Aalto University
School of Chemical
Technology

School of Chemical Technology
Degree Programme of Chemical Technology

Igor Saavedra

MODEL-BASED OPTIMIZATION OF A COMPACTCOOKING G2 DIGESTING PROCESS STAGE

Master's thesis for the degree of Master of Science in Technology submitted for inspection, Espoo, 31 December 2015.

Supervisor Prof. Sirkka-Liisa Jämsä-Jounela
Instructors Dr. Ing. Aldo Cipriano
D.Sc. Olli Joutsimo

Aalto University
School of Chemical Technology

ABSTRACT OF MASTER'S THESIS

Author **Igor Saavedra**

Thesis title **Model-based Optimization of a CompactCooking G2 Digesting Process Stage**

Department **Biotechnology and Chemical Technology**

Abstract

A CompactCooking™ G2 (Valmet) digesting system represents a challenging process stage to be optimized in the context of a kraft pulp mill. Its highly non-linear behavior due to liquor recycling and heat integration poses a barrier to traditional trial-and-error optimization conducted by physical lab-scale simulation. Hence, this thesis aims to design a solution based on numerical simulation and mathematical optimization, whose results can be directly applied on industrial-scale as computed optimal set-points for the supervisory control.

Based on published, first-principles, pulp digester models, a customized dynamic model was developed in Matlab/Simulink to simulate a complete CompactCooking™ G2 stage. The process model is founded on Purdue wood reaction kinetics and Härkönen chips bed compaction models, and it seamlessly takes into account process characteristics mentioned above. The non-linear model was validated by comparison against historical data of an industrial unit (200 h), and then employed in the design of a steady-state optimizer for this process stage by means of linear programming.

Simulation results showed very good agreement in terms of liquors residual alkali, weak black liquor solids, and blowline kappa, despite high uncertainty on disturbances data and model simplifications. However, simulated kappa showed higher sensitivity to temperature fluctuations than the plant signal, likely indicating the need for more detail when modelling heat transfer phenomena. As to the optimization goal, a base case scenario (plant steady-state) was identified from industrial data to attempt process economics optimization. The results showed a potential for increasing profit or reducing variable costs in at least 2 USD/ADt, which for a modern pulp mill represents annual benefits between 1 – 2 million USD depending on production rate and mill availability.

Further, the simulation model showed remarkable results when used in a novel process analysis technique, called here simulated contribution, letting to explain the variability of blowline kappa in terms of multiple-time-scale process dynamics.

In conclusion, a model-based optimization method has been successfully designed for the CompactCooking™ G2 system, and potential economic benefits should encourage industrial testing and further work to develop a real-time optimizer software technology.

Professorship **Process Control**	Professorship code **KE-90**
Thesis supervisor **Prof. Sirkka-Liisa Jämsä-Jounela**	Pages **157+18**
Thesis advisors **Dr. Ing. Aldo Cipriano** **D.Sc. Olli Joutsimo**	Language **English**
Keywords **pulp digester, CompactCooking G2, dynamic simulation, model-based optimization, model-based process analysis**	Date **31.12.2015**

Preface

I have been studying kraft pulping processes since I entered the South American pulp industry as a trainee research engineer four years ago. A modern kraft pulp mill represents a challenging and interesting process system to learn about for a young chemical engineer. Unfortunately, although pulp production is an important economic activity for South America, I was not able to find the specialized knowledge I needed at home.

I came to know about Finland as a forerunner in the pulp and paper industry through my job, from where I was given the support to study there, along with other colleagues, in order to learn as much as I could about related fields to the kraft pulp mill process. Thus, I began studies in Åbo Akademi compulsively consuming knowledge about wood and fiber chemistry, biomass combustion and ash chemistry, and the new trends of transforming kraft pulp mill into future biorefineries. After that, I moved to Aalto-yliopisto attracted by the idea of acquiring knowledge on process automation, including subjects such as modelling, simulation, control, optimization, and monitoring of chemical processes; topics that may be the fundamentals to the process systems engineering discipline. This thesis hence crystallizes a bunch of ideas related to the above matters, and although it is certainly not the most advanced work on its field, it aims to be useful for anyone interested in modelling, simulation and optimization of pulp digesters. The code itself is indebted to the original spirit of Castro and Doyle's Pulp Mill Benchmark Model from which I learned a lot. Open innovation is certainly the best way to innovate and probably the most natural one, as sharing words and ideas should be in our genetic code.

I am greatly indebted to the Finnish higher education system. Thus I am thankful to all lecturers and professors from whom I learned during my time in Finland. Special acknowledgments to Prof. Sirkka-Liisa Jämsä-Jounela and Alexey Zakharov from Aalto-yliopisto, who taught me most of the mathematical techniques found here; and to Jan Gustafsson, Anna Sundberg, and Pedro Fardim from Åbo Akademi for their teaching in wood and paper chemistry subjects. Also, I wish to acknowledge Aldo Cipriano for his feedback and comments, and Olli Joutsimo for his patience and support.

Future, experts say, is all about knowledge-, bio- and digital-economy. South American pulp industry is blessed regarding its forest resources but is (light) years behind forerunners in terms of advancing process technologies, likely, due to shortsighted decision-making, poor collaboration between industry and local universities, and low investment in R&D. Hopefully, the effort to bring new knowledge to this industry will not be a vain attempt.

Finally, I would like to express my gratitude to my beloved ones, to Loreto and Alex that even travelled to share some time along, and to my colleagues with whom we kill freezing cold times. My special gratitude also to Onu, Evi, Leila, Sanna, Anni, Aleksi, Vahid, Moses, José, Vincent, Anatoly and all the Axelbandet members. I know I am the worst at keeping in touch, but I keep the best memories of all of you… after all, life may not be more than a bunch of memories.

Igor Saavedra

Table of Contents

Algebraic Notation

Simulation Part

R_g	Universal gas constant	$8.314\,\frac{\mathrm{J}}{\mathrm{mol \cdot K}}$
g	Gravity acceleration	$9.81\,\frac{\mathrm{m}}{\mathrm{s^2}}$
A	Cross-sectional area	$\mathrm{m^2}$
D	Diffusivity coefficient	$\frac{\mathrm{cm^2}}{\mathrm{min}}$
T	Temperature	K
P	Pressure	Pa
F	Volumetric flow rate	$\frac{\mathrm{m^3}}{\mathrm{min}}$
$\tilde{F}$	Mass flow rate	$\frac{\mathrm{kg}}{\mathrm{min}}$
ρ	Density	$\frac{\mathrm{kg}}{\mathrm{m^3}}$
s	Rotational speed	rpm
z	Axial space dimension	m
t	Time dimension	min
τ	Retention time	min
w	Molar mass	$\frac{\mathrm{g}}{\mathrm{mol}}$
ρ_i	Basic concentration of wood components	$\frac{\mathrm{kg\ of}\ i}{\mathrm{m^3 sub}}$
C_j	Mass concentration of liquor components	$\frac{\mathrm{kg\ of}\ j}{\mathrm{m^3 e/f}}$
$\hat{C}_j$	Molar concentration of liquor components	$\frac{\mathrm{kmol\ of}\ j}{\mathrm{m^3 e/f}}$
C_P	Mass-specific heat capacity	$\frac{\mathrm{J}}{\mathrm{kg \cdot K}}$
$\bar{C}_P$	Volume-specific heat capacity	$\frac{\mathrm{J}}{\mathrm{m^3 K}}$
h	Mass-specific enthalpy	$\frac{\mathrm{J}}{\mathrm{kg}}$
H_R	Mass-specific heat of reaction	$\frac{\mathrm{J}}{\mathrm{kg}}$
E_a	Activation energy	$\frac{\mathrm{J}}{\mathrm{mol}}$
k_0	Pre-exponential factor	$\frac{\mathrm{ad\ hoc}}{\mathrm{min}}$
k	Reaction rate constant	$\frac{\mathrm{ad\ hoc}}{\mathrm{min}}$
U	Overall heat transfer coefficient	$\frac{\mathrm{J}}{\mathrm{min \cdot m^2 K}}$
R_i	Volume-specific reaction rate of wood components	$\frac{\mathrm{kg\ of}\ i}{\mathrm{m^3 sub \cdot min}}$
R_j	Volume-specific reaction rate of liquor components	$\frac{\mathrm{kg\ of}\ j}{\mathrm{m^3 e/f \cdot min}}$
u	Superficial velocity	$\frac{\mathrm{m}}{\mathrm{min}}$

v	Interstitial velocity	idem
$\hat{R}_{1,2}$	Specific liquid pressure drop parameter	$\frac{\mathrm{Pa}}{\mathrm{m}}\left(\frac{\mathrm{min}}{\mathrm{m}}\right)^{1,2}$
$[\eta]$	Polymer-solvent intrinsic viscosity	$\frac{\mathrm{ml}}{\mathrm{g}}$
n	Volume-specific number of bonds	$\frac{\mathrm{mol\_bond}}{\mathrm{m^3sub}}$
M	Volume-specific number of polymers	$\frac{\mathrm{mol\_poly}}{\mathrm{m^3sub}}$
N	Volume-specific number of monomers	$\frac{\mathrm{mol\_mono}}{\mathrm{m^3sub}}$
DP_n	Number-average degree of polymerization	$\frac{\mathrm{mol\_mono}}{\mathrm{mol\_poly}}$
DP_w	Weight-average degree of polymerization	idem
DP_v	Viscosity-average degree of polymerization	idem
K, α	Mark-Houwink parameters	
κ	Pulp kappa number	
Y	Pulp yield	$\frac{\mathrm{BDkg}}{\mathrm{BDkg}}$
c^*	Pulp consistency	$\frac{\mathrm{BDkg}}{\mathrm{kg}}$
$x^\dagger$	Mass fraction	$\frac{\mathrm{kgDS}}{\mathrm{kg}}$
$\tilde{x}$	Mass fraction on dry-basis	$\frac{\mathrm{kgDS}}{\mathrm{kgDS}}$
η	Void volume fraction of the chips bed	$\frac{\mathrm{m^3f}}{\mathrm{m^3st}}$
ε	Void volume fraction inside chips	$\frac{\mathrm{m^3e}}{\mathrm{m^3sub}}$
P_ε	Penetration degree	$\frac{\mathrm{m^3}}{\mathrm{m^3e}}$
K_ε	Chip permeability	$\mathrm{cm^2}$
L_l	Chip length	cm
L_c	Chip thickness	cm
L_w	Chip width	cm
μ	Liquor dynamic viscosity	$\mathrm{Pa \cdot min}$
γ	Ratio of volume fractions	
m	Fed chips moisture	$\frac{\mathrm{kg}}{\mathrm{kg}}, \frac{\mathrm{kg}}{\mathrm{BDkg}}$
ρ_{basic}	Fed chips basic density	$\frac{\mathrm{BDkg}}{\mathrm{m^3sub}}$
ρ_{bulk}	Fed chips bulk density	$\frac{\mathrm{BDkg}}{\mathrm{m^3st}}$
ρ_{ws}	Wood substance density	$\frac{\mathrm{BDkg}}{\mathrm{m^3s}}$

* Mass fraction of pulp, express in AD, BD or OD units (see Abbreviations)
† Mass fraction of components other than pulp, expressed in DS units (see Abbreviations)

Optimization Part

F_{pulp}	Pulp production rate	$\frac{\mathrm{ADt}}{\mathrm{min}}$
Q_{WBL}	WBL energy content delivery rate as HHV	$\frac{\mathrm{MWh}}{\mathrm{min}}$
F_{wood}	Wood consumption rate	$\frac{\mathrm{m^3sub}}{\mathrm{min}}$
Q_{steam}	MP steam effective latent heat transfer rate	$\frac{\mathrm{MWh}}{\mathrm{min}}$
F_{WL}	White liquor consumption rate	$\frac{\mathrm{tNa_2O}}{\mathrm{min}}$
p_{pulp}	Unbleached pulp price	$\frac{\mathrm{USD}}{\mathrm{ADt}}$
p_{EE}	Electric energy price	$\frac{\mathrm{USD}}{\mathrm{MWh}}$
p_{wood}	Wood price	$\frac{\mathrm{USD}}{\mathrm{m^3sub}}$
p_{WL}	White liquor cost	$\frac{\mathrm{USD}}{\mathrm{tNa_2O}}$
η_{RL}	Energy conversion efficiency of the whole recovery	
η_{TG}	Energy conversion efficiency of turbo generators	
y	Output variable	
u	Input variable	

Abbreviations and Subscripts

AGU	Anhydrous glucose unit
AD*	Air dry mass of pulp
BD†	Bone dry mass of pulp
DS	Dry solids mass
DCS	Distributed control system
C	Cellulose
H	Hemicellulose
GM‡	Glucomannan
E	Extractives
X§	Xylan
CH	Carbohydrates (polysaccharides)

* Per definition 1 AD = 0.9 BD
† Also referred as oven dry mass of pulp (OD)
‡ Galactoglucomannan in SW and glucomannan in HW
§ Arabinoglucoronoxylan in SW and glucoronoxylan in HW

DP	Average degree of polymerization
HHV	Higher heating value
LHV	Lower heating value
HP	High pressure
MP	Medium pressure
LP	Low pressure
EA/W[*]	Effective alkali-to-wood ratio
L/W	Liquor-to-wood ratio
L	Lignin
L_F	Fast lignin (high reactivity)
L_S	Slow lignin (low reactivity)
HW	Hardwood (broad-leaves trees)
SW	Softwood (coniferous trees)
WBL	Weak black liquor
c	Chips phase (“solid under bark” phase)
s	Chips solid phase (wood substance volume)
l	Liquid phase
e	Entrapped liquid phase (chips internal porosity)
f	Free liquid phase (chips bed porosity)
st[†]	Stereo volume (bulk volume)
i	Index for chips solid phase components
j	Index for liquid phase components
k	Index for the grid point (discretized axial dimension)
cs	Polymer chain scission
w	Water
cm	Chip meter
wm	Weightometer

[*] Also referred as effective alkali charge (EA%)
[†] In terms of units m^3st [=] $m^3sub + m^3f$ [=] $m^3s + m^3e + m^3f$ [=] $m^3s + m^3l$

1 Introduction

The pulp and paper industry is a global, dynamic and competitive economic sector. Although world consumption of its products used to increase steadily, until the beginning of the last global recession when reached almost 400 Mt/y in 2007 (FAO, 2014), worldwide economic and cultural changes are driving the production rate into a stagnation phase that is strongly rising competition. This scenario affects especially market pulp producers, who confront major challenges in terms of: increasing operating costs, higher quality demand, low mill availability, and ever more restrictive environmental legislation.

To addresses these issues, pulp companies can take actions at different levels of the automation pyramid in an effort to optimize profitability and remain competitive. At the plant level, companies can greatly benefit from studies on modelling, simulation and control to optimize process economics and product quality, since it requires a low capital investment and can yield a very high return. In this sense, process systems engineering plays a key role providing theory, tools and methods to improve automation technologies in the process industries.

In the case of the pulp and paper industry, wide research has been done in modelling, simulation and control of the kraft pulp mill process, the dominant pulping process technology; and research has been specially intensive regarding modelling of pulp digesters, core reactors of the mills (Dahlquist, 2008; Blanco et al., 2009). However, research tends to focus mainly on theoretical aspects of process systems engineering, ignoring to deliver means for practical implementation of automation solutions at industrial-scale. Moreover, as process technologies advance, available research models need to be updated and thus a constant modelling effort is needed.

1.1 Problem statement

The digesting or cooking stage of a kraft pulp mill process represents a key area for the economic performance of a mill. As the main consumer of medium-pressure (MP) steam and white liquor, its consumption rates impact on the profit margin of the whole mill. Moreover, cooking kappa fluctuations greatly affect all the remainder process stages by impacting on overall yield, specific

consumptions of bleaching agents, and heating value of the black liquor sent to the recovery line.

The operation of a modern continuous digesting process, including those implementing CompactCooking™ or Lo-Solids™ techniques, is especially challenging: highly interacting unit operations due to liquor recycling and heat integration, high uncertainty and delay in the measurement of key disturbances, and complex physicochemical phenomena inside reactors. All the above configures a difficult task for mill personnel trying to optimize cooking set-points, commonly referred as “the cooking recipe”. Conventionally, this optimization task is performed by laboratory trials that physically simulate different cooking conditions; however, available laboratory equipment simplifies the complexity of industrial scale systems, and key interaction effects cannot even be evaluated by these experiments.

1.2 Goals and scope

This thesis aims to accomplish model-based optimization of a continuous digesting process stage commercialized as CompactCooking™ G2 (Valmet) by designing a solution based on numerical simulation and mathematical optimization that not neglect key interactions within the process.

The optimizer shall be able to calculate an improved cooking recipe by performing steady-state optimization of a process model. The model will take into account interactions between the impregnator and the digester vessels as part of the flow and heat-recovery configurations in the process system. The modelling effort for phenomena inside vessels tries to avoid excessively long computation times; hence, only pulping reaction kinetics, as from Purdue model, and chips column compaction, as from Härkönen model, are to be dynamically simulated in a single axial dimension.

Although an optimization routine will be designed and tested, its actual implementation as part of a process automation system remains outside the scope of the thesis. Likewise, evaluating the wide variety of optimization algorithms and/or multi-objective approaches is not considered, thus only a linear programming approach for single-objective optimization will be designed, applied and discussed.

1.3 Methodology and contribution

This thesis contributes a novel, first-principles, dynamic simulator of the CompactCooking™ G2 process system, which is designed, tested, and validated for optimization purposes. The simulation model will be used to identify a plant steady-state, from which the optimization routine, given an objective function, can start to search for an improved steady-state that complies with target production rate and cooking kappa, as well as additional operational constraints such as limits on: temperatures, alkali concentrations, compacting pressures, or pulp viscosity. The simulator and optimizer will be implemented in Matlab/Simulink.

To the best knowledge of the author, an open-source, dynamic simulator of this process has not made public elsewhere. Although commercial software, such as CADSIM Plus™ or IDEAS™, might permit to simulate this system in a resembling manner, its closed source implementation does not allow analyzing and improving the fundamental model architecture. Furthermore, this work shall contribute by evaluating the applicability of a model-based optimization approach for the CompactCooking™ G2 system, which can provide a conceptual basis for developing hereafter a real-time optimizer technology.

1.4 Structure of the thesis

This thesis is divided into eleven chapters grouped in two parts. A literature part comprises Chapters 2 to 4; Chapter 2 briefly reviews the fundamentals of the kraft pulp mill process; Chapter 3 expands on the digesting process stage; and Chapter 4 delves into mathematical models with application to simulation, control and optimization of continuous pulp digesters. An experimental part includes Chapters 5 to 10; Chapter 5 presents the global methodology; Chapter 6 describes the process studied; Chapter 7 explains the mathematical modelling and model implementation; Chapter 8 presents the simulation results discussing model uncertainties; Chapter 9 describes the design of the process economics optimizer; and Chapter 10 discuss the optimization results concerning the applicability of the whole model-based approach to a real process. Finally, Chapter 11 concludes by summarizing main results and indicating future development lines. In addition, Appendix A analyses the CompactCooking™ G2 process by means of a novel technique called here simulated contribution.

LITERATURE PART

2 The Kraft Pulp Mill

To fully understand the problem statement and objectives of the thesis, it is necessary to comprehend the fundamentals of the kraft pulp mill process. Accordingly, the literature part begin by briefly describing the mill as a chemical process system. First, general terms are defined in order to contextualize the industrial role of a pulp mill, and then the mill-wide process is described.

2.1 Industry facts and terms

Pulp is a term that can be defined in different ways depending on our standpoint. The following explains several meanings of the term pulp, as well as common categorization methods for its different types, conventionally referred as pulp grades. Besides, some historical facts are covered about the development of the kraft pulping process. For a thorough treatment of these topics the reader can consult Sixta (2006) and Holik (2006).

From an economic perspective, pulp denotes an intermediate product primarily used as feedstock in the production of paper products. In that context, market pulp refers to a variety of pulp produced in a pulp mill that is sold as a commodity for further processing in another location, normally a paper mill.

In the field of materials science, pulp refers to an assemblage of vegetal fibers obtained by dismantling the internal, fibrous structure of a plant. The vast majority of plants, vascular plants, can be chemically referred as lignocellulosic biomass, i.e., their vascular tissue cells are constituted by a biopolymer of cellulose, hemicellulose and lignin that forms the cell walls. A simplified picture is that cellulose and hemicellulose form the main fractions of the cell wall, whereas lignin concentrates into an intercellular layer that cements multiple cells altogether constituting the plant tissue. Most of these plant cells show an elongated shape and are therefore commonly denoted as fibers.

For process engineers, pulp means a suspension or semisolid material of fibers and is categorized based on the properties of the fibers, the nature of the fibers source, and the pulping process applied. Pulping, as the name suggests, refers to the process by which the lignocellulosic biomass is transformed into pulp.

Fibers themselves are termed virgin (primary) or recovered (secondary) depending on whether the feedstock was a newly harvested plant source or recovered paper. Likewise, pulp is termed wood (hardwood or softwood) or non-wood based on the taxonomy of the biomass source. Among pulps of virgin fibers, many pulp grades are distinguished due to the large variety of pulping techniques and fiber sources available. Pulping techniques vary from complete mechanical to complete chemical processes with several combinations in between; their suitability depends on the desired properties of the fibers, which in turns depends on the final product to be manufactured, commonly a paper product though not exclusively. According to the pulping technique, names for the pulp grades arise naturally, such as mechanical, thermomechanical, semichemical, or chemical pulps. Among the latter, four important subgrades must be mentioned: (i) soda, (ii) sulfite, (iii) kraft (sulfate), and (iv) organosolv.

Chemical pulping has become predominant within the pulp and paper industry due to changes in the paper products market, as well as to advances in the process technologies themselves. Indeed, kraft pulp grades represent today almost 74% of the global wood pulp production, which reached 174 million ADt in 2013 (FAO, 2014). Furthermore, new kraft pulp mills have recently started operations, and several mill projects are waiting to enter construction phase or are already under construction (RISI, 2014)

The kraft pulping process was accidentally invented by Carl Dahl, a German chemist, during his research to improve the recovery of chemicals in the soda pulping process. Although the research aim was not advancing pulping itself, he was led to discover that the addition of sodium sulfide (Na_2S) to the soda pulping produces a “kraft”[*] pulp (see Figure 2.1). The invention was patented in 1884, and the first kraft pulp mill started operations during 1890 in Sweden. However, it was not until the development of the Tomlinson’s recovery boiler and chlorine bleaching techniques, since the 1930s, that the process starts gaining predominance. The Tomlinson’s boiler gave an economical edge over the sulfite alternative, leading process at that time, thanks to significant improvements in the recovery of chemicals and energy. On the other hand, chlorine bleaching allowed achieving higher pulp brightness without compromising the characteristic strength

[*] The word for strong in German

properties of the kraft pulps, and made also possible to apply the kraft process to a wide variety of raw materials attaining high quality pulps.

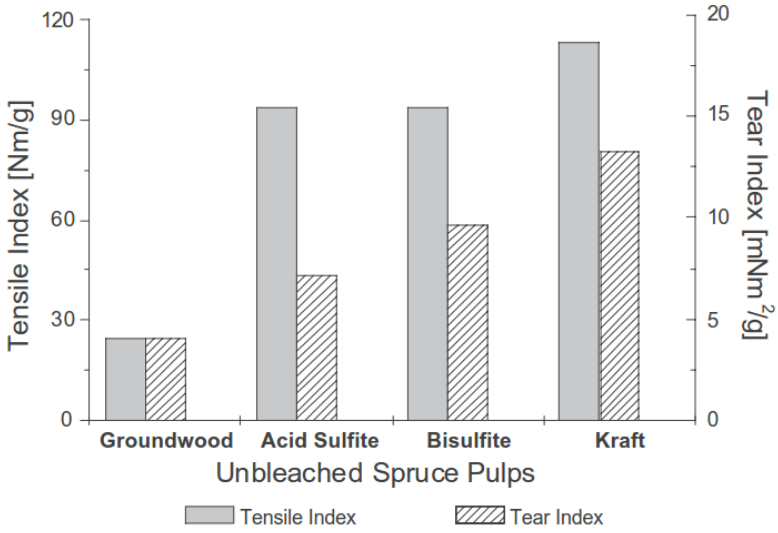

Figure 2.1. Pulp sheet properties of unbleached spruce pulp grades (45 SR). (Sixta, 2006)

Currently, modified kraft processes are the dominant technologies in chemical pulping probably because of these two unique features: (i) versatility for processing a wide variety of raw materials achieving superior pulp properties, and (ii) highly profitable process economics due to an integrated recovery cycle of chemicals and energy. Indeed, modern mills are self-sufficient in the generation of process steam and electrical power, and even able to sell a considerable amount of electrical energy to the grid.

In a global perspective, the production capacity of hardwood and softwood kraft pulps is shifting in recent decades from the traditionally strong pulping countries in North America and Scandinavia to South America and Russia. This is allegedly explained by substantial differences in growth rate of forest plantations, as well as raw materials and labor costs. Companies from the former countries are pursuing a transformation of traditional kraft pulp mills into the new concept of biorefineries or multiple bioproduct mills, in order to avoid mill shutdowns and to reinvigorate their pulping economic sector by creating products of higher value-added. On the other hand, the new players rely on the advantages of their natural environments and opt for a strategy of cost reduction and efficiency increment.

2.2 Mill-wide process description

A kraft pulp mill can be defined as an industrial process plant that transforms, applying a kraft process, a lignocellulosic biomass resource into an intermediate fiber product. The latter represents either an: (i) unbleached, (ii) bleached, or (iii) dissolving pulp grade, which can be used for further manufacturing of products such as paper and board, textiles, or cellulose derivates (e.g., carboxymethyl cellulose). The difference between these grades is given along the mill description below.

From a forest plantation, wood is transported to the mill in the form of logs, which usually correspond to the upper part of trees as the lower part is more suitable for other types of wood products. These logs are collectively termed roundwood. The roundwood entering the mill go through a series of unit operations grouped into process stages. Each stage is designated by a unique name and associated to a layout area; since there is usually one area per process stage, mill personnel refer to the concept of process stage as an “area”, and this convention may also be used along the thesis. Functionally related areas are grouped into higher-level abstractions of process stages called “lines”. Figure **2.2** shows a block flow diagram of the mill-wide process identifying main areas and lines.

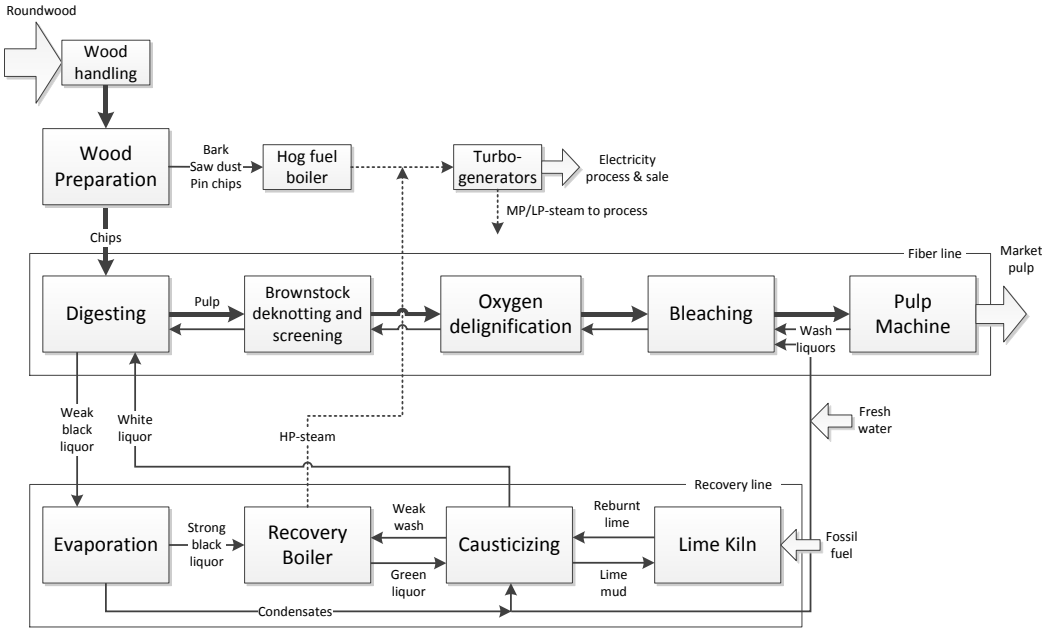

Figure 2.2. Block flow diagram of the kraft pulp mill process.

Environmental emissions, such as liquid effluents, solid wastes and air emissions, are not drawn in the diagram for sake of simplicity. However, the main known disadvantages of the kraft pulp mill process are: (i) malodorous gases formed during digesting due to the presence of sodium sulfide; and (ii) bleaching filtrates containing adsorbable organic halides (AOX) caused by the use of chlorine-based bleaching agents.

The following sections concisely describe the main areas of a generic kraft pulp mill producing a wood bleached pulp grade. For a comprehensive description of the kraft pulp mill process, the reader is encourage to consult Fardim (2011) and Tikka (2008). The summarized information found here is also based on Biermann (1996), Sixta (2006), and Ek et al. (2009).

2.2.1 Wood line

The roundwood entering the mill must be debarked, chipped, and screened before being sent to the pulp digesting stage; these three mechanical operations constitute the wood preparation area. Prior to this, logs should have been measured and eventually deiced, cut, and stored as part of the wood handling operations.

Logs arrive by trunks or rail cars that are unloaded, for preference, directly into the debarker infeed. At peak arrival, most of the trucks are unloaded on the wood yard where logs can be piled up. In this sense, the yard acts as a process inventory to level out the seasonal variation in the arrival of logs.

A good practice is to debark logs as soon as possible because the dryer they become, the more difficult the debarking may result. However, bark adhesion varies with wood species, harvesting time, felling age, and storage conditions. The chemical composition of bark is fairly different from wood, understood as the xylem, and for this reason bark represents a process contaminant. Bark, nevertheless, is appreciated for a higher heating value compare to wood, thus is commonly burnt in a hog fuel boiler to generate steam and electricity.

Other common process contaminants comprise sand, stones, metal pieces and plastics residues. All of them may be found on the plantation ground and sent to the mill during the loading of trucks. Sand can be washed before or during debarking. Stones and big metal pieces should be separated by traps incorporated in the debarking unit. For smaller metal pieces, metal detectors are

place along conveyor belts of the area in order to stop them and remove the contaminant. Plastics residues are probably the most difficult contaminants to deal with, and there is no equipment designed to trap them during wood preparation.

After debarking, wood is immediately processed in the log chipper. Since the final size and shape of the chip varies stochastically around a target, a chip screening operation takes place to ensure homogeneity of woodchips for the digesting area. Screening divides the input stream of chips into three fractions: accepted, oversize and fines. Oversize fraction can be processed in a chip conditioner in order to generate a new accepted fraction; fines instead are mixed with bark and sent to the hog fuel boiler.

To absorb variations of input and output flow rates in the wood preparation stage, a chip storage unit, such as a chip pile or silo, acts as a process inventory and it is commonly placed between chipping and screening operations.

2.2.2 Fiber line

The fiber line comprises the areas of digesting, brownstock screening, oxygen delignification, bleaching, and pulp machine.

The screened chips enter the digesting area where steam and chemical reagents, mainly sodium sulfide (Na_2S) and sodium hydroxide (NaOH) dissolved in aqueous phase, provide the conditions of temperature (in the range of 130 – 170 C) and chemical potential to promote alkaline delignification of wood. Fibers are more prompt to separate from each other as lignin degrades, and thus solid woodchips become a pulp suspension. Alkaline delignification comprises a series of chemical reactions of the wood that are desired to be as selective as possible towards lignin degradation; however, parallel degradation of hemicellulose and cellulose also occurs. Once the target lignin content has been reached, the delignification can be stopped by decreasing the temperature (usually below 95 C) and washing the pulp. The foregoing operation is conventionally termed cooking or digesting, and the resulting pulp is called crude pulp or brownstock.

The main fraction of cooking reagents is fed as a clear solution called white liquor. As the delignification advances, partial degradation and solubilization of lignin turns the coloration of the aqueous phase into a dark-brown tone, the resulting liquid phase is therefore called black liquor. According to the

concentration of dissolved matter on it, black liquor is conventionally denoted as weak or strong instead of diluted or concentrated. At the end of the cook, weak black liquor (WBL) is obtained and it can be concentrated to attain a combustible material for the recovery boiler, in which also a fraction of the cooking reagents can be regenerated.

The crude pulp should be processed through a system of screeners and cyclones in order to remove knots, shives, or other previously present contaminants that can damage equipment or be detrimental for the pulp quality. This separation stage corresponds to the brownstock deknotting and screening area. In simple ideas, knots refer to uncooked portions of a woodchip; and shives, to uncooked fiber bundles. Both can be recovered as part of the accepted pulp fraction to avoid a yield loss by recirculating them to the digesting area, although this can affect the homogeneity of the cook.

Lignin content on the crude pulp can be further lowered, with higher selectivity than during cooking, by means of mixing the pulp with oxygen gas in a pressurized reactor. This represents the oxygen delignification stage, up to which the resulting pulp is denoted unbleached due to its brown coloration. Mills producing unbleached pulp grades can stop their pulping process at this point, or even dismiss this stage completely to reduce process costs.

In order to remove coloration, pulp is said to be bleached by means of chlorine- and oxygen-based oxidants such as chlorine (Cl_2), chlorine dioxide (Cl_2O), hydrogen peroxide (H_2O_2), oxygen (O_2), or ozone (O_3). Bleaching may be defined as the selective removal of colored compounds (chromophores) in order to increase the pulp brightness, i.e., its light reflectance at a particular wavelength measured according to a standard protocol. This stage is usually performed by applying bleaching agents in a multi-step sequential process. Bleaching sequences without chlorine (Cl_2) are called elemental-chlorine free (ECF), whereas sequences without any chlorine-based oxidant correspond to totally-chlorine free (TCF). Currently, ECF sequences are preferred when balancing process cost and allowed environmental impact; however, TCF technology is known to be more benign to the environment. Bleached kraft pulp grades are commonly required to show a brightness value above 89%-ISO; the initial brightness of unbleached kraft pulps is typically between 55 – 60%-ISO.

At the end of the bleaching sequence, a bleached pulp grade is obtained that should be chemically composed of cellulose, hemicellulose and almost no lignin. Further purification of this pulp to remove hemicellulose would produce a dissolving pulp grade. However, the industrial approach to produce dissolving grades through a kraft process usually involves removing most of the hemicellulose before the cooking stage, which is conventionally known as a pre-hydrolysis kraft (PHK) operation.

Finally, the bleached pulp is dried in the form of a sheet formed at the pulp machine stage. Actually, this stage highly resembles a paper machine process but without the equipment for pulp refining and paper additives application. A thorough description of a paper machine can be found on Holik (2006).

Between the foregoing stages, pulp storage tanks should be placed to absorb flow rate variations along the fiber line. More details are reviewed about the digesting stage and pulp quality variables on the next Chapter.

2.2.3 Recovery line

The recovery line includes the areas of evaporation, recovery boiler, causticizing and lime kiln.

The weak black liquor exiting the digesting area contains most of the organic wood compounds removed during the cook and the inorganic chemicals charged as white liquor addition; its dry solids content typically range between 13 – 18%. The organic material consists primarily of lignin fragments (high molecular-weight), and aliphatic carboxylic acids (low molecular-weight) originated from the degradation of the wood carbohydrates fraction, i.e., cellulose and hemicellulose. The higher heating value of the kraft black liquor usually range between 13 – 15 MJ/kg dry solids, greatly depending on the wood species, white liquor charge, and unbleached pulp yield. For purpose of firing most of the water must be separated, this is done in the evaporation area by a multi-effect system with steam in up to 7 – 9 heat-integrated effects. The resulting strong black liquor may achieve a dry solids content of 70 – 85%.

The strong black liquor is sent to the recovery boiler area where the organic material is combusted to generate high-pressure steam (480 – 500 C at 70 – 100 bar) for the turbo generators. Along the process, the sulfide ion (S^{-2}) tends to oxidized into sulfate (SO_4^{-2}), thus a reduction is needed to regenerate the active

ion for the cooking. The recovery boiler provides this reductive environment where thermochemical reduction of sulfate may happen, such that the inorganic cooking chemicals can be recovered in the form of a smelt containing sodium carbonate (Na_2CO_3) and sodium sulfide (Na_2S). The smelt is dissolved in water, then clarified or filtered to remove solid impurities, called dregs, and finally sent to the causticizing area for the preparation of white liquor. The dissolved smelt shows a green coloration and is thus called green liquor.

The flue gas exiting the boiler furnace carries a considerable dust load; hence the gas is passed through electrostatic precipitators in order to retain the solid particles. As dust contains a significant amount of sulfur, it may reenter the process, with or without purification, such that a sulfur loss is avoided.

In order to regenerate the white liquor, the carbonate ion (CO_3^{-2}) in the green liquor must be exchanged for a hydroxide ion (OH^-). This is achieved during the causticizing stage by mixing the green liquor with reburnt lime mud in a slaker reactor, where the fast slaking reaction (Eq. 2.1) occurs, and then giving enough retention time to the liquor in a train of causticizer reactors, thus the causticizing reaction (Eq. 2.2) can reach as high as possible conversion.

$$CaO_{(s)} + H_2O \rightarrow Ca(OH)_{2(aq)} \quad \textbf{2.1}$$

$$Na_2CO_{3(aq)} + Ca(OH)_{2(aq)} \rightarrow 2NaOH_{(aq)} + CaCO_{3(s)} \quad \textbf{2.2}$$

Heavy insoluble particles settle in the classifier section of the slaker reactor. These solids are called grits, and together with the dregs represent a purge of impurities for the whole mill process. These impurities correspond to an insoluble form of inorganic ions unwanted within the process; the latter are termed non-process elements (NPEs) and tend to accumulate within the mill due to its degree of closure.

The regenerated white liquor is filtered to separate the remainder lime mud, which is sent back to the lime kiln area for regenerating the calcium oxide (CaO) by calcination (Eq. 2.3). The latter is a very endothermic process requiring high temperature (above 820 C), achieved by firing fuel oil or natural gas in a refractory rotary kiln to which the return mud is fed.

$$CaCO_{3(s)} \rightarrow CaO_{(s)} + CO_{2(g)} \quad \textbf{2.3}$$

3 Pulp Digesting Stage

Several challenges are confront when engaging on tasks of modelling, simulation, control, and optimization of kraft pulp digesters. Naturally, first-principles modelling requires understanding the phenomenological dimension of the digesting operations as much as possible, and actually all these tasks demand some background on the process chemistry and technology of the stage. Consequently, this Chapter expands on the kraft digesting stage providing the reader essential information to understand the experimental part. Otherwise stated, the summarized information found here has been taken from Fardim (2011), Biermann (1996), Sixta (2006), Ek et al. (2009) or Sjöström (1993).

3.1 Woodchips as raw material

Wood is a biological, heterogeneous material that poses several difficulties in its processing concerning the production of pulp. In fact, wood was not an important source of fibers until the beginning of the Industrial Revolution, period up to which cotton was the common raw material for the production of paper, main end-product of the current woodpulp production.

Wood as a renewable resource is regenerated in the growing of forest plantations. The trees from the plantation are logged and transported to the pulp mill, where they are debarked and chipped to a size that enables, as much as possible, an homogeneous condition for the chemical reactions of wood during digesting without decreasing the intrinsic length of the fibers or provoking severe damage to their structure. Figure 3.1 shows the scheme of a woodchip and its common dimensions.

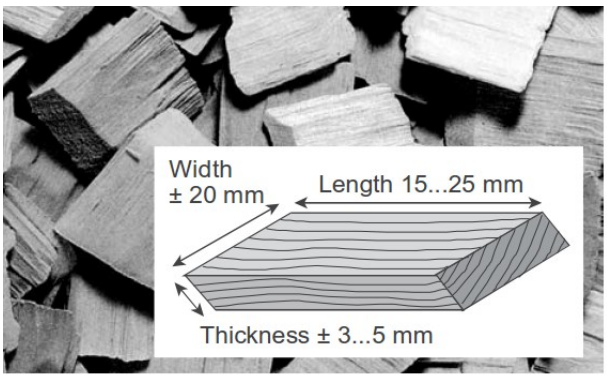

Figure 3.1 Typical dimensions of woodchips. (Sixta, 2006)

Woodchips correspond to parts of the xylem, a type of transport tissue of trees. The xylem presents a very complex structure with several substructures at different scales, i.e., from its molecular dimensions to the macroscopic tissue level. Figure 3.2 schematically depicts wood structures at different scales. Fibrils composing the cell wall layers can be described as nanocomposites of biopolymers, namely lignin, cellulose, hemicellulose and pectin. While lignin is a randomly cross-linked polymer of phenylpropane units, the remainder constituents are linear polysaccharides containing glucose along with several other monosaccharides.

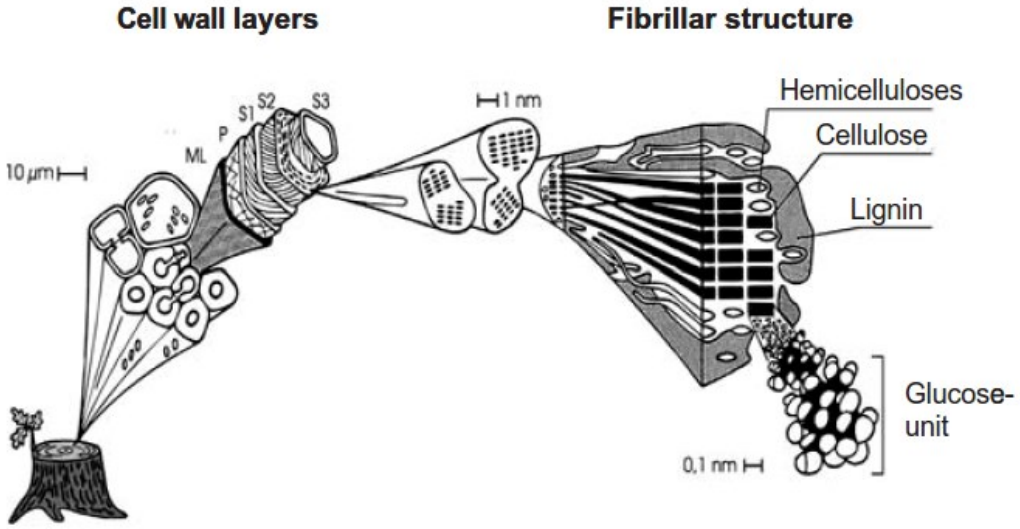

Figure 3.2. Wood xylem multi-scale structures. (Sixta, 2006)

Depending on the wood species, the mass percentage of these biopolymers in the xylem may drastically vary. In this sense, the chemical composition of wood in terms of its polymeric constituents is a critical factor to consider in the design of pulping processes. Table 3.1 shows the chemical composition for several wood species relevant in chemical pulping. The reader could easily recognize a pattern in the composition of softwood (gymnosperms) versus hardwood (angiosperms) tree species. Although the main aim of chemical pulping is the removal lignin, both types of species are actually needed in the industry because their fibers present very distinct properties, especially considering their average length in which softwood fibers usually tend to be longer than hardwood ones.

Table 3.1. Chemical composition of various wood species. Adapted from Sjöström (1993)

All values are given as % of the dry wood mass; extractives are obtained by dichloromethane followed by ethanol extraction; glucomannan includes galactose and acetyl groups in softwood; glucoronoxylan includes arabinose in softwood and acetyl groups in hardwood.

Species	Extractives	Lignin	Cellulose	Glucomannan	Glucoronoxylan	Other polysaccharides	Residual constituents
Softwoods							
Pinus radiata	1.8	27.2	37.4	20.4	8.5	4.3	0.4
Pinus sylvestris	3.5	27.7	40.0	16.0	8.9	3.6	0.3
Picea abies	1.7	27.4	41.7	16.3	8.6	3.4	0.9
Picea glauca	2.1	27.5	39.5	17.2	10.4	3.0	0.3
Larix sibirica	1.8	26.8	41.4	14.1	6.8	8.7	0.4
Hardwood							
Eucalyptus globulus	1.3	21.9	51.3	1.4	19.9	3.9	0.3
Betula papyrifera	2.6	21.4	39.4	1.4	29.7	3.4	2.1
Betula pendula	3.2	22.0	41.0	2.3	27.5	2.6	1.4
Acer rubrum	3.2	25.4	42.0	3.1	22.1	3.7	0.5
Acacia mollissima	1.8	20.8	42.9	2.6	28.2	2.8	0.9
Fagus sylvatica	1.2	24.8	39.4	1.3	27.8	4.2	1.3

In the above table, the extractives fraction refers to non-polymeric mass found in the xylem tissue that can be separated by a particular solid-liquid extraction (leaching) procedure. Extractives usually contain salts, lipids and phenolic compounds of low molecular masses. The fractions of glucomannan and glucoronoxylan (or simply xylan) form the hemicellulose previously mentioned. Whereas cellulose chemical composition remains the same independent of the species, the composition of lignin and hemicelluloses vary significantly among different species, but following also a distinct pattern between softwood and hardwood. Further, cellulose is a linear, unbranched homopolymer composed of anhydrous glucose unit, while hemicelluloses are branched heteropolymers composed of several different monosaccharides. Table 3.2 lists the most common monosaccharides found in wood polysaccharides.

Table 3.2. Most common monosaccharides in plant cell walls. Adapted from Ek et al. (2009)

Monosaccharide	Letter code	Occurrence
D-Glucose	Glc	Cellulose, glucomannan
D-Mannose	Man	Glucomannan
D-Xylose	Xyl	Xylan
D-Galactose	Gal	Glucomannan, Pectin
L-Arabinose	Ara	Xylan, Pectin
4-O-methyl D-glucuronic acid	4-O-Me-GlcUA	Xylan
D-Galacturonic acid	GalUA	Pectin
L-Rhamnose	Rha	Pectin, traces in xylan
L-Fucose	Fuc	Xylan, traces in pectin

Regarding lignin, three types of monomers, denoted as monolignols, compose most of its mass, though also some unusual monolignols may be present depending on the wood species. Figure 3.3 depicts the structure of monolignols and their common linkages.

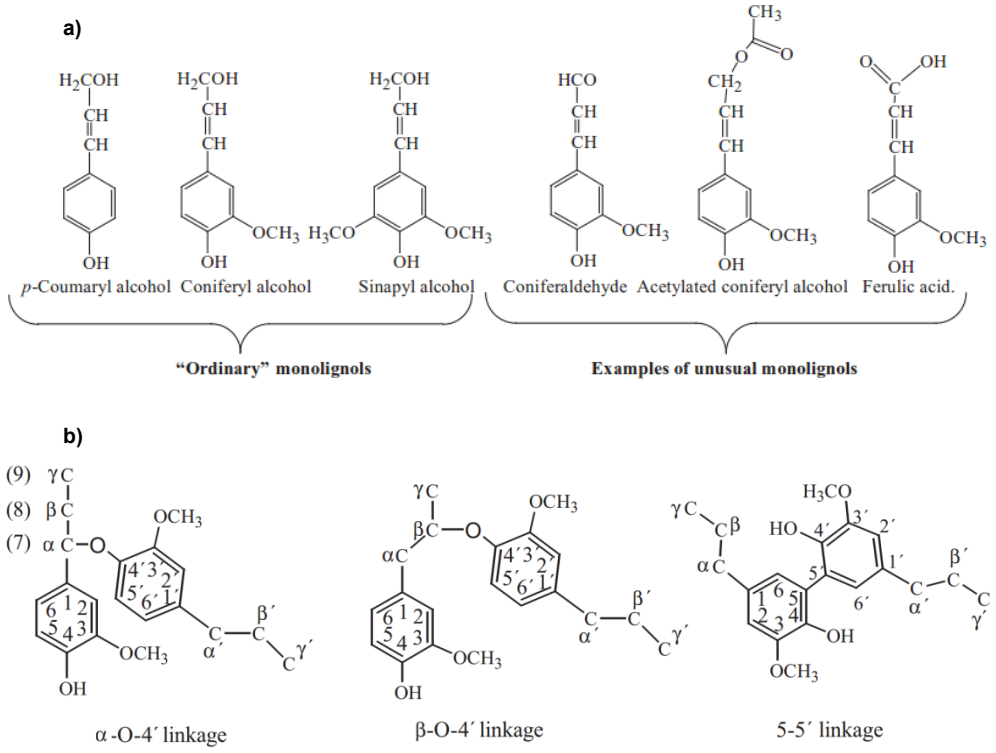

Figure 3.3. Lignin forming structures: a) monomers forming the lignin polymer, b) common linkages between lignin monomers. Adapted from Ek et al. (2009)

The difference between common monolignols lies in the degree of methoxylation of the fundamental phenylpropane structure, which confer them a differential ability to cross-link with other monomers. Hence, the reactivity of lignin is closely connected to its composition in terms of types of monolignols. When incorporated into the lignin, *p*-coumaryl, coniferyl, and sinapyl alcohols are referred as *p*-hydroxyphenyl (H), guaiacyl (G), and syringyl (S) units, respectively. Further, softwood lignin primarily comprises guaiacyl units, whereas hardwood lignin is mostly a mixture of guaiacyl and syringyl units.

3.2 Chemistry of kraft cooking

The aim of kraft pulping is to convert the solid woodchips into a pulp suspension. The first stage of the pulping process is denoted as digesting or cooking, comprehending it as the reaction stage that allow separating single fibers from the wood tissue while trying to the preserve the fiber structure undamaged during the removal of lignin, which acts a “glue” between single fibers. To achieve this, kraft cooking processes exploit alkali- and sulfur-mediated reactions of the wood in an aqueous medium denoted as white liquor. Ideally, this liquor is an aqueous solution containing only sodium hydroxide and sodium sulfide, but at the industrial realm it can contains several other salts accumulated in the kraft process (non-process elements). Table 3.3 shows a typical composition of an industrial white liquor sample.

Table 3.3.Typical composition of the white liquor. Adapted from Sixta (2006)

Compounds	g/l as NaOH	g/l as Na_2O	g/l as compound
NaOH	90.0	70.0	90.0
Na_2S	40.0	31.0	39.0
Na_2CO_3	19.8	15.3	26.2
Na_2SO_4	4.5	3.5	8.0
$Na_2S_2O_3$	2.0	1.6	4.0
Na_2SO_3	0.6	0.4	0.9
Total alkali (TA)	156.9	121.5	170.6
Total sulfur (TS)	47.1	36.5	19.7
Active alkali (AA)	130.0	101.0	
Effective alkali (EA)	110.0	85.0	

At the very high pH of the white liquor, due to the concentration of sodium hydroxide, sodium sulfide is almost completely hydrolyzed according to

$$Na_2S + H_2O \rightarrow NaSH + NaOH \tag{3.1}$$

and the sodium hydroxide thus generated represents other important source of alkali available for cooking reactions. In order to account for this contribution, the white liquor is usually characterized according to its content of active alkali or effective alkali, which describe aggregated fictitious species defined as follows

$$AA = NaOH + Na_2S \tag{3.2}$$

$$EA = NaOH + \tfrac{1}{2}Na_2S \tag{3.3}$$

where the summands in the equation should be expressed like sodium equivalents as mass of NaOH or Na_2O. Actually, the active reagents in cooking reactions are the hydroxide (OH^-) and hydrosulfide (HS^-) ions; thus, based on the above values, two mole ratios are defined for describing the composition of the white liquor that are denoted as its sulphidity and causticity[*].

$$\frac{Sulfidity\ \%}{100} = \frac{Na_2S}{NaOH+Na_2S} = \frac{2[HS^-]}{[OH^-]+[HS^-]} = \frac{2(AA-EA)}{AA} \tag{3.4}$$

$$\frac{Causticity\ \%}{100} = \frac{NaOH}{NaOH+Na_2S} = \frac{[OH^-]-[HS^-]}{[OH^-]+[HS^-]} = \frac{2\cdot EA-AA}{AA} \tag{3.5}$$

In addition to this, several other variables are defined to describe the performance of the white liquor regeneration in the kraft process, such as the total alkali, total sulfur, efficiency of green liquor causticizing, and efficiency of the black liquor sulfate reduction.

$$TA = \sum Na\ compounds \tag{3.6}$$

$$TS = \sum S\ compounds \tag{3.7}$$

$$Causticizing\ effiency\ \% = \frac{NaOH}{NaOH+Na_2CO_3}\cdot 100 \tag{3.8}$$

$$Reduction\ effiency\% = \frac{Na_2S}{Na_2S+Na_2SO_4}\cdot 100 \tag{3.9}$$

[*] This name is also given to the causticizing efficiency in Scandinavian countries

A kraft cook is typically performed at a temperature in the range of 130 – 170 C and an overpressure of 5 to 10 bars to prevent boiling of the white liquor. Lower temperatures are preferable in order to avoid extreme degradation of the polysaccharides. Likewise, it is desirable to have reached a complete penetration of the white liquor into the woodchips before rising temperature, such that the wood substance reacts as homogenous as possible within the chips. This penetration stage is designated as woodchips impregnation, being usually performed at a temperature below 100 C and eventually under pressurized conditions to accelerate the process. After impregnation, the actual cook takes place until it is stopped by a sudden decrease of temperature and displacement of the black liquor generated, i.e., the white liquor containing dissolved wood substance.

During the cook, lignin is cleaved in a series of different reaction paths according to the reactivity of lignin moieties. Phenolic units are more easily cleaved than non-phenolic ones, as they can experience several degradation processes, including nucleophilic addition, elimination, or electron-transfer reactions. Figure 3.4 shows the basic mechanism of hydroxide ion attack to the phenolic lignin and the formation of the quinone intermediate.

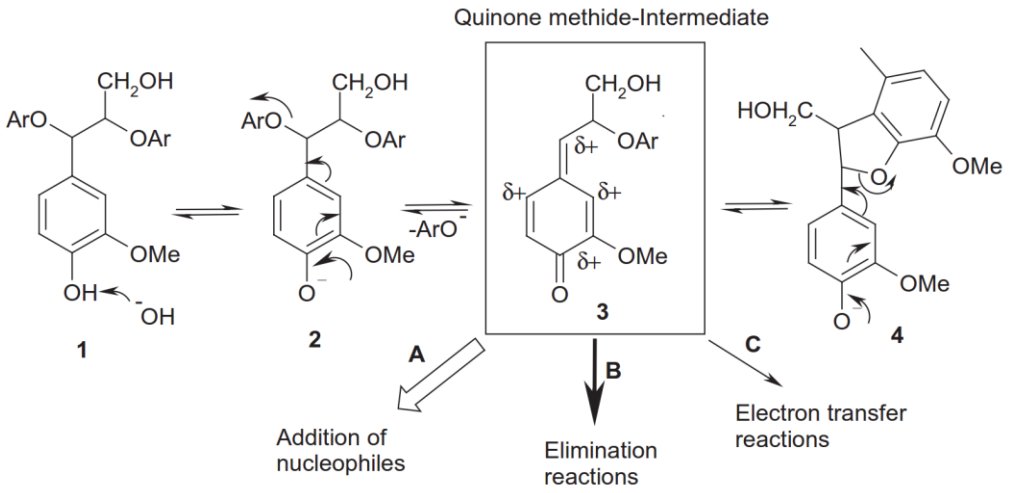

Figure 3.4. Reactions paths for phenolic lignin cleavage. (Sixta, 2006)

Lignin may also experience undesired condensation reactions that create stable carbon-carbon bonds between lignin units hindering its degradation. This can occur especially during the last phase of the cook and is promoted by a low alkali concentration.

In the case of wood carbohydrates, hemicelluloses are very labile to temperature and alkali attack, being easily degraded during the first phase of the cook; cellulose, instead, is a stronger polysaccharide that can resist well the alkaline medium, though it can also degrade especially in its amorphous regions and at the end of the cook. Polysaccharide reactions are conventionally grouped into three degradation mechanisms: peeling and stopping, oxidative peeling, and alkaline hydrolysis. Figure 3.5 shows the positions of attack on the polysaccharide related to different degradation mechanisms. Reducing end units may undergo peeling or stopping reactions, thus the extent of depolymerization is controlled by the relative reaction rate between both mechanisms, as long as oxidative peeling or alkaline hydrolysis are not occurring at significant reaction rates. Stopping reactions turn the original form of the reducing end group of the polysaccharide into a more stable form that resists peeling reactions.

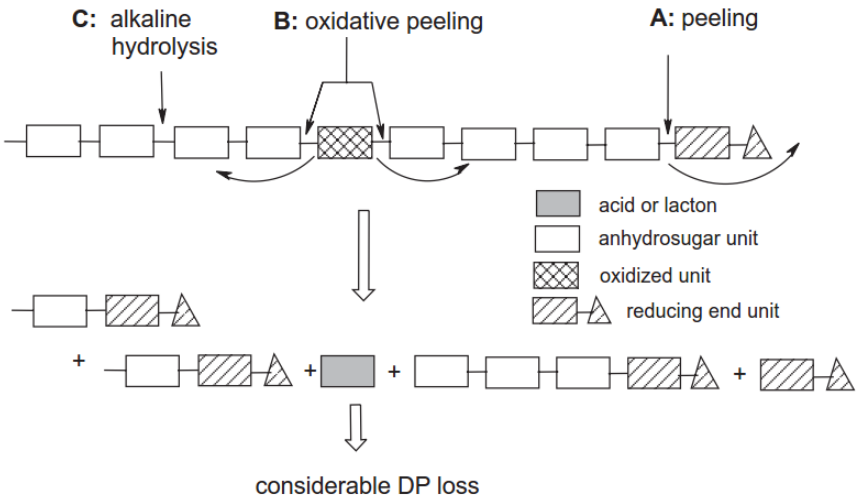

Figure 3.5. Schematic model of polysaccharides degradation under alkaline conditions. (Sixta, 2006)

Besides the above mechanisms, several other reactions, specifically affecting some types of polysaccharides, are of great importance in the cooking stage. For example, the formation of hexenuric acids in hardwood xylan, due to its side chains containing 4-O-methylglucuronic acids, has attracted special interest during last years as it seems to be involved in the deterioration of pulp bleachability. Likewise, deacetylation of hemicelluloses is a relevant phenomenon that affects the initial phase of the cook in terms of neutralizing the available alkali; and chromophores formation from low-molecular mass carbohydrates, resulting at the residual phase of the cook, represents a critical

process that should be avoided in order to facilitate the bleaching of the cooked pulp. Figure 3.6 summarizes the main reactions of wood components during the distinct phases of the kraft cook.

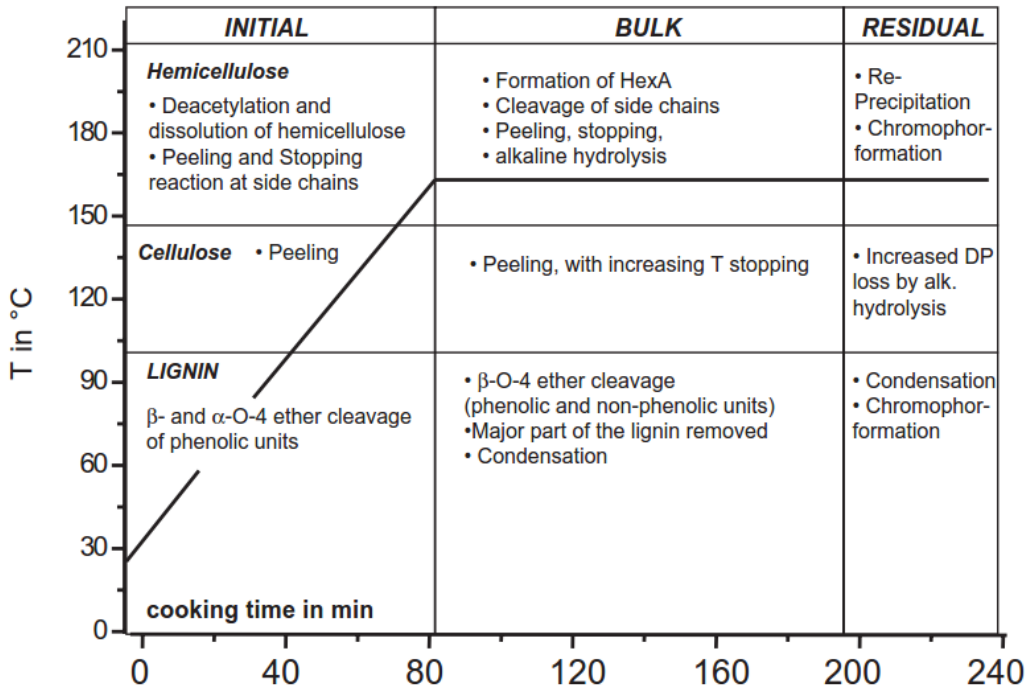

Figure 3.6. Phases of the cook and respective reactions in wood polymers. (Sixta, 2006)

Although the distinction of three phases in kraft cooking is only a conceptual scheme, experimental observations support this idea regarding how carbohydrates and lignin percentages in the wood substance change their decreasing trends over time and temperature of the cook. Figure 3.7 illustrates the experimental behavior of cooking phases in softwood kraft digesting.

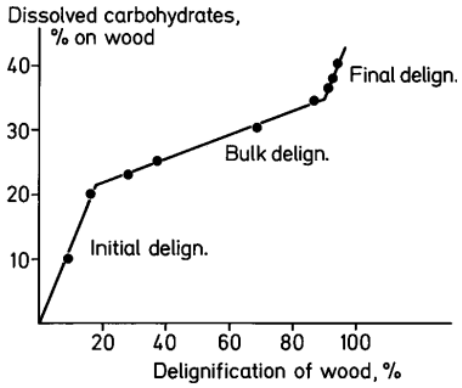

Figure 3.7. Selectivity changes in kraft cooking of softwood. (Ek et al., 2009)

3.3 Equipment and instrumentation

Kraft cooking technology has tremendously evolved from its initial implementation in conventional batch cooking reactors to modern continuous pulp digesters. The first, industrial-scale, continuous cooking reactor was invented by Johan Richter, a Norwegian mechanical engineer, who can be considered as the father of continuous pulping as he conceived the pioneering design of the Kamyr digester (see Figure 3.8). Although the latter apparatus was early patented in the 1940s, it took several years of continuous improvements to scale up the technology for its successful application in the pulp and paper industry. While the first Kamyr reactor was design to produce about 30 ADt/d, modern digesters are meant for a production rate of up to 4500 ADt/d.

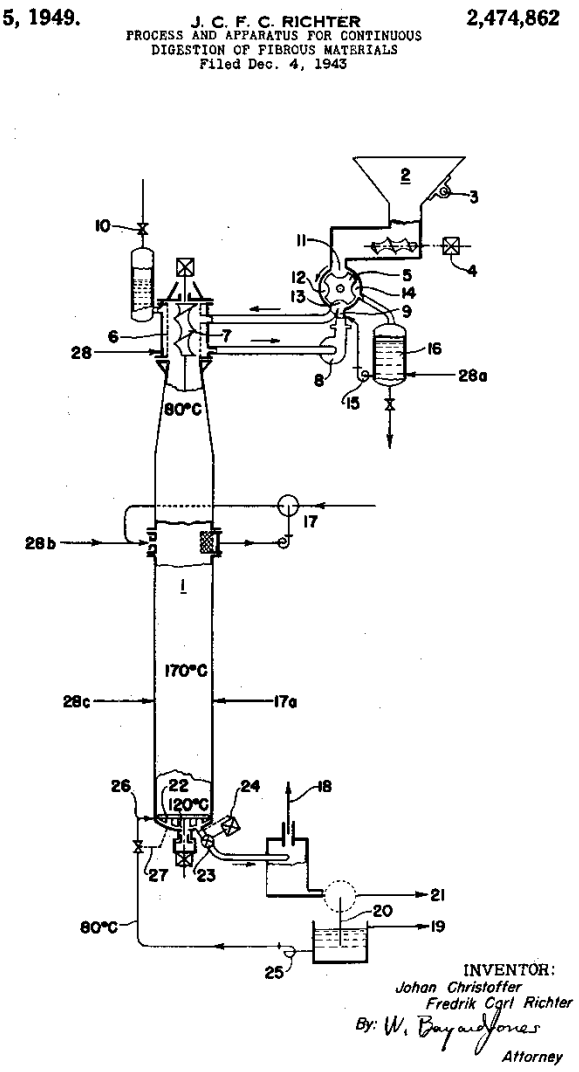

Figure 3.8. Design of the first Kamyr digester. (Richter, 1949)

From the single-vessel, continuous cooking process conceived in the application of first Kamyr digesters, several two-vessel, modified cooking processes have been developed in recent decades. In the latter processes, the first vessel is usually referred as the impregnator and the second one as the digester. Currently, CompactCooking™ G2 (Valmet) and LoSolids™ (Andritz) technologies represent the latest advances in continuous digesting, both leveraging the integration of heat recovery and liquor recycling systems within the basis of a two-vessel process configuration. The main difference between these competing technologies used to be the heating method of the digester. The former technology mainly leverages the direct contact of the steam with the cooking liquor; whereas the latter utilizes indirect heating by means of steam heat-exchangers. Based on this, CompactCooking™ reactors used to be referred as steam/liquor-phase vessels, while LoSolids™ reactors as hydraulic vessels. Figure 3.9 shows the evolution of continuous cooking processes stemming from the pioneering Kamyr invention.

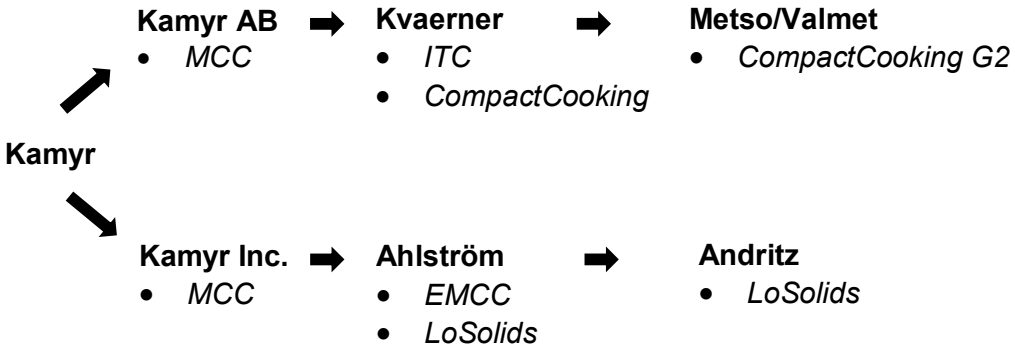

Figure 3.9. Evolution of continuous cooking technologies. Adapted from Laakso (2008)

Along with the invention of the Kamyr digester, several other process apparatuses had to be designed in order to allow a controlled, continuous functioning of the cooking reactor. In this sense, the chip feeding and the in-digester washing systems have represented major challenges for the companies involved in the technological evolution of the Kamyr design. The chip feeding system used to comprise: a chip silo, a chip meter, a low-pressure feeder, a steaming vessel, a chip chute and/or a high-pressure feeder. However, through an effort of process intensification, companies have been able to consolidate the functions of these apparatuses into a few ones, thus reducing the capital and operating costs of the continuous cooking technology.

Naturally, the design of the process equipment has also been influenced by the progress in process chemistry knowledge. Thus, each iteration of the technology aims to modify in certain way the profiles of process variables established along the vessels, including temperature, bed compaction, concentration of hydroxide ion (OH^-), hydrosulfide ion (HS^-) and dissolved matter, such that the quality of the cooked pulp is improved. In this sense, the use of extraction screens along the vessels has been a crucial element letting to test different cooking strategies. An extraction screen can be basically understood as a means of separating the cooking liquor from the chips slurry that pass through a certain height of a vessel. This separation has several effects in the profiles and therefore extracted flow rates must be carefully controlled.

Besides the use of common instruments, such as flow meters, pressure and temperature sensors, special instrumentation has been designed for cooking processes in order to sense the concentration of reagents in cooking liquors and the fraction of lignin remaining in the cooked pulp. Thus, alkali meters are currently essential instruments for controlling of alkali charges distributed to the vessels, same as kappa analyzers are for controlling the primary set-point of the digesting process: the cooking kappa.

3.4 Control and optimization

As mentioned already, the cooking stage is designed to transform woodchips into pulp. However, pulp as a suspension is not properly obtained until “blowing” the cooked woodchips, i.e., provoking a sudden change in the pressure difference between the internal liquor within the cooked chip (entrapped liquor) and the outer liquor medium (free liquor) such that single fibers can be dispersed from the wood tissue. This fiberization phenomenon is possible due to partial removal of lignin, allowing the dismantling of the tissue structure into single fibers. Hence, the extent of lignin removal is a primary, controlled variable of the digesting process.

There are several analytical methods to measure the lignin mass fraction of a pulp sample; however, few of them are suitable for control purposes. Industrially, the usual method corresponds to the determination of the kappa number, which represents a number obtained by a titration method that correlates fairly well to the lignin fraction in the pulp sample. Kappa analyzers have automated the

procedure and are able to measure the kappa number every few minutes, thus permitting the automatic control of the extent of lignin removal.

The set-point kappa number of the cooked pulp is referred as the target cooking kappa, and its value is set according to the design of the whole fiber line. Controlling the cooking kappa is the most challenging aspect of the digesting stage, as it depends on the whole reaction history of a chips parcel passing through the digesting vessels. Although several control strategies have been developed over the years, the H-factor control remains the usual philosophy taken from the control of batch digesters. This strategy relies on the calculation of a severity parameter, originally defined by Vroom (1957), that estimates the extent of delignification based on a simple kinetic model, which considers residence time and temperature that a chips parcel experienced during its pass through the vessels. In order to set the target H-factor of the stage, this strategy requires an experimental correlation between the calculated severity parameter and the cooking kappa. Figure 3.10 depicts the basic structure of the kappa control based on the H-factor concept.

As the H-factor neglects the effects of reagent concentration in the extent of delignification, additional controlled variables are defined to maintained these variables under control; hence, the ratios of liquor-to-wood (L/W) and alkali-to-wood (A/W) are defined as the amount of liquor volume (m^3/BDt) and sodium hydroxide mass per unit bone dry wood mass (w/w%) respectively. As previously defined, these ratios are actually meaningful for batch digesters; however, they can be easily generalized to continuous cooking by considering the flow rate of each entity instead of the unknown filled volume in the continuous vessel. Due to the fact that digesting vessels may have several extraction screens to separate the liquor passing through them, more than one L/W ratio could be necessary to describe flow conditions along the length of the vessels. Likewise, the total alkali charge (A/W) must be split in a two-vessel system, thus leading to the definition of fresh alkali charges of each vessel. The set of H-factor, L/W and A/W targets is usually referred as the “cooking recipe” of the process, and these values can be adjusted in wide intervals while still complying with a set-point cooking kappa, thus founding the feasibility of process optimization. In any case, the optimization of the cooking recipe can be a very difficult task due to the intrinsic complexity of the process.

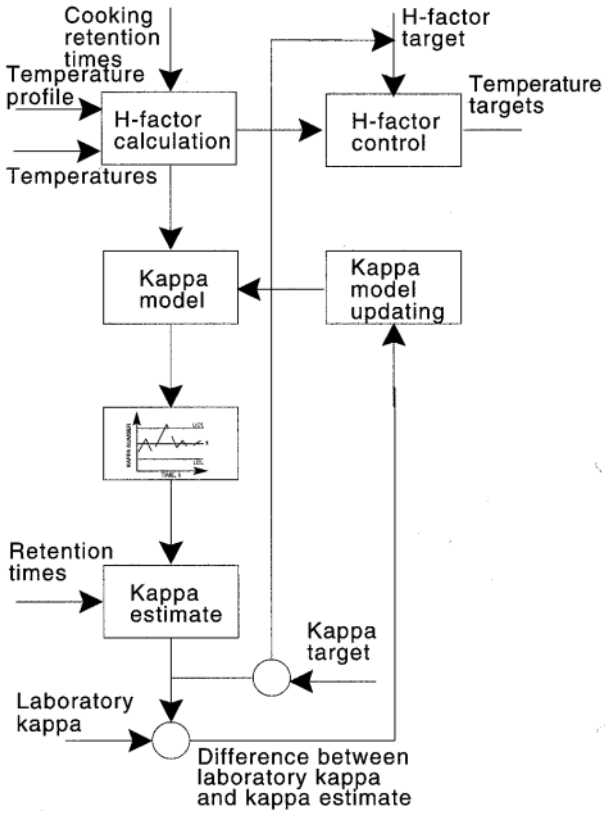

Figure 3.10. Control strategy for cooking kappa based on the H-factor concept. (Leiviskä, 2000)

Although the control of the digesting stage is fundamentally design around the stabilization of the cooking kappa, the ultimate variables of interest are the physico-mechanical properties of the pulp sheet, such as tensile, tear or burst indices, formed either with brownstock or bleached pulp depending on the final product of the mill. These properties cannot be measured with the sufficient sampling time such that the information can be used in automatic control loops; therefore, they represent monitored outputs rather than controlled variables, which should, however, warn mill personnel about the need of changes in the cooking recipe over long periods of time. In a way to compensate long delays in the measurement of these properties, the intrinsic viscosity of a pulp sample, usually dissolved in a Cuen* solution, is measured with higher frequency to obtain predictive information about the development of the pulp sheet properties. In general, the higher the viscosity, the greater the tensile index, while the lower the tear index (antagonistic properties). In any case, the relation between pulp

* cupriethylenediamine hydroxide

intrinsic viscosity and pulp sheet indices is far from linear; indeed, under a critical value of viscosity, pulp sheet indices and intrinsic viscosity show an exponential relation, a behavior that is often detrimental for the quality of the pulp.

Regarding the control of the production rate, it must be noted that the cooking kappa tightly correlates to the yield of the cook; therefore, given a set-point cooking kappa, a target production rate can be achieved based on an empirical model between the yield and kappa of the cooked pulp, which allows calculating a set-point woodchips feed rate. In this sense, the actual cooking yield is not a controlled variable of the stage but rather a monitored variable over a long period of time.

4 Mathematical Models on Pulp Digesters

This Chapter is based on a review of the main contributions in the field of mathematical modelling of continuous pulp digesters. The aim here is to show the reader the evolution of first-principles models with application to kraft cooking, and to describe with deeper details the models that will be used as foundation for the simulation task of this thesis: Purdue kinetic and Härkönen bed compaction models. After presenting a list of highlighted contributions, four sections expand on modelling of reaction kinetics, bed compaction, mass transfer, and quality variables. Finally, the application of pulp digester models to the domains of process simulation, control, and optimization is review at the end of the Chapter.

The main driving forces in the field of mathematical modelling of continuous digesters are probably the academic research effort in cooking reaction kinetics, the advances in computational power, the emergence of new modelling and simulation software platforms, and the interest and funding from the industry for the development of process simulators. In this way, the early steady-state simulation models of a single-vessel stage have evolved into dynamic process simulators that include complex flowsheet configuration, or into very detailed simulators of a digester describing its three-dimensional fluid dynamics.

From the pioneering efforts in Purdue University and University of Washington, two families of kinetic models have arisen which are known as the Purdue and Gustafson models respectively. They have been the base for developing digester models with an increasing degree of sophistication, and while the former was

naturally designed to deal with the complex chemical composition of the wood substance, the latter emphasized a more detail description of delignification coupled to diffusion phenomena. Likewise, from the former Helsinki University of Technology (today part of Aalto University) a key contribution in modelling of bed compaction was conceived that has been the foundation for modelling the complex momentum transfer between chips and liquor phases within digesting vessels. More recently, Aalto University is also contributing a novel kinetic model with an unparalleled degree of sophistication, which will be probably the base for further advancing pulp digester models. Table 4.1 lists below a selection of fundamental contributions on modelling of pulp digesters briefly describing the essential features of each work, the explanation of some concepts is left for the remainder sections of this Chapter.

Table 4.1. List of main contributions on mathematical models applied to kraft pulp digesting

Vroom (1957), Wilder & Daleski (1965), Aurell & Hartler (1965a, 1965b) Kleinert (1966), Lémon & Teder (1973)	Pioneering works on wood reactions kinetics of kraft cooking. Vroom's original H-Factor concept is published, a severity parameter to describe the extent of delignification depending on the batch cooking time and temperature curve.
Hatton (1973, 1976), Kerr (1970), Kerr & Uprichard (1976), Akhtaruzzaman & Virkola (1979, 1980)	Empirical models relating chip dimensions, cooking yields, kappa number, H-factor and effective alkali consumption for softwood and hardwood kraft cooking. Data from these and the above experiences were later used for benchmarking kinetic models.
McKibbins (1960), Neretnieks (1972)	Pioneering works on alkali mass transfer in woodchips applying diffusion theory.
Johnsson (1970)	First digester model based on the single chip balance approach, simulating the mass transfer of alkali and wood reactions with a simple kinetic law to describe the extent of delignification.
Smith (1974)	First version of the Purdue kinetic model. Wood substance is represented as 5 different components reacting in parallel, kinetic laws are developed to be regressed from experimental data. Reactions dependence on $[OH^-]$ and $[HS^-]$ is considered.

Christensen (1982)	Improved Purdue kinetic model by using a search algorithm to adjust parameters for softwood and hardwood species. Consumption of dissolved reagents is also modelled.
Gustafson et al. (1983)	First version of the Gustafson kinetic model. The kraft cook is modelled as 3 successive phases: initial, bulk and residual. Wood substance is represented as 2 components; kinetic laws are developed to be regressed from experimental data. Reactions dependence on $[OH^-]$ and $[HS^-]$ is considered.
Kubes et al. (1983)	Development of a pulp intrinsic viscosity model and a severity parameter to describe the extent of cellulose depolymerization, the G-factor.
Härkönen (1987)	First 2D steady-state, continuous digester model with emphasis on chips and liquor flow dynamics using a simple kinetic model. This contributed a framework for bed compaction modelling used in all later developments (Härkönen correlations). *(Härkönen, 1984)*
Saltin (1992)	A dynamic, continuous digester model using the Purdue kinetics and a simplified Härkönen bed compaction model. Implemented in GEMS.
Agarwal (1993)	A steady-state, continuous digester model using Gustafson kinetics and implemented by the single chip approach. It also incorporated a viscosity model derived from Kubes et al. work and introduced the modelling of diffusion and chip thickness by a sphere-equivalent chip model. Implemented in GEMS. *(Agarwal & Gustafson, 1997)*
Montané et al. (1994)	First fractal kinetic model of delignification. It contributed a new conceptual approach to describe cooking reactions.
Michelsen (1995)	A dynamic, continuous digester model using a simplified Purdue-like kinetics and a modified Härkönen bed compaction model that involves solving a dynamic momentum balance for the chips phase. First modelling approach of chip level variations. Implemented in MATLAB. *(Michelsen & Foss, 1994, 1996)*

Lindström (1997)	A kinetic model of delignification with a Purdue-like structure that includes the effect of [Na^+] on reaction rates. *(Lindgren & Lindström, 1997)*
Wisnewski (1997)	A dynamic, continuous digester model with improved Purdue kinetics but fixed bed compaction profile. It is also modelled the liquor concentration of dissolved wood substance and the chip internal porosity. Implemented in MATLAB. *(Wisnewski, Doyle, & Kayihan, 1997)*
He et al. (1999)	First 3D model of a continuous digester (CFD) based on Härkönen bed compaction, Michelsen fluid dynamics assumptions, and a simplified kinetic model.
Bhartiya et al. (2001)	Continuation of Wisnewski et al. work incorporating advances made by Michelsen. It also contributed a modelling approach for grade transition. Implemented in MATLAB. *(Bhartiya, Dufour, & Doyle, 2003)*
Malkov (2002)	A model describing the liquor penetration of woodchips, not yet integrated in any digester model.
Andersson (2003)	A kinetic model that combines Purdue and Gustafson approaches. Wood substance is represented by 5x3 components.
Kayihan et al. (2005)	A dynamic, continuous digester model based on Purdue kinetics, modified Härkönen bed compaction, and Agarwal diffusion and chip thickness. It is solved by a novel cinematic approach allowing to model chip level and stochastic changes in chip size distribution. Implemented in MATLAB.
Rantanen (2006)	A dynamic, continuous digester model based on Gustafson kinetics, Saltin simplified bed compaction, and Agarwal diffusion and chip thickness. It is applied to describe a LoSolids™ process (two-vessel stage) with grade transition. Implemented in MATLAB. *(Rantanen, Similä, & Ahvenlampi, 2005)*
Fan (2005), Pougatch et al. (2006)	Continuation of He et al. work improving fluid dynamics modelling and code implementation.

Simão et al. (2005), Danielsson et al. (2006)	Development of kinetic models to describe hexenuronic acids (HexA) formation and degradation.
Nguyen & Dang (2006), Bogren (2008)	Fractal kinetic models fitted to describe delignification of *Eucaplyptus nitens* and *Pinus sylvestris* respectively.
Grénman et al. (2010)	Woodchip anisotropy model describing the 3D chip structure and internal diffusion. Purdue, Gustafson and Andersson kinetic models are coupled and compared regarding delignification in the 3D modelled structure of the chip.
Nieminen et al. (2014a, 2014b)	New kinetic models of lignin and carbohydrates degradation. Delignification can be described with varying degrees of sophistication (including Donnan equilibrium); and carbs degradation is modelled based on the reaction mechanism of peeling, stopping and alkaline hydrolysis. Reactions dependence on $[OH^-]$, $[HS^-]$ and $[Na^+]$ is considered.
Nieminen et al. (2015)	New viscosity model leveraging the information from the mechanistic carbs degradation model previously proposed.

4.1 Wood reaction kinetics

Inside the cooking reactors, the basic density of chips and the concentration of liquor components vary as a result of a series of wood reactions referred as delignification and carbohydrates degradation (or simply cooking reactions). Although it is impossible to model all these reactions due to their heterogeneity and complexity, researchers have modelled instead apparent reaction rates describing the degradation of lumped wood components and associated consumption of cooking reagents. This is the underlying idea of all kinetic models of wood delignification and carbohydrates degradation.

Andersson et al. (2002) and Nieminen & Sixta (2012) have compared the accuracy of several kinetic models as applied to simulate well-controlled laboratory batch cooks. From their results, the Purdue model seems to be the best structure weighing complexity and computation efficiency, as it is able to follow the trajectory of the cook with higher accuracy given a good adjustment of its parameters. In the context of kinetic models often used in continuous digester models, it is presented below only the structures of the Purdue and Gustafson models. A brief comparison of other models can be found on Nieminen (2015).

4.1.1 Purdue model

This model represents wood substance degradation as a process of parallel reactions of each polymer. Lignin receives as special treatment as it divided into two types, fast and slow, intending to capture the reactivity difference between lignin moieties. Reaction rates are expressed as depending on the mass concentration of sodium hydroxide and sodium hydrosulfide. Besides, some portion of each wood polymer may be considered unreactive, thus leading to the possibility to create 2·5 entities. Eqs. 4.1 to 4.6 constitute the mathematical structure of the model as adapted from Wisnewski et al. (1997).

$$\rho_i = \rho_i(t) \;\; i \in \{L_F, L_S, C, GM, X\}$$

$$C_j = C_j(t) \;\; j \in \{NaOH, NaSH, DS\}$$

$$-R_i = e_f\left(k_{ai}{C_{NaOH}}^{1/2} + k_{bi}{C_{NaOH}}^{1/2}{C_{NaSH}}^{1/2}\right)(\rho_i - \rho_i^{\infty}) \qquad 4.1$$

$$k_{\Theta,i} = k_{\Theta 0,i}\exp\left(\frac{-E_{\Theta i}}{R_g T}\right) \;\; \Theta \in \{a, b\} \qquad 4.2$$

$$\varepsilon R_{NaOH} = \beta_{EAL}\left(R_{L_F} + R_{L_S}\right) + \beta_{EAC}(R_C + R_{GM} + R_X) \qquad 4.3$$

$$\varepsilon R_{NaSH} = \beta_{ESL}\left(R_{L_F} + R_{L_S}\right) \qquad 4.4$$

$$\varepsilon R_{DS} = -\sum_i R_i \qquad 4.5$$

$$\rho_i^{\infty} = \alpha_i^{\infty}\rho_{basic} \qquad 4.6$$

Table 4.2. Parameters of the Purdue kinetic model. Adapted from Wisnewski et al. (1997)

Species	Parameter		L_F	L_S	C	GM	X
Softwood	$k_{a,i}$	m^3/kg·min	0.2809	$6.035\cdot10^{10}$	6.4509	1.5607	$1.0197\cdot10^{4}$
	$k_{b,i}$	m^3/kg·min	9.26	0.489	28.09	10.41	$5.7226\cdot10^{16}$
	α_i^{∞}		0.00	0.00	0.71	0.25	0.00
	$\beta_{EAL/C}$		0.166		0.395		
	β_{ESL}		0.039				
Hardwood	$k_{a,i}$	m^3/kg·min	0.3954	$1.457\cdot10^{11}$	28.09	7.075	$5.8267\cdot10^{3}$
	$k_{b,i}$	m^3/kg·min	12.49	1.873	124.9	47.86	$3.225\cdot10^{16}$
	α_i^{∞}		0.00	0.00	0.65	0.25	0.00
	$\beta_{EAL/EAC}$		0.210		0.490		
	β_{ESL}		0.050				
Common	$E_{a,i}$	kJ/mol·K	29.3	115	34.7	25.1	73.3
	$E_{b,i}$	kJ/mol·K	31.4	37.7	41.9	37.7	167

The e_f terms are called effectiveness factors and were meant to be adjusted such that the model matches the behavior of an industrial cooking reactor. In any case, the model can be better adjusted by regressing the whole set of parameters from laboratory batch cooks, but at the obvious higher cost of funding this work.

The basic idea of parallel wood reactions contained in the Purdue model has also been the base for developing specific kraft cooking kinetic models of certain wood species, as in the *Eucalyptus globulus* batch cooking model of Sixta & Rutkowska (2006).

4.1.2 Gustafson model

Contrary to the above, the Gustafson model represents the wood substance as only 2 entities, and the kraft cook is modelled by explicitly following the phenomenological description of 3 consecutive stages: initial, bulk, and residual. Thus, this model changes the reaction rate expressions according to the extent of delignification. Although it is arguable that these phases are truly the product of intrinsic changes in reaction rates, the model gives good results requiring less parameters to be regressed and being more computationally efficient than the above. Eqs. 4.7 to 4.11 constitute the mathematical structure of the Gustafsson kinetic model as adapted from Gustafson et al. (1983) and Agarwal & Gustafson (1997).

$$x_i = x_i(t) \;\; i \in \{L, CH\}$$

$$\hat{C}_j = \hat{C}_j(z,t) \;\; j \in \{OH, SH, DS\}$$

$$stage = \begin{cases} initial & x_L > 22.5\% \\ bulk & 22.5\% > x_L > 2.2\% \\ residual & 2.2\% > x_L \end{cases} \quad \textbf{4.7}$$

$$-R_L = \begin{cases} 36.2T^{0.5} e^{\frac{-4807.69}{T}} x_L & initial \\ \left(e^{35.19 - \frac{17200}{T}} \hat{C}_{OH} + e^{29.33 - \frac{14400}{T}} {\hat{C}_{OH}}^{0.5} {\hat{C}_{SH}}^{0.4} \right) x_L & bulk \\ e^{19.64 - \frac{10804}{T}} {\hat{C}_{OH}}^{0.7} x_L & residual \end{cases} \quad \textbf{4.8}$$

$$R_{CH} = \begin{cases} 2.53 R_L \hat{C}_{OH}^{\,0.11} & initial \\ 0.47 R_L & bulk \\ 2.19 R_L & residual \end{cases} \quad \textbf{4.9}$$

$$\varepsilon R_{OH} = (0.045 R_L + 0.09 R_{CH}) \rho_{basic} \quad \textbf{4.10}$$

$$\varepsilon R_{DS} = -(R_L + R_{CH}) \rho_{basic} \quad \textbf{4.11}$$

The Gustafson model was originally regressed with softwood cooking data, however, it has been later adapted to describe hardwood (*Eucalyptus globulus)* kraft cooking (Santos et al., 1997; Gilarranz et al., 2002). Likewise, it was also extended to model the degradation of carbohydrates distinguishing between cellulose and hemicellulose (Pu et al., 1991).

4.2 Chips bed compaction

Similarly as a liquid column has an associated liquid pressure, we can visualize a solid pressure associated to the chips column formed inside a vessel that arises from the contact between individual chips. According to Härkönen (1984), this solid pressure, termed chips or compacting pressure, would vary due to several forces exerted on the chips, including their weight, their buoyancy, as well as the friction caused by the motion of chips and liquor. Variations of the compacting pressure would be a cause for the rearrangement of individual chips within the bed that forms the chips column; in turn, this would provoke changes of bed porosity and compaction along the vessel.

In fact, bed porosity is what concerns most when modelling compaction, since the void volume of the bed determines the residence times of chips and liquor phases affecting the extent of delignification reactions. In this sense, Härkönen (1987) also noted that the extent of delignification affects the porosity of the chips bed due to the softening of the chips, allowing their rearrangement in a denser and more compacted form. Encouraged on these observations, he pioneered an investigation to determine a mathematical correlation between void volume of the bed, the pulp kappa number, and the external compacting pressure exerted over the chips bed as formed in a lab-scale digester.

4.2.1 Härkönen correlations

Härkönen correlation of the bed void volume, expressed by the Eq. 4.12, has been used in all kinds of first-principles pulp digester models that include a description of the bed compaction phenomenon.

$$\eta = k_0 + \left(\frac{P_c}{10^4}\right)^{k_1} (-k_2 + k_3 \ln(\kappa)) \qquad \textbf{4.12}$$

Furthermore, Härkönen (1987) also proposed using a modified form of the Ergun equation (Ergun, 1952) to describe the pressure drop of the liquid flowing through the chips bed, given by Eq. (4.13). In his modified version, some terms are simply grouped into two empirical coefficients, $\hat{R}_1$ and $\hat{R}_2$, that must be determined from laboratory experiments.

$$\frac{\Delta P_l}{\Delta z} = \hat{R}_1 \frac{(1-\eta)^2}{\eta^3} u_l + \hat{R}_2 \frac{(1-\eta)}{\eta^3} {u_l}^2 \qquad \textbf{4.13}$$

The above correlation was used by Härkönen to construct a model of the compacting pressure P_c inside a vessel, which used together with the void volume correlation allows to simulate compaction phenomena of the reactor. Although he characterized the parameters of his correlations solely for a specific woodchips furnish, i.e., a chips sample of a particular wood species and size distribution, other researchers has continued its work obtaining values at different conditions and also investigating the dependence of the parameters to other variables of the cook (Lee & Bennington, 2005; Alaqqad et al., 2012).

Table 4.3. Parameters of Härkönen correlations for different wood furnishes. Adapted from Lee (2002)
These values should be considered only as examples of a particular chip size distribution (described in the source) for each wood species. R_1 and R_2 are given in units of 10^5·Pa·s/m^2 and 10^6·Pa·s^2/m^3 respectively

Wood furnish	k_0	k_1	k_2	k_3	R_1	R_2
Härkönen's values	0.644	0.59	0.831	0.139	0.046	3.9
Scandinavian pine	0.663	0.56	0.788	0.133	0.52	1.5
Scandinavian birch	0.630	0.64	0.697	0.151	2.8	-1.2
River red gum	0.591	0.56	0.645	0.148	5.5	0.75

4.2.2 Compacting pressure models

Härkönen (1987) formulated his model of the compacting pressure in a complex manner whose numerical solution represented a difficult task. For this reason, Saltin (1992) suggested the use of a simplified model, which approaches Härkönen results being computationally more efficient. Saltin model can be derived from a static force balance in an infinitesimal section of the vessel and its mathematical expression is the following

$$\frac{dP_c}{dz} = \big((1-\eta)\rho_c - \eta\rho_l\big)g - \mu\frac{P_c}{D} \pm \frac{dP_l}{dz} \qquad \textbf{4.14}$$

where the sign of third term in the right-hand side of the equation should be changed according to co-current or counter-current liquor flow regimen. Eq. 4.14 has been used later by other researchers (Poulakka & Kortela, 2005; Rantanen, 2006; Laakso, 2008) but with a subtle modification, thus becoming transformed into

$$\frac{dP_c}{dz} = (\rho_c - \rho_l)(1-\eta)g - \mu\frac{P_c}{D} \pm \frac{dP_l}{dz} \qquad \textbf{4.15}$$

4.3 Chip size phenomena (mass transfer)

Mass transfer phenomena inside a vessel are intrinsically connected to the chip size distribution and the internal chip structures. Liquor penetration and reagents diffusion are the main mass transfer processes affecting the digesting performance; therefore, models of these phenomena are especially relevant for building digester models. While the first attempts to model the liquor penetration and the effects of chip internal structures have been relatively recent (Sergey Malkov, 2002; Grénman et al., 2010), efforts to include diffusion effects on digester models can be traced back to the original implementations of the Gustafson and Purdue kinetic models.

4.3.1 Diffusion and chip size

Based on the work of McKibbins (1960), distinct diffusivity coefficients were defined by the developers of the Purdue and Gustafson models, representing fundamental differences in the way that mass balances were established when implementing their respective kinetic models.

Early Purdue model developers (Smith, 1974; Christensen, 1982) regarded diffusion as a transport process that can be averaged by omitting the spatial

dimension from the Fick's law. In this sense, they developed mass balances for lumped volumes of chips and liquor phases defining a diffusion term that depends on the average concentration difference of species in each phase. That is, the chip size is not explicitly modelled but rather related to the parameters of a lumped diffusivity coefficient defined as

$$D = 6.1321\sqrt{T}e^{(-4870/R_gT)}\ \frac{1}{\text{min}} \tag{4.16}$$

On the other hand, Gustafson model developers (Gustafson et al., 1983; Agarwal, 1993; Agarwal & Gustafson, 1997) implemented their kinetic model by the single chip approach representing the physical form of the chip with different ideal geometries, such as an infinite slab, an infinite cylinder, and a perfect sphere, as suggested by Neretnieks (1972). In this way, they were able to explicitly include the chip size in the calculation of the diffusive transport. Actually, these ideal forms allow reducing the dimensionality of the 3D diffusive transport into one abstract dimension, which would represent the controlling dimension, either thickness, length, width or a transformed dimension that depends on all of them. Accordingly, Gustafson et al. (1983) defined a true diffusivity coefficient,

$$D = 5.7 \cdot 10^{-2}\sqrt{T}e^{(-4870/R_gT)}\left(0.02x_L + 0.13\hat{C}_{OH}{}^{0.55} + 0.58\right)\ \frac{\text{cm}^2}{\text{min}} \tag{4.17}$$

which is used when establishing mass balances for a single, generic chip under the infinite slab, infinite cylinder, or perfect sphere representation.

In a general perspective, Purdue developers have often established mass balances that highlight mass transfer by advection, assuming plug flow motion of chips and liquor; Gustafson developers, instead, have tended to focus on the diffusive transfer of cooking reagents from the surrounding liquor to the chip center. Although diffusivity coefficients may vary depending on the chemical species, both lines of development usually consider only one, common coefficient for modelling diffusion of all liquor components.

4.3.2 Liquor penetration

The penetration of cooking liquors into woodchips should have a special relevance when modeling the impregnator or the impregnation zone of a single-vessel system, where it is presumed to occur; however, few authors (Malkov, 2002; Malkov et al., 2003) appear to have researched this phenomenon aiming to

develop a first-principles model useful for building digester models. Moreover, liquor penetration is usually an omitted phenomenon in digester models under the assumption that chips are instantaneously and completely penetrated once entering the digesting stage.

Malkov et al. (2003) presented a relatively simple equation for describing penetration dynamics into a single chip,

$$\Delta P = \frac{\mu}{K_\varepsilon}\left(\frac{L_l}{2}\right)^2 P_\varepsilon \frac{dP_\varepsilon}{dt} \quad \textbf{4.18}$$

This approach only requires the experimental determination of one parameter: the permeability coefficient K_ε. However, the model relies on the simulation of the pressure difference ΔP between inside the chip and surroundings, which is actually the difficult part to be coded for integrating this equation into a digester model. Thus, when weighing the pros and cons of this integration, model developers seem inclined to neglect this feature in favor of improving models of more general phenomena.

4.4 Pulp quality variables

A digester model can be understood as a set of differential and algebraic equations derived from conservation principles of mass, energy and momentum. Based on this, the model allows simulating streams of mass and energy that are described in terms of species concentrations, temperatures, and flow rates. However, digester models become of greater relevance for industry when they can also simulate particular quality variables that are functions of the above entities through rather complex ways of dependence. In this sense, three categories of variables can be distinguished among quality variables associated to the digesting stage: (i) variables depending on basic concentrations (wood polymers “densities”), (ii) variables depending on molecular characteristics of the wood polymers, (iii) and variables predicting properties of the pulp sheet (product).

4.4.1 Yield, kappa and screen reject

In the first category, we can consider definitions of the cooking yield, cooking kappa, and screening reject (equivalent to screened yield). Cooking yield can be easily computed as the ratio of the remaining wood substance mass to the

original bone dry mass of the fed chips; by the contrary, cooking kappa and screening reject may require further analysis. In the case of the former, the kappa number is presumed proportional to the lignin content, although other wood components are known to interfere in the standard kappa method, and therefore a general correlation widely applied for relating both variables is

$$x_L = \theta_{\kappa L}\kappa \tag{4.19}$$

where $\theta_{\kappa L}$ may vary in the range of 0.13 – 0.20 depending on the wood species and cooking conditions (Dence, 1992; Jääskeläinen et al., 2005). Regarding screening reject, Gustafson et al. (1983) found that the simulated variance (normalized second moment) of the lignin profile along the chip thickness correlates fairly well to the screening reject percentage. In fact, these variables show a negative correlation in such a way that the steeper the lignin profile, the higher the reject percentage; mathematically, this relation can be expressed as

$$\frac{1}{reject} \propto \frac{\int_{-\frac{L_C}{2}}^{\frac{L_C}{2}} x_L \chi^2 d\chi}{\int_{-\frac{L_C}{2}}^{\frac{L_C}{2}} x_L d\chi} \tag{4.20}$$

where χ is an auxiliary variable moving along the chip thickness dimension.

4.4.2 DP and intrinsic viscosity

In the second category, we may consider modeling efforts to explain the decrease of pulp intrinsic viscosity and cellulose degree of polymerization (DP) along the cook. Kubes et al. (1983) made the first attempts to model those phenomena, contributing the experimental determination of a depolymerization kinetic rate law of the pulp cellulose. Based on this, Agarwal & Gustafson (1993, 1997) and Miyanishi & Shimada (2001) implemented depolymerization models of the pulp cellulose in continuous digester models by coupling them with Gustafson and Purdue kinetic models respectively.

Originally, none of the foregoing authors explicitly stated and/or disclosed the values of the kinetic rate law. However, by reexamining the work of Kubes et al., Sixta (2006) arrived to the following expression

$$\frac{1}{DP_{v,t}} - \frac{1}{DP_{v,t_0}} = 4.35 \cdot 10^{15} \exp\left(-\frac{179 \pm 4 \frac{\text{kJ}}{\text{mol}}}{R_g T}\right) \hat{C}_{OH}{}^{1.77} t \tag{4.21}$$

which is valid to describe the decrease of cellulose DP during a batch kraft cook, either of softwood or hardwood chips. This expression has the form of the Ekenstam equation (af Ekenstam, 1936), where the depolymerization rate constant of the Ekenstam form corresponds to

$$k = 4.35 \cdot 10^{15} \exp\left(-\frac{179 \pm 4 \frac{\text{kJ}}{\text{mol}}}{R_g T}\right) \hat{C}_{OH}{}^{1.77} \quad \textbf{4.22}$$

Based on the above, this thesis will show the derivation of a novel depolymerization model that allows describing the change of cellulose DP in continuous digesters. The latter variable is phenomelogically related to the pulp intrinsic viscosity, and indeed it is the variable that actually grounds the predictive power of the intrinsic viscosity about pulp sheet properties. The relation between the pulp intrinsic viscosity and the cellulose DP has not been completely clarified, but it is often assumed as a weighted-sum over intrinsic viscosities of every pulp polysaccharide fraction (Agarwal & Gustafson, 1997; da Silva Perez & van Heiningen, 2002, 2015), i.e.,

$$[\eta] = \sum_i [\eta]_i x_i \quad \textbf{4.23}$$

where the intrinsic viscosity of a single polysaccharide fraction can be explained by its viscosity-average degree of polymerization (DP_v) according to the Mark-Houwink equation as follows,

$$[\eta]_i = K_i DP_{v,i}{}^{\alpha_i} \quad \textbf{4.24}$$

Should be mentioned that it exist several definitions of the DP, including number-average DP, weight-average DP, and viscosity-average DP. The latter is of especial relevance in this context due to its relation to the intrinsic viscosity of polymer solutions, expressed by the Mark-Houwink equation. However, the parameters of the Mark-Houwink expression have not been determined for every wood polysaccharide except cellulose; even more, the parameters found in the literature for cellulose dissolved in Cuen, the usual solvent in industrial practice, show high uncertainty with K values ranging from 0.42 to 2.45 and α values ranging from 0.771 to 0.905 (Oberlerchner et al., 2015). The lack of information and the discrepancies in these parameters suggest that further experimental research is needed in this subject in order to support the development of reliable

models. Table 4.4 summarizes some values for the Mark-Houwink parameters of cellulose dissolved in Cuen.

Table 4.4. Mark-Houwink parameters of cellulose dissolved in 5% Cuen at 25 ºC. *K is given in units of ml/g*

K	α	Source
2.45	0.70	Kes & Christensen (2013)
1.87	0.771	Łojewski et al. (2010)
1.65	0.90	Evans & Wallis (1989)
0.42	1	Marx-Figini (1978), DP < 950
2.28	0.76	Marx-Figini (1978), DP > 950
1.37	0.905	Immergut & Eirich (1953)

4.4.3 Z-span, tensile and tear indices

The third category of quality variables strictly represent variables associated to the product rather than the process performance. Despite the obvious importance of models on this subject, very little information has been found in the literature. In fact, only two articles have been discovered that can be applied in the building of digester models.

In the first article, Emsley et al. (1997) developed a pseudo first-principles, dynamic model of the zero-span index variation of the kraft insulation paper during its normal lifetime. In principle, this model could be adapted to describe a predictive z-span index associated to the pulp along the kraft cook, in the same way that the Ekenstam equation was adapted from a context of acid dissolution of pure cellulose to the kraft cooking of woodpulp. The z-span model of Emsley et al. can be expressed as

$$\frac{dI_{zspan}}{dt} = \theta_1 \frac{1}{DP^2} \frac{dDP}{dt} + \theta_2 DP \qquad 4.25$$

where the empirical constant θ_1 and θ_2 should be positive defined.

In the second article, Molin & Teder (2002) found linear correlations between tensile and tear indices and the ratio of cellulose to hemicellulose mass fractions in the pulp. These correlations could be used as the base for developing more advanced empirical models with predictive power on said indices. The correlations of Molin and Teder can be expressed as follows

$$\frac{1}{I_{tensile}} \propto \frac{x_C}{x_H} \quad \textbf{4.26}$$

$$I_{tear} \propto \frac{x_C}{x_H} \quad \textbf{4.27}$$

4.5 Applications on control and optimization

Digester models have been widely applied to investigate the performance of digesting stages against changes in operational parameters. The basic research approach starts with the simulation of steady-state profiles established along the vessels. Later, it can advance to the study of process dynamics, and the design of novel control structures, process optimization methods, or fault detection and monitoring algorithms. Except for the works on process optimization, reviewing all this literature is clearly outside the scope of the thesis; therefore, only some particularly relevant works are now mentioned as examples.

Kayihan et al. (1996) presented a model of a two-vessel system, based on Purdue kinetics, as a digester benchmark model for system identification and controller design. This model was further utilized by Doyle & Kayihan (1999) to investigate the feasibility of kappa profile control by a model predictive controller. Later, Castro & Doyle (2002, 2004a) even developed a whole pulp mill benchmark model using the previous digester model. The latter model has been an especially fruitful work in the field of modeling and simulation for the pulp and paper industry. Likewise, other research groups have use digester models to simulate particular process technologies such as EMCC and LoSolids™ processes (Miyanishi & Shimada, 2001; Walkush & Gustafson, 2002; Rolandi & Romagnoli, 2003); to study specific problems on chips bed compaction (Poulakka & Kortela, 2005; Laakso, 2008); or to design advanced control strategies for kappa stabilization (Ahvenlampi, Rantanen, & Tervaskanto, 2006).

Regarding process optimization of pulp digesters, fewer works have been published in comparison to the vast amount of articles on control of digesters. Sidrak (1991), likely the first published contribution, applied a dynamic optimization algorithm to compute optimal set-points of a Kamyr digester; Silva & Biscaia Jr. (2003) used genetic algorithms to search for Pareto optimal sets of operational conditions also in a single-vessel Kamyr digester; Rolandi & Romagnoli (2004) developed optimization routines with application to a whole LoSolids™ digesting stage as a part of an integrated decision support system,

leveraging for this purpose the optimization capabilities of the modelling platform (gPROMS). Mercangöz & Doyle (2008) applied a linear optimization approach, which leads to the approach elaborated in this thesis, to search for optimal set-points in the Pulp Mill Benchmark Model. Zakharov & Jämsä-Jounela (2011) improved the optimization method of the previous authors in the application to the same problem. Finally, Bhat, Srinivasa, & Pathath (2012) have secured a patent concerning the steady-state optimization of digesting stages by means of customizing digester models and calibrating them with plant data.

EXPERIMENTAL PART

5 Methods

The optimization goal of the thesis logically requires a simulation model of the CompactCooking™ G2 digesting process stage. Since none was available when starting the thesis, this work comprises both tasks of process simulation and optimization. Figure 5.1 shows a summarized workflow diagram of thesis.

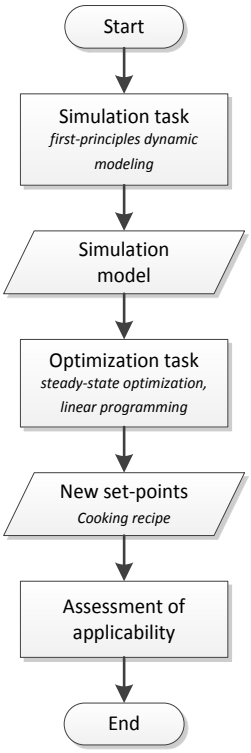

Figure 5.1. Workflow diagram of the thesis

Several mathematical modelling techniques may allow the completion of the process simulation task. Among these techniques, first-principle modelling has been chosen for two main reasons: (i) since published models on the field of kraft pulp digesting permit leveraging decades of accumulated knowledge, and (ii) because the resulting model provides a general architecture applicable to a wide variety of wood species and vessels dimensions, feature that would not be attainable by other modelling techniques (e.g., system identification). For the optimization goal, a single-objective linear programming approach is proposed in order to obtain a heuristically optimized new cooking recipe, i.e., set-points for the digesting stage. In this sense, the last part aims solely to evaluate the applicability of model-based optimization, which is done by estimating potential

benefits on the process economics under different objective functions and constraints sets.

Although steady-state optimization is performed, the simulator is designed to be dynamic. A steady-state (static) simulator should be computationally less intensive to perform this type of optimization; however, static simulators cannot be truly validated on the basis of mill data since the mill is always showing a dynamic behavior. One could argue that from plant data a steady-state condition can be determined and then compared against simulated one, but this would require identifying at least more than one steady-state to properly talk about validating a steady-state simulator. On the contrary, a dynamic simulator can be straightforward validated by comparison of measured and simulated dynamic signals. What is to be compared remains a critical factor that must be addressed during the mathematical modelling. In a simple phenomenon, e.g. water tank level fluctuation, it may be evident the comparability relation between measured and simulated signals; however, complex phenomena, including those of continuous digesters, require a careful judgment based on chemical engineering knowledge in order to identify comparable variables between real and simulated processes.

Technically speaking, the simulation task involves mathematical modelling with distributed parameter systems, implementation of model equations on a Matlab/Simulink environment, and numerical solving by means of Simulink integration capabilities. The process flow configuration is represented by a Simulink file, and unit operations are modelled making use of C MEX S-functions. The latter take parts of code from the pulp mill benchmark model of Castro & Doyle (2004), a simulation model of a generic kraft pulp mill open-sourced for the academic community. The source code[*] of the S-functions is compiled using GNU GCC 4.8.4 running on a Linux-based 64-bit operating system. A special S-function requires to be linked to libfreesteam[†] (freesteam 2.1) to correctly model heat transfer from the steam. The optimization task comprises identifying a plant steady-state, linearizing the process model around it, and statically optimizing the

[*] This code and related files are released under the GNU GPL following the spirit of open innovation of Castro and Doyle's work
https://github.com/utopicaCL/optidige

[†] Open source implementation of the international-standard IAPWS-IF97 of steam tables
http://freesteam.sourceforge.net/

process by calling Matlab `linprog()` function. The whole optimization routine is implemented as a Matlab script. All computations are performed running MATLAB R2014a on an Intel Core i7-4800MQ 2.7 GHz CPU. Computation times greatly depend upon model architecture in relation mainly to: (i) the number of algebraic loops introduce by representing liquor recycles, and (ii) the resolution of the discretization mesh in the distributed parameter models.

More details about the methods of each task are found on Chapter 7 and 9 respectively. The assessment of applicability of the model-based optimization approach is elaborated along Chapters 8 and 10, which present the results of the simulation and optimization tasks correspondingly.

6 Process Description

The digesting process studied corresponds to a CompactCooking™ G2 system (Valmet), a two-vessel, continuous, steam/liquor-phase, industrial kraft cooking technology. It represents the state-of-the-art in steam/liquor-phase techniques, and aims to be a process designed for fewer equipment requirements than the competition. This system can be tailored for a wide range of production rates of up to almost 4000 ADt/d (Valmet, 2014). As any kraft digesting process, its purpose is to transform wood chips into crude pulp of a particular kappa number using white liquor and steam, and generating at the same time a stream of weak black liquor that contains degraded wood substance and spent reagents. The crude pulp is further processed in the remaining stages of the fiber line, and the weak black liquor sent to the recovery line. The reader can found details on the process chemistry and technology of the kraft digesting in Chapter 3.

Figure 6.1 shows the process flow diagram of a particular CompactCooking™ G2 implementation that is to be dynamically modelled and simulated in this thesis. As it can be inferred from the diagram, this process is highly non-linear and interacting due to complex flow configuration combined with heat integration. Figure 6.2 also depicts the assembly of the two-vessel system and inner parts. Below, a description is given of the main process features intending to explain the essential functioning of the equipment.

This implementation fundamentally consists of the following major equipment: (i) the chip metering device; (ii) two tubular moving bed reactors (“vessels”),

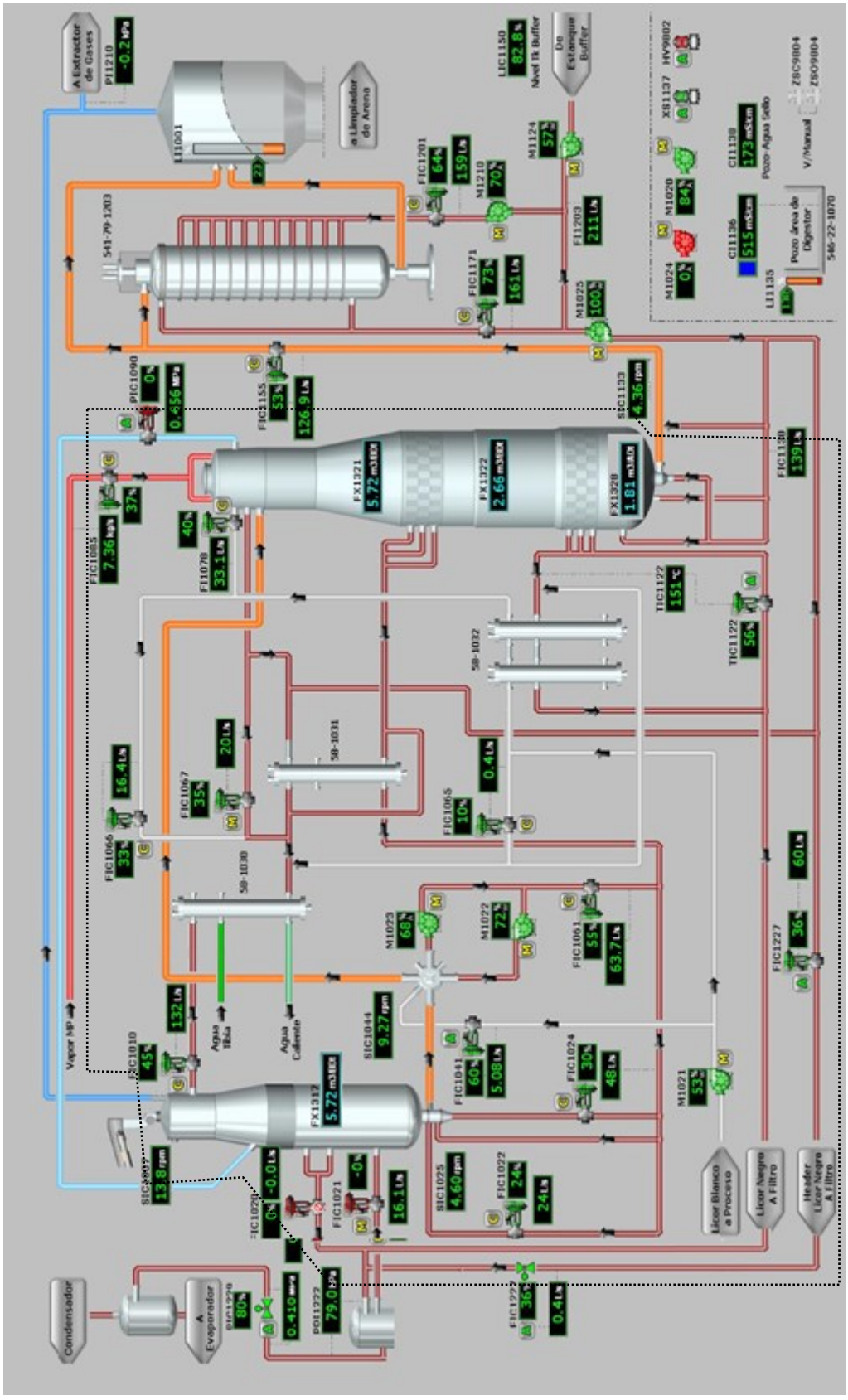

Figure 6.1. Process flow diagram of the CompactCooking™ G2 implementation to be modelled and simulated.

impregnator (impbin) and digester, fitted with side screens and bottom scrappers; (iii) the high-pressure feeding device; (iv) three heat-exchangers: the white liquor heater, the transfer liquor heater, and the impbin cooler; (v) the fiber screen filter; (vi) the pressure diffusion washer; and (vi) centrifugal pumps. Furthermore, the digester includes a special device called top separator and an integrated washer at the bottom end. Non-essential equipment of the system, in terms of influencing cooking reactions, comprises: (i) a flash evaporation tank, (ii) a weak black liquor cooler (heat-exchanger), and (iii) a blow tank.

Woodchips are transported to the digesting area by a conveyor belt that discharges in the chip metering device. This device comprises two components: a chip chute (buffer) and a chip meter. The former receives and accumulates chips over a minimum level; whereas the latter is a specially designed rotating wheel with pockets able to deliver a specific volume of chips per revolution. By adjusting the frequency set-point of its speed controller, the chip meter can be used to manipulate the bulk volumetric flow rate of woodchips entering the digesting stage. Naturally, the chip chute should maintain a minimum level to ensure complete filling of the chip meter pockets.

From the chip meter, chips fall by gravity into the impregnator vessel where a moving bed of chips retains them for a certain time. Analogously, chips transferred to the digester top separator fall over the moving bed of this other vessel, in which they reside during a controlled period of time. Logically, the average retention time of chips is affected by the actual volume of chips in the bed and the motion speed of the same. The former simply depends on the bed porosity, whereas the latter is determined by a complex momentum balance.

The chips bed moves slowly several meters downward until reaching its outlet at the bottom end of the vessel. Through the chips bed, a hot aqueous phase flows in co-current mode carrying active chemical reagents that promote wood delignification reactions, the hydroxide (OH^-) and hydrosulfide (HS^-) ions, and removing degraded substances from the wood. By convention, the bed is referred as “the chips column” and the aqueous phase as “the liquor”. Chips and liquor move at different speeds and separately define levels within each vessel.

Exiting chips from the impregnator pass through the high-pressure feeding device which provides impulse to reach the top of the digester and maintains a pressure

seal in the pipe connection to the digester top separator. This feeding device comprises the actual high-pressure feeder and two centrifugal pumps that generate a recycle of liquor at high-pressure. The feeder is a specially designed rotating plug with four through-holes and a screen at the bottom of the feeder housing, such that while one through-hole is being filled, another is discharging chips into the pipe connected to the top separator with an excess of liquor, and sucked liquor from the previous filled plug plus the returning liquor excess is being recycled at high-pressure to the discharging plug. Whilst the impregnator is operated at atmospheric pressure, the pipe connection from feeder to digester and the digester steam phase may reach a pressure over 1.0 and 0.5 MPa(g) respectively.

Chips entering the digester pass through the top separator, a special device designed to separate the liquor excess from the transferred chips by means of a screw and screen. This device should remain above the digester chips column, thus in contact with the steam phase formed due to the direct injection of MP steam to the digester top. The fed MP steam, at a nominal superheated condition of 210 C and 1050 kPa(g), rapidly transfers its latent heat to the entering chips slurry. Ideally, most of the heat should be transferred to the retained chips slurry fraction, such that the main temperature rise occur in the mass of chips and liquor falling over the bed.

The steam phase, enclosed within the digester top, reaches a near saturation condition that depends mainly on the flow rates and temperatures of the following streams: MP steam, entering chips slurry, return transfer liquor, and vapor relief. The steam phase temperature is one of the variables that most affect the cook along the digester and therefore the final cooking kappa; hence, it is referred as “the cooking temperature” and is usually cascade controlled as part of the H-factor and kappa number control (see Section 3.4). Its set-point value is changed in the range of 130 – 160 C, following H-factor set-point changes which mainly depend on the fed wood species, the mill production rate and the white liquor charge. Alternatively, since the liquor phase at the top liquor level establishes a steady gradient of temperature with the steam phase (4 – 6 C), it may also be considered as the cooking temperature for control purposes. Along the digester, the temperature rises some degrees as a result of the heat liberated by exothermic reactions; whereas in the bottom end, a sudden drop of temperature

should take place due to cold wash liquor entering counter-currently. In this manner, the cook can be stopped and cooking reagents washed away. If chips have reached (a well-chosen) target cooking kappa, it should be possible to disaggregate the fibers by a sudden change of pressure that is referred as “blow”. To avoid mechanical damage to the fibers, cooked chips are blown at the lowest temperature possible after the pressure diffusion washer, discharging the washed crude pulp into the blow tank (see Section 3.3).

In the case of the impregnator, the temperature profile is fairly different from the one established along the digester. First of all, this vessel is not pressurized and directly receives ambient temperature fluctuations associated with the entering chips stream. Besides, the top liquor stream, connected to a top flange but actually distributed through an internal central pipe at a middle level, flashes due to a sudden pressure change and fumes are liberated to the atmosphere. Liquor flashing is a design feature to achieve a so-called “chip steaming” process that should aid removing air from the chips, avoiding column movement disturbances due to high buoyancy and improving the subsequent impregnation process. (see Section 3.2)

The liquor phase flowing through a bed can also be separated, to some extent, in order to influence the compaction of the bed and consistency of the exiting chip stream. This phase separation is performed by means of side screens located at different levels of the vessel; these so-called “extraction screens” define boundaries for establishing vessel zones, thus five zones can be distinguished in this CompactCooking™ G2 system: impbin top, impbin bottom, cook zone 1 (digester top), cook zone 2 (digester bottom), and wash zone (digester bottom end). The separated liquor streams will be termed middle extraction, upper extraction, and lower extraction as seen in Figure 6.1. Likewise, the return liquor stream obtained from the top separator will be simply termed transfer liquor. The transfer liquor is separated such that the reagents concentration within the digester can be better controlled by adding a new stream of fresh white liquor at the top of the digester, and also because it has been added in a considerable excess simply to aid the transport of chips from the high-pressure feeder to the digester top located several meters higher.

Chips exit from a vessel guided by the movement of the bottom scrapper and aided by the addition of dilution liquor, thus its outflow rate can be manipulated by

means of the scrapper rotational speed. The chips column moves downward primarily due to gravity and the action of the bottom scraper as it removes the processed chips; however, the momentum balance is more complex and the column may show discontinuities and stoppage due to high compaction and wall friction. These plugging phenomena are conventionally referred as “hangs”, and digester hangs are more likely to occur due to the operating conditions of this vessel. This faulty condition should be extremely avoided due to its great impact on process quality variables. An experienced operator may be able to read the signals of an incipient plugging, recognize a hang occurrence, and take manual control of the vessel in order to solve the process fault. Liquor channeling through the chips bed is also another common fault that operators must solved, as it can affect the homogeneity of the cook and lead to higher reject rate at the brownstock deknotting and screening area.

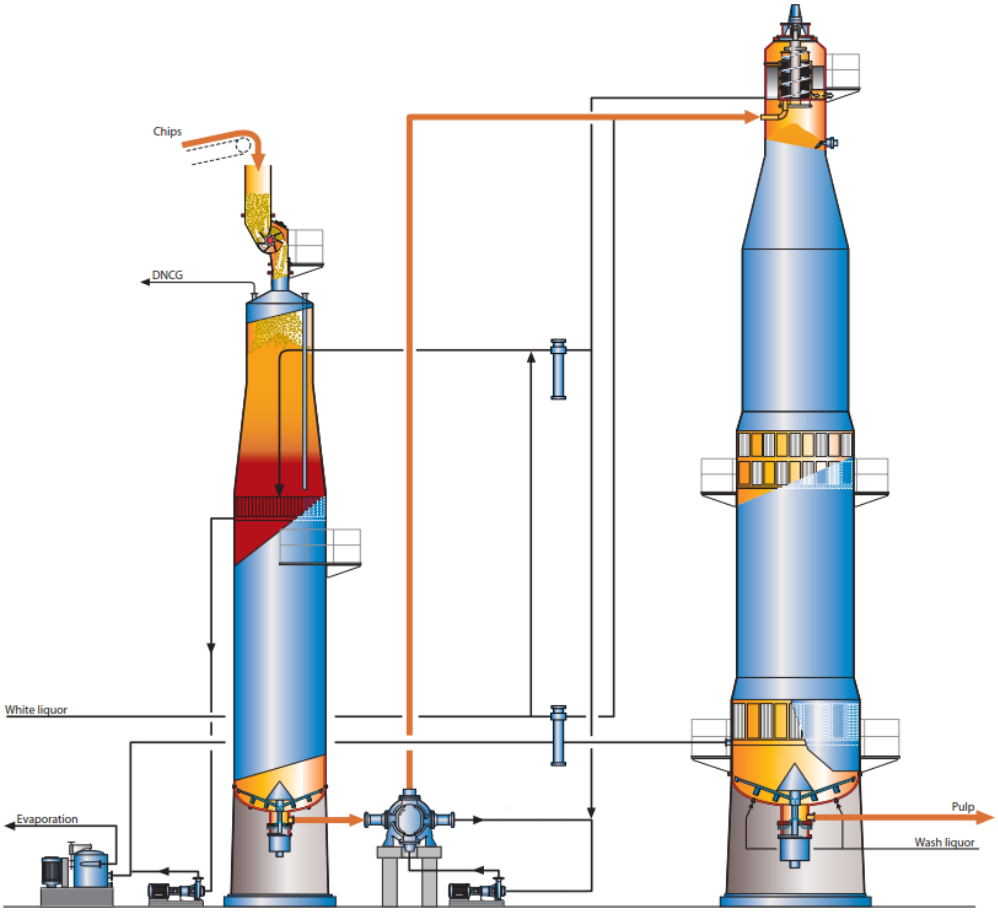

Figure 6.2. Outline of the vessels assembly. Adapted from Valmet (2014).

Whilst the chips flow configuration is relatively simple and straightforward, the liquor flow configuration involves several splitting and mixing points, which establish three main liquor recycling paths: (i) transfer liquor from the digester top separator to impregnator bottom, (ii) extraction liquor from the digester upper screen to impregnator top, and (iii) reject liquor from fiber-filter to impregnator bottom. Besides liquor recycling, the system also incorporates heat integration. Heat-exchangers configures a local heat recovery network that allows: (i) to preheat the white liquor fed to the digester by recovering heat from the lower extraction, (ii) to increase temperature of the transfer liquor by recuperating heat from the upper extraction, (iii) and to constrain the maximum temperature of the impregnator top liquor by releasing heat to the plant-wide heat-integration network.

Liquor splitting and recycling allows controlling the reagents distribution, namely alkali concentration, as well as liquor-to-wood ratios for different zones of the vessels. On the other hand, local heat integration permits to decrease steam consumption thus lowering process costs. However, the added interaction effects are likely contributing to a highly non-linear behavior with multiple-time-scale dynamics that may pose hard challenges to the control and the optimization of the system. Although this is only an hypothesis, it is interesting to note that current research on the subject have shown how a characteristic process behavior with multiple-time-scale dynamics arises from the condition of material recycling and/or heat integration within a process; and how important can be designing a control system to deal with fast and slow dynamics (Baldea & Daoutidis, 2012).

Aiming to model and simulate this process stage, we finish this description by listing in Table 6.1 physical input and output streams of the process seen as an atomic block. Each independent stream may have multiple associated process variables, which must be classified as logical inputs or outputs of the process model. As it will be explained later, this classification depends upon the model architecture and affects simulation capabilities.

Table 6.1. List of physical inputs and outputs of the process seen as an atomic block.

Stream name			
Inputs		Outputs	
1	Woodchips	1	Cooked pulp
2	MP steam	2	Weak black liquor
3	White liquor	3	Hot water
4	Wash liquor	4	Relief vapor
5	Warm water	5	Flashed vapor

7 Simulator Design

The workflow diagram for the simulation task is shown in Figure 7.1. Although this indicates a clear and straightforward way to proceed, the reader should be warned that modelling a process involves much more of a creative and ingenious task than following a standard procedure.

First, the process design is studied and analyzed as a system of input, output and state variables, i.e., under the mathematical paradigm of state-space representation. Based on this and considering the goal of the second task, an abstraction of the actual process flow diagram is made intending to capture the necessary details for process optimization. This first abstraction entails discarding or aggregating some unit operations or process streams; henceforth logical inputs and outputs can be established and state variables later defined. It might not be wrong saying that defining states is the key of first-principles modelling, as they represent hypothetical entities that allow researchers to apply a scientific reasoning (hypothetical-deductive) to prove the validity of model hypotheses.

Once the model is mathematically formulated in the state-space representation, whether as an ordinary differential equations (ODE) or differential algebraic equations (DAE) system, it can be implemented in ad hoc simulation software such as Matlab/Simulink, OpenModelica or gPROMS. This work implements the conceptual process model in the Matlab/Simulink environment. Hence, model implementation means here either representing equations in C or Matlab programming languages, or graphically representing them in the Simulink interface.

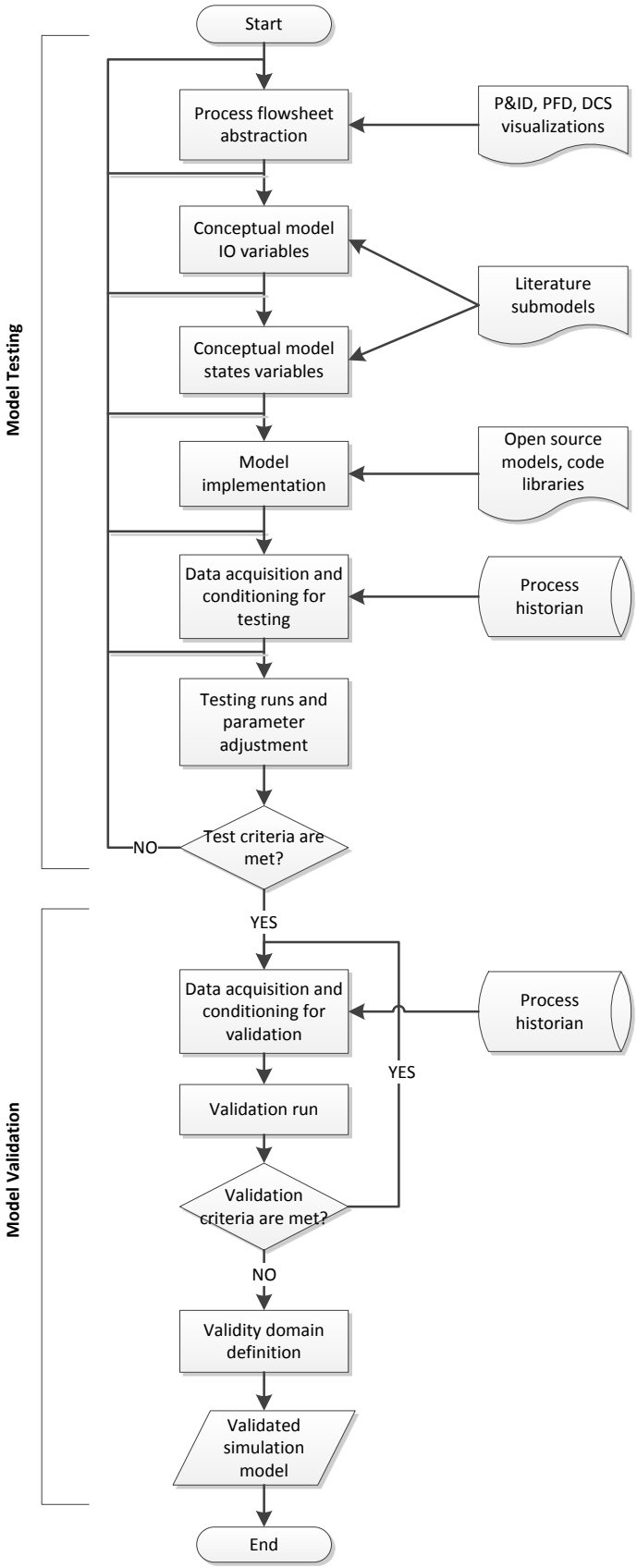

Figure 7.1. Workflow diagram for the design of the simulator.

The implemented model, i.e., the simulation model, contains several parameters whose values are in principle unknowns, thus additional information is needed to estimate them apart from process historian data. This information usually represents laboratory analyses of complex chemical compositions, e.g. wood composition, or experimental data needed to determine correlation parameters, e.g. parameters in Härkönen equations. However, obtaining these data at the laboratory is very time-consuming and therefore outside the thesis scope. A practical solution instead is to calibrate them starting from a guess based on available literature values. This model calibration could be formulated as an optimization problem on itself, but it is also a major effort concerning its implementation and execution. As a result, the chosen approach is a heuristic parameter adjustment starting from literature values, and guided by the process knowledge of the author under the condition that results should be “reasonable”. In this sense, the latter configures a subjective validation criterion, which can be complemented with other criteria in relation to model verification, face validity, parameter sensitivity analysis, or model reproductive/predictive power.

The validation of mathematical models is actually a matter of discussion, and there is no consensus about how a process model must be validated or what should be understood for model validity. In this thesis, we follow the paradigm of Sargent (2011) but grouping some of its ideas into two distinct concepts: model testing and model validation. Model testing comprises validating the conceptual model, verifying the model implementation, balancing computation times versus model complexity, and adjusting model parameters such that the historical data used in this calibration is reproduced successfully under particular test criteria. Model validation instead involves solely operational validation, i.e., assessing model degradation or failure when trying to reproduce historical data not used during calibration. In this way, we can explorer the model validity domain and identify extreme conditions leading to model failure.

7.1 Simulation model architecture

Our optimization goal entails computing set-points that affect the cooking reactions, i.e., computing an optimized cooking recipe. Therefore, some unit operations can be neglected since by design they cannot influence phenomena inside the vessels: the flash evaporation tank, the weak black liquor cooler, and the blow tank.

After the first testing attempts, however, it became clear that computation times are too long when representing all liquor recycles due to the number of algebraic loops; thus, additional unit operations were excluded to decrease this number, and then computation times achieved a fast pace of almost 800 times faster than real time. These last excluded operations correspond to the pressure diffusion washer and the fiber filter. Figure 7.2 shows the resulting abstraction of the CompactCooking™ G2 process flow configuration as implemented into a Simulink model. To aid the convergence of the Simulink algebraic loop solver, memory blocks were inserted at different places in the paths of the loops. By trial-and-error and after some attempts, the positions shown here resulted well enough to speed up the model initialization.

The omission of the pressure diffuser implies that the wash zone losses important information needed for its simulation, since temperature and composition of the wash liquor entering the digester bottom depends on the washing performance of the pressure diffuser. Likewise, the filter reject composition and temperature depends on the mixing inside the fiber filter. Nevertheless, neglecting a fiber filter model allowed to make use of measure data for the now input signal, the temperature of the filter reject stream, which improved the general accuracy of the simulation model when trying to reproduce “incomplete” industrial data, i.e., lacking of other temperature signals needed as input in the simulation. More on this will be discussed later on in Section 8.1. For the moment, it should be noted that depending on the unit operations included, the selection of logical inputs and outputs will change.

Table 7.1 lists a rigorous set of inputs required for simulating the CompactCooking™ G2 stage represented in the Simulink model. An ideal implementation of this process technology would be instrumented in a way that all these signals, except split fractions, are measured online. Certainly, this would be an expensive instrumentation and indeed not completely feasible, since there is no online chemical analyzers of the wood composition up to the present date. However, one could expect that at least all signals of flow rates and temperatures be available at the mill site, as they only need relatively cheap sensors, and that the remainder disturbances be measured offline in a regular basis.

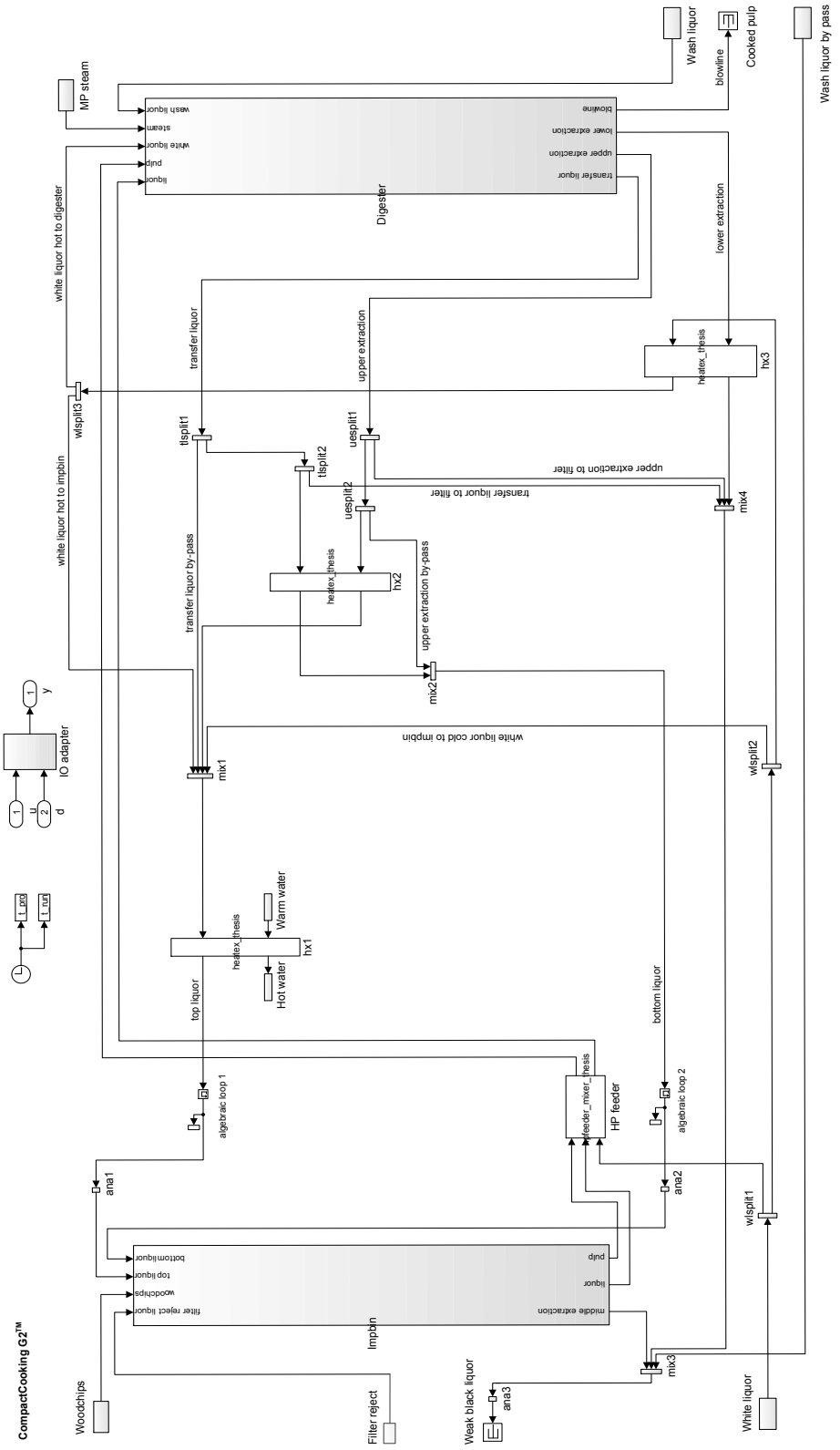

Figure 7.2. Top-level diagram of the CompactCooking™ G2 Simulink model.

Table 7.1. Logical inputs of the simulation model.

	Input variable name	Unit
Manipulated variables		
1	Chip meter speed	rpm
2	MP steam flow rate	kg/s
3	White liquor flow rate	l/s
4	Wash liquor flow rate	l/s
5	Middle extraction flow rate	l/s
6	Transfer liquor flow rate	l/s
7	Upper extraction flow rate	l/s
8	Lower extraction flow rate	l/s
9	Filter reject split fraction	v/v%
10	White liquor split fraction 1	v/v%
11	White liquor split fraction 2	v/v%
12	White liquor split fraction 3	v/v%
13	Transfer liquor split fraction 1	v/v%
14	Transfer liquor split fraction 2	v/v%
15	Upper liquor split fraction 1	v/v%
16	Upper liquor split fraction 2	v/v%
Disturbances		
1	Chips basic density	BDkg/m^3sub
2	Chips bulk density	BDkg/m^3st
3	Chips moisture	w/w%
4	Chip chute temp.	C
5	MP steam temp.	C
6	White liquor temp.	C
7	Wash liquor temp.	C
8	Filter reject temp.	C
9	MP steam pressure	kPa(g)
10	Wash liquor by-pass flow rate	l/s
11	White liquor NaOH conc.	g/l
12	White liquor NaSH conc.	g/l
13	White liquor total solids	g/l
14	Wash liquor NaOH conc.	g/l

15	Wash liquor NaSH conc.	g/l
16	Wash liquor total solids	g/l

To clarify, split fractions are held as inputs of the simulation because they contribute the sufficient number of freedom degrees to distribute liquor throughout the flow network, complying with a mass continuity constraint that, in this case, implies volume continuity because liquor density is assumed unmodified at the split point. Values of split fractions are computed based on actual flow rate measurements. Since it can exist redundant ways to compute them, depending on the placement scheme of flow meters, data reconciliation may be needed.

As stated in Chapter 5, to validate a simulation model we need to define comparable variables between simulated outputs and measured signals in the real process. Table 7.2 lists the selected outputs from the simulation model, distinguishing between a set of comparable and non-comparable ones. Analogous to the list of simulation inputs, the set of comparable outputs defines an ideal instrumentation for the process, which in this case is completely feasible with online sensors (calculated outputs only depend on the remainder measurements).

Non-comparable outputs listed here are selected for optimization purposes. Although some of these signals are not even measurable up to date, they permit introducing meaningful physical constraints in the optimization. For example, compacting pressures allow estimating the risk of plugging when operating with particular liquor-to-wood (L/W) ratios. Likewise, the chemical composition of the cooked pulp could be correlated to physico-mechanical properties of the pulp sheet, allowing the incorporation of these quality variables in the optimization task (see Section 3.4).

Table 7.2. Selected logical outputs of the simulation model.

	Output variable name	**Unit**
Comparable selected outputs		
1	Cooked pulp prod. rate	ADt/d
2	WBL solids prod. rate	tDS/d
3	Cooking kappa	κ

4	Cooking yield	w/w%
5	Cooking wood specific consumption	m^3sub/ADt
6	Blowline consistency	w/v%
7	WBL solids fraction	w/v%
8	Cooked pulp intrinsic viscosity	ml/g
9	Cooked pulp carry-over	kgDS/Adt
10	Impbin top temp.	C
11	Digester top temp.	C
12	Top liquor temp.	C
13	Bottom liquor temp.	C
14	Middle extraction temp.	C
15	Transfer liquor temp.	C
16	Upper extraction temp.	C
17	Lower extraction temp.	C
18	Blowline temp.	C
19	White liquor hot temp.	C
20	Lower extraction cold temp.	C
21	Top liquor hot temp.	C
22	Hot water temp.	C
23	Top liquor EA conc.	g/l
24	Bottom liquor EA conc.	g/l
25	Middle extraction EA conc.	g/l
26	Transfer liquor EA conc.	g/l
27	Upper extraction EA conc.	g/l
28	Lower extraction EA conc.	g/l
29	Blowline EA conc.	g/l
30	Top liquor flow rate	l/s
31	Bottom liquor flow rate	l/s
32	Blowline flow rate	l/s
33	EA/W total	w/w%
34	EA/W impbin fresh	w/w%
35	EA/W digester fresh	w/w%
36	L/W impbin top	m^3/BDt
37	L/W impbin bottom	m^3/BDt
38	L/W digester cook zone 1	m^3/BDt

39	L/W digester cook zone 2	m^3/BDt
40	DF digester wash zone	m^3/ADt
41	H-factor	H
Non-comparable selected outputs		
42	Impbin max. compacting pressure	kPa
43	Digester max. compacting pressure	kPa
44	WBL enthalpy flow as HHV	MJ/min
45	MP steam enthalpy flow	MJ/min
46	WBL solids HHV	MJ/kg dry
47	MP steam effective lambda	MJ/kg
48	Chips flow rate	m^3sub/min
49	Cooked pulp lignin content	w/w%
50	Cooked pulp cellulose content	w/w%
51	Cooked pulp glucomannan content	w/w%
52	Cooked pulp xylan content	w/w%
53	WBL solids lignin content	w/w%
54	WBL solids carbs content	w/w%
55	WBL solids extractives content	w/w%
56	WBL solids ash content	w/w%
57	Blowline consistency	w/w%
58	WBL solids fraction	w/w%
59	Lower extraction flow rate check	l/s

7.1.1 Vessel submodel architecture

The essence of the process simulator lies on the conceptual modelling of an infinitesimal control volume of a vessel. The results of this thesis, in turn, rely on the S-function that implements this submodel to represent vessel zones. There, several phenomelogical models are merged to describe as “realistic” as possible what is allegedly occurring within digesting reactors.

Impregnator and digester have several similarities that justify simulating both vessels with the same S-function. Thus, these units are constituted by its necessary instances, such that extraction streams can be represented by punctually splitting the liquor stream flowing through the vessel. Figure 7.3 and Figure 7.4 show the subsystems created within the Simulink model for representing each vessel.

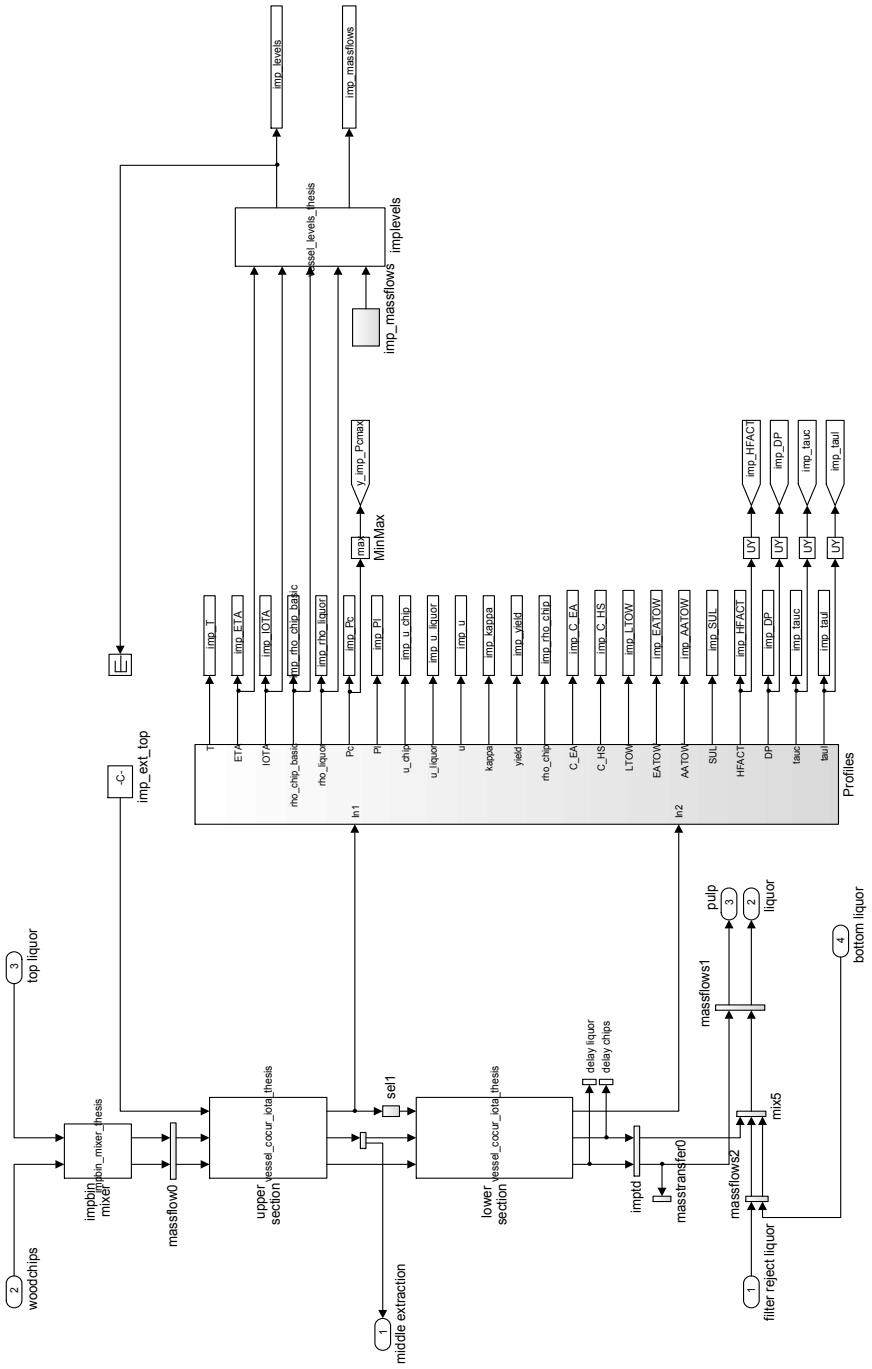

Figure 7.3. Impregnator vessel subsystem diagram.

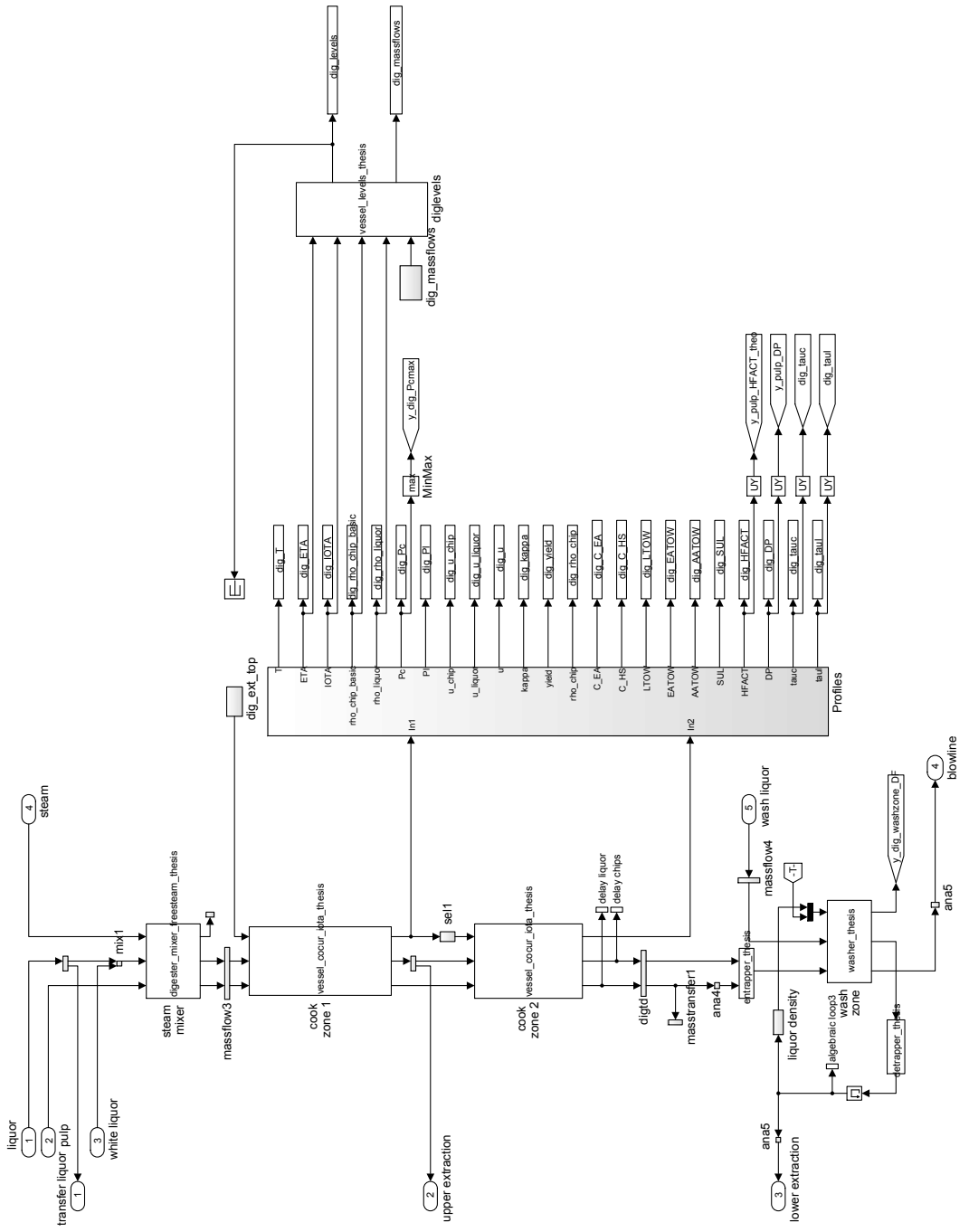

Figure 7.4. Digester vessel subsystem diagram.

The features of the vessel zone S-function (vessel_cocur_thesis) impose conditions for all the remainder parts of the Simulink model, including number of components per liquor and chip signals, as well as the physical meaning of the signals values.

In the case of the digester, an additional submodel is used to simulate the wash zone as an ideal washer. This approach creates an extra algebraic loop, since we need to match the lower extraction flow rate from the input data with the output value computed by the ideal washer.

7.2 Mathematical modelling

As the reader may have noted, we are explaining the design of the process simulator from the general to the particular. Let us now deepen into the mathematical and logical structure of the equations system of each submodel, understanding its underlying assumptions and physical meaning.

7.2.1 Main assumptions

Below are listed the main assumptions and simplifications of the process model:

- Vessels are moving bed reactors
    - Chips and liquor move as plug flow
    - Chips and liquor are in thermal equilibrium in radial direction
    - Flows are always co-current from top to bottom, except in the digester wash zone
    - Chips are a porous solid composed of wood substance and entrapped liquor filling the pores
    - Vessels inside can be describe as a three-phase reacting system of the wood substance degrading into the pores liquor, from which mass is being transferred to and from the free liquor surrounding the chips and completely filling the void volume of the chips bed
    - Bed compaction affects only the form and spatial arrangement of chips but not their individual volumes
    - Liquor streams are incompressible flows
    - Radial gradients of temperature, pressure, or concentration within phases can be neglected

    - Additionally, radial gradients between entrapped and free liquor are neglected to decrease numerical burden
    - Chips are completely and instantaneously penetrated with liquor when entering the impregnator
    - Levels of chips and liquor are held constant
    - Pulp consistency in extraction liquors is negligible
    - Phenomena associated to the chip size and its distribution can be neglected
- Heat-exchangers are perfectly mixed tanks
    - The heat exchange occurs between hot and cold sides at a constant area-global heat transfer coefficient (UA)
    - The liquor composition vary due to mixing and retention time, but no reaction occurs inside heat-exchangers
- Pipes transport delays are negligible
    - No reaction occurs inside pipes
- All equipment is adiabatically isolated

From the above several deductions can be made, such as that: (i) no aerial phase is modelled; (ii) the chips bed is compressible as an aggregate, but volume continuity and incompressibility hold valid for chips and liquor streams; (iii) chips and liquor phases have the same temperature profile; (iv) no diffusion or heat transfer need to be modelled in radial direction; (v) no heat losses occur to the environment; (vi) and that the spatial representation of all phenomena is lumped into one axial dimension.

Although levels were tried to be dynamically simulated, computation times excessively increased and the numerical stability of the simulation became compromised due to high stiffness. Thus, it seems that the modelling approach of levels variations requires some refinement before obtaining a practical solution for a normal PC. Similarly, dynamic momentum balances were conceptualized but not implemented, previewing the numerical problems they can introduce and the long time it can take to solved them.

The following headings will now explain the conceptual modelling of process equipment and its mathematical formulation. The reader can find explanations to algebraic symbols on the first pages of this work.

7.2.2 Vessels

As it has been emphasized, the vessel submodel is the fundamental element of the thesis work. Therefore, an extensive discussion is elaborated in this Chapter aiming to clarify its underlying equations through their derivation.

This submodel corresponds to a distributed parameter system of a multiphase reacting system, where axial distribution of conserved quantities occurs due to advection caused by plug flow motion of the chips and liquor phases. Time-dependence variation of the conserved quantities of each phase is described by continuity equations, resulting from applying conservation laws of mass, energy and momentum to an infinitesimal control volume. The final result is a set of coupled non-linear first-order partial differential equations (PDEs) in Euler formulation, which are solved by the method of lines regarding variables of concentration and temperature, and by a steady-state approach in the case of pressure and velocity variables. Since flow velocities do not change due to a true dynamic equation, variable transport delays are introduced at the vessel outlet to compensate neglected effects of momentum dynamics.

Figure 7.5 depicts the logical relations of the phases and phase variables in an infinitesimal, cross-sectional, control volume of a vessel. The solid phase corresponds to the wood substance; the entrapped liquor phase to the liquid filling the chips pores; and the free liquor phase to the liquid surrounding the chips. Chips phase therefore refers to the sum of solid and entrapped liquor phases.

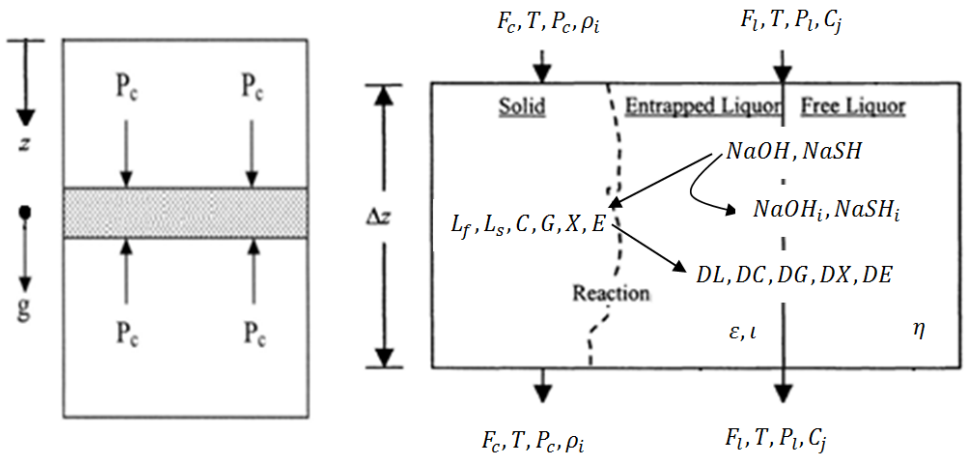

Figure 7.5. Outline of an infinitesimal control volume in a vessel cross-section.

Each phase occupies a certain fraction of the total control volume. These fractions can be expressed in several ways depending on the volume-basis; however, the definitions used here are as follows

$$\eta = \frac{\Delta V - \Delta V_c}{\Delta V} = \frac{\Delta V_f}{\Delta V} \quad \textbf{7.1}$$

$$\varepsilon = \frac{\Delta V_c - \Delta V_s}{\Delta V_c} = \frac{\Delta V_e}{\Delta V_c} \quad \textbf{7.2}$$

Flows through the vessels are describes in a volume-basis except in the wash zone, which requires mass-basis to correctly implement the mass balances of the ideal washer model.

7.2.2.1 Bed compaction

Let us start by explaining the model of the compaction phenomenon implemented in this thesis. Bed porosity (compaction) can be express as a function of compacting pressure and the kappa number (see Section 4.2), thus modelling compaction basically means calculating these two variables. The kappa number is indirectly obtained from mass and energy balances; whereas the former directly from momentum balances. In fact, there are several ways to establish these balances, as well as kinetic models to include in them, and this constitutes the basis for a variety of vessel models (see Chapter 4).

The computation of kappa number will be explained later. Now, we treat the simultaneous calculation of compacting and free liquor pressures, since these are interdependent variables, aiming to derive equations from which we can compute both variables as functions of the axial coordinate and time,

$$P_c = P_c(z, t)$$

$$P_f = P_f(z, t)$$

7.2.2.1.1 Definitions

First, let us recall definitions of the superficial and interstitial velocity given by Eqs. 7.3 and 7.4 respectively,

$$F_c = Au_c = Av_c(1 - \eta) \quad \textbf{7.3}$$

$$F_f = Au_f = Av_f\eta \quad \textbf{7.4}$$

Averaged momentum balances can be derived with any of these phase velocity definitions and, in principle, they should be equivalent. However, if we include an interphase friction term following the approach of Härkönen (1984), i.e., using a modified Ergun equation (Ergun, 1952), then we will have dissimilar terms depending on the phase velocity definition we choose. The empirical parameters of the modified Ergun equation are usually correlated with superficial velocity, thus our approach is to define the interphase friction, Eq. 7.5, also in relation to the superficial velocity. This account for friction between the viscous flows of chips and free liquor, and it will represent momentum transfer per unit of stereo volume and time.

$$\psi_{\Lambda} = \hat{R}_1 \frac{(1-\eta)^2}{\eta^3} \Delta u + \hat{R}_2 \frac{(1-\eta)}{\eta^3} \Delta u |\Delta u| \qquad 7.5$$

$$\Delta u = u_f - u_c \qquad 7.6$$

It must be mentioned that other authors, who have published vessel models describing the compaction phenomenon, use superficial velocity (Saltin, 1992; Rantanen, 2006; Laakso, 2008), interstitial velocity (Härkönen, 1987; Michelsen, 1995; Bhartiya et al., 2003) or give no explicit information about this choice (Kayihan et al., 2005). However, this selection is clearly a matter of interpretation, considering that the empirical coefficients of Eq. 7.5 are always regressed with data of superficial velocity and bed porosity obtained from experiments in which liquor is flowing top down through a packed bed of chips, a fairly different scenario than the real flow pattern in an industrial vessel. Nevertheless, the natural choice in two- or three-dimensions models (Härkönen, 1987; Pougatch et al., 2006) is the interstitial velocity, since superficial velocity is meant only for describing a lumped flow model in one-dimension.

Given the definitions of Eqs. 7.5 and 7.6, the interphase friction term ψ_{Λ} should be negative in the liquor phase momentum balance and positive in the chips case. In this way, it models a momentum transfer when one phase is moving faster through and in relation to the other.

In addition to the above, we can also include in the momentum balances a term to describe sliding friction of the chips column and the vessel wall. Härkönen (1984) also proposed the definition of a force volume, which is based on the idea of the sliding friction force as proportional to the normal reaction of the wall

against the pressure exerted by the chips column over an infinitesimal area of the vessel cylinder, i.e.,

$$dF_{\mu} = \mu dN = \mu P_c \pi D dz(1-\eta) \tag{7.7}$$

and the force volume is

$$\psi_{\mu} = \frac{dF_{\mu}}{dV} = \frac{\mu dN}{dV} = \frac{\mu P_c \pi D dz(1-\eta)}{\frac{1}{4}\pi D^2 dz} = \frac{4\mu P_c(1-\eta)}{D} \tag{7.8}$$

This force volume is actually a sink term of momentum per unit of stereo volume and time, which is to be included in the momentum balance of the chips phase. A subtle difference has been introduced in equation (7.8) in relation to the original definition of Härkönen, the factor $(1-\eta)$ represents here that the exerted force by the column is only proportional to the volume occupied by the chips phase. This element naturally implies that if no chips phase is present, then no sliding friction should occurs.

With the concepts provided, we are now able to postulate momentum balances for the chips and free liquor phases. In the following equations, the density of each phase is estimated according to the formulas below

$$\rho_c = \rho_{ws}(1-\varepsilon) + \rho_e \varepsilon \tag{7.9}$$

$$\rho_e = \sum_j C_{e,j} + \rho_w \tag{7.10}$$

$$\rho_f = \sum_j C_{f,j} + \rho_w \tag{7.11}$$

where

$$\varepsilon = 1 - \frac{\sum_i \rho_i}{\rho_{ws}} \tag{7.12}$$

Given these estimates, the density of water must remain constant to avoid violating mass balances.

7.2.2.1.2 Liquor phase momentum continuity

We postulate the momentum balance of the liquor phase in an infinitesimal control volume as follows

$$A\eta\Delta z\rho_f\left(u_f(z,t+\Delta t)-u_f(z,t)\right) = F_f\rho_f\Delta t u_f(z,t)-F_f\rho_f\Delta t u_f(z+\Delta z,t)+A\eta\Delta t P_f(z,t) - A\eta\Delta t P_f(z+\Delta z,t)+A\eta\Delta z\rho_f g\Delta t-\psi_\Lambda A\eta\Delta z\Delta t \quad \textbf{7.13}$$

multiplying by $\frac{1}{\Delta t\Delta z}$, taking limits as $\Delta t\to 0\wedge\Delta z\to 0$, introducing Eq. 7.4, and clearing the temporal derivative we get

$$\frac{\partial u_f}{\partial t}=-u_f\frac{\partial u_f}{\partial z}-\frac{1}{\rho_f}\frac{\partial P_f}{\partial z}+g-\frac{1}{\rho_f}\psi_\Lambda \quad \textbf{7.14}$$

Several fluid dynamics effects could be included in the balance Eq. 7.13; however, our goal for the moment is to consider only major, obvious effects, such as advective momentum transfer, pressure forces, gravity and momentum transfer due to viscous friction between phases.

Since the momentum is a vector quantity, the sign of the terms in the balance reflect not only whether momentum is entering or exiting the control volume, but also the direction of these momentum quantities. The term ψ_Λ is preceded by a negative sign due its definition. The sign of the pressure terms instead are explained according to the direction of impulses exerted by the immediate volumes above and below the control volume of free liquor.

To solve the dynamic Eq. 7.14, we would have to compute somehow the partial derivative of the liquor pressure. Although there are methods for it[*], their numerical complexity suggests choosing an alternative and more practical solution. Thus, we simply solve the equation in the steady-state condition neglecting also the advection term, i.e., we compute at each step of the dynamic integration an approximate profile of the liquor pressure given by

$$\frac{dP_f}{dz}=\rho_f g-\psi_\Lambda \quad \textbf{7.15}$$

Considering the discretized axial dimension, the actual equation to implement is

$$P_{f,k}=\left(\rho_{f_k}g-\left(\hat{R}_1\frac{(1-\eta_k)^2}{{\eta_k}^3}\Delta u_k+\hat{R}_2\frac{(1-\eta_k)}{{\eta_k}^3}\Delta u_k|\Delta u_k|\right)\right)\Delta z+P_{f,k-1} \quad \textbf{7.16}$$

[*] The reader can consult Patankar (1980)

The reader should bear in mind that several implicit assumptions may be made already when establishing a balance equation. In the case of Eq. 7.13, it is assumed a local, constant phase density (incompressible flow), despite the density may change along the pathline of a fluid parcel due to mass transfer phenomena. Likewise, balance equations in the next secctions may involve implicit assumptions needed to obtain a numerically solvable form.

7.2.2.1.3 Chips phase momentum balance

Analogously to the liquor case, a momentum balance is postulated for an infinitesimal control volume according to Eq. 7.17. The effects considered here include advective momentum transfer, pressure forces, gravity, buoyancy, sliding friction, and interphase friction.

$$\begin{aligned} A(1-\eta)\Delta z\rho_c\big(u_c(z,t+\Delta t)-u_c(z,t)\big) \\ = F_c\rho_c\Delta t u_c(z,t) - F_c\rho_c\Delta t u_c(z+\Delta z,t) + A(1-\eta)\Delta t P_c(z,t) \\ - A(1-\eta)\Delta t P_c(z+\Delta z,t) + A(1-\eta)\Delta z\rho_c g\Delta t - A(1-\eta)\Delta z\rho_f g\Delta t \\ + A(1-\eta)\Delta t P_f(z,t) - A(1-\eta)\Delta t P_f(z+\Delta z,t) - \psi_\mu A(1-\eta)\Delta z\Delta t \\ + \psi_\Lambda A(1-\eta)\Delta z\Delta t \end{aligned} \qquad \textbf{7.17}$$

multiplying by $\frac{1}{\Delta t\Delta z}$, taking limits as $\Delta t \to 0 \wedge \Delta z \to 0$, introducing Eq. 7.3, and clearing the temporal derivative we get

$$\frac{\partial u_c}{\partial t} = -u_c\frac{\partial u_c}{\partial z} - \frac{1}{\rho_c}\frac{\partial P_c}{\partial z} + \left(1-\frac{\rho_f}{\rho_c}\right)g - \frac{1}{\rho_c}\frac{\partial P_f}{\partial z} - \frac{1}{\rho_c}\psi_\mu + \frac{1}{\rho_c}\psi_\Lambda \qquad \textbf{7.18}$$

A distinctive feature of the balance Eq. 7.17 is that the free liquor exerts a pressure force over the chips, which does not generate a reaction force in the reverse sense because the chips phase would behave as a inelastic compressible bed (though individual chips are incompressible).

The dynamic Eq. 7.18 could be solved with relatively less numerical complexity than in the liquor case. First Michelsen (1995) and then Bhartiya et al. (2003), following Michelsen's approach, have achieved to solve a similar dynamic equation postulated for the change of momentum described by the interstitial velocity. However, considering the scope and time limitation of the thesis, we will

follow the same steady-state approach applied before. Thus, we neglect the advection term and solve the equation at steady-state given by

$$\frac{dP_c}{dz} = (\rho_c - \rho_f)g - \frac{dP_f}{dz} - \psi_\mu + \psi_\Lambda \qquad \textbf{7.19}$$

In terms of the discretized axial dimension, the equation to be implemented is

$$P_{c,k} = \left((\rho_{c,k} - \rho_{f,k})g - \frac{4\mu P_{c,k}(1-\eta_k)}{D_k} + \left(\hat{R}_1 \frac{(1-\eta_k)^2}{{\eta_k}^3}\Delta u_k + \hat{R}_2 \frac{(1-\eta_k)}{{\eta_k}^3}\Delta u_k|\Delta u_k|\right)\right)\Delta z - (P_{f,k} - P_{f,k-1}) + P_{c,k-1} \qquad \textbf{7.20}$$

Since the compacting pressure and the bed porosity result to be interdependent variables, Eq. 7.20 must be solved simultaneously with the bed porosity correlation (Eq. 4.12). Numerically, this is achieved by creating an intrinsic iteration loop during the dynamic simulation. The difficulty of this approach lies in the initialization of states. Once this has been successfully done, the intrinsic loop keeps driving both equations to convergence along the dynamic integration, thus satisfying them simultaneously

Since the bed porosity correlation could yield a negative value at a high compacting pressure, a saturation minimum limit should be defined. Moreover, a compacting degree near zero can cause extreme stiffness in the simulation, and therefore the limit should not be too small either.

Equation 7.19 resembles the static compacting pressure model used by Rantanen (2006) and Laakso (2008), who allegedly taken it from Saltin (1992). The differences lie in that these authors did not consider interphase friction as an independent term and multiplied the first term on the right-hand side of the equation by $(1-\eta)$ (see Section 4.2.2). Moreover, these authors claim that the sign of the pressure liquor derivative should be changed depending whether the flow regime is co-current or counter-current; but this seems to be a wrong conception, since the sign of this term changes intrinsically according to Eqs. 7.5 and 7.15 when the free liquor flows co-currently $(u_f > 0)$ or counter-currently $(u_f < 0)$

It is worth noting that the approach used to solve the compaction model results to be the same of Rantanen (2006). However, Rantanen did not discuss in terms of

momentum balances. Michelsen (1995) instead is probably the author who has most elaborated on dynamic momentun balances within digesting vessels, but strangely he did not consider buoyancy in his equations, and neither did Bhartiya et al. (2003) who merged Michelsen's work with the Purdue kinetic model.

As a final remark, the compacting pressure derivate can be decoupled from the liquor pressure by introducing Eq. 7.15 in 7.19 to obtain the following form

$$\frac{dP_c}{dz} = \left(\rho_c - 2\rho_f\right)g - \frac{4\mu P_c(1-\eta)}{D} + 2\left(\hat{R}_1\frac{(1-\eta)^2}{\eta^3}\Delta u + \hat{R}_2\frac{(1-\eta)}{\eta^3}\Delta u|\Delta u|\right) \quad \textbf{7.21}$$

which easily explains why high L/W ratios in co-current flow regime, i.e., high values of Δu, tend to increase the risk of plugging inside vessels by leading to an extreme compacting pressure.

However, the relation between the L/W ratio, usually defined as an apparent value on the basis of the set-point infeed woodchip mass flow (see Section 7.2.5), and the Δu value is not linear, thus the risk of plugging can rise when increasing production rate in spite of operating at low L/W ratios. Based on the definition of the L/W ratio

$$L/W = \frac{F_f + \varepsilon F_c}{F_c \rho_{basic}\cdot\frac{\mathrm{t}}{1000\mathrm{kg}}} \quad \textbf{7.22}$$

we can get the below expression to estimate Δu inside vessels by introducing Eq. 7.95 in 7.22.

$$\Delta u = \left(L/W - \frac{1+\varepsilon}{\rho_{basic}\cdot\frac{\mathrm{t}}{1000\mathrm{kg}}}\right)\frac{s_{cm}\theta_{cm}\rho_{bulk}\cdot\frac{\mathrm{t}}{1000\mathrm{kg}}}{A} \quad \textbf{7.23}$$

This value could be used as an index to monitor the risk of plugging, thereby overcoming the limitation in the definition of the L/W ratio that lumps flows of free and entrapped liquor. Indeed, we can better define a new monitored variable, for example, the ratio of flow difference to wood (ΔF/W) given by

$$\Delta F/W = \frac{F_f - F_c}{F_c \rho_{basic}\cdot\frac{\mathrm{t}}{1000\mathrm{kg}}} = \left(L/W - \frac{1+\varepsilon}{\rho_{basic}\cdot\frac{\mathrm{t}}{1000\mathrm{kg}}}\right) \quad \textbf{7.24}$$

If this ratio is zero then the value of Δu is zero, implying that bed compaction is solely influenced by gravity, wall friction and chips softening (kappa number) but not by interphase friction. As a case example, let us consider a basic density in

the infeed equal to 382 BDkg/m^3sub and a chips internal porosity of 0.85 (value that could be representative for the cook zone 1), with these data we calculate a L/W ratio of 4.84 m^3l/ BDt needed for obtaining ΔF/W equal to zero. Thus, operating with a higher L/W ratio would imply enhanced compaction, since ΔF/W becomes greater than zero and the same happens to Δu. On the contrary, a negative value for the new ratio implies a decompacting effect on the chips column. In any case, the proposed ratio requires accurately estimating or measuring the chips internal porosity at the vessel zone being monitored, since the value of ε significantly impacts the calculation.

7.2.2.1.4 Flow velocities

In principle, momentum balances allow us to derive expression for calculating either pressures or velocities. We have used these balances to compute pressure profiles; therefore, flow velocity profiles remain unknown and additional information is required. A simple solution is to approximate the velocity profile of each phase by the following equations valid in the steady-state,

$$u_{c,k} = \frac{F_c(t)}{A_k} \quad \textbf{7.25}$$

$$u_{f,k} = \frac{F_f(t)}{A_k} \quad \textbf{7.26}$$

To compensate for the lost momentum dynamics, a transport variable delay is introduced at the vessel outlet that observes the retention time of fluid parcels going through the vessel. Obviously, this approach is coherent as long as the bottom scrapper speed does not affect significantly the flow rate of the entering fluid parcels.

7.2.2.2 Woodchips degradation

To this point we have obtained equations to compute pressure and velocity variables. The former are coupled to the kappa number, phase densities, and volume fractions. The kappa number depends exclusively on the basic concentration of woodchips components. Density variables, instead, depend on the latter along with the concentrations of liquor components, such as dissolved organics, inorganic reagents, and inerts. Volume fractions depend on pressure variables and the kappa number due to the structure of the Härkönen correlation.

Expressions to compute concentration variables will be now derived from mass balances, in which a kinetic model is required to describe apparent wood reactions rates. Reaction rates in turn strongly depend on temperature variables, for which computation formulas will be derived from energy balances. The set of mathematical expressions to compute concentration and temperature variables will be referred as the wood delignification and carbohydrates degradation model, or simply wood degradation model.

This thesis uses the original Purdue kinetic model with some minor modifications and implements it under several simplifying assumptions (see Section 7.2.1). Those simplifications could be overcome in order to achieve a more detailed wood degradation model similar to the work of Wisnewski et al. (1997), Bhartiya et al. (2003) or Kayihan et al. (2005). However, computation times may become extremely long due to a considerable increase in the number of states. In this sense, current simplifications represent a proof of concept to the challenge of designing a practical, dynamic simulator for the CompactCooking™ G2 stage.

The wood substance is represented as composed of five reaction variant components, defined by the original Purdue model (see Section 4.1.1), plus one pseudo-invariant component, wood extractives. Liquor phases are composed of nine variant components plus one pseudo-invariant, dissolved extractives, and two invariants, inerts and water. Wood and liquor components are respectively indexed with the subscripts i and j given below

$$i \in \{L_F, L_S, C, GM, X, E\}$$

$$j \in \{NaOH, NaSH, NaOH_r, NaSH_r, INERT, DL_F, DL_S, DC, DGM, DX, DE\}$$

Since flows inside vessels are represented in a volume-basis, the concentration of water in liquor phases is kept constant at a particular value of the water density. On the contrary, the concentration of inerts can vary according to the values contributed by the entering streams. As already mentioned, extractives are instantaneously leached when entering the impregnator. The concentration of reaction variant components is obviously affected by the wood degradation model. Once mass and energy balances be established, we will obtain expressions to compute concentration and temperature variables as functions of the axial coordinate and time, which under our simplifying assumptions will comply with

$$\rho_{s,i} = \rho_i(z,t)$$

$$C_{e,j} = C_{f,j} = C_j(z,t)$$

$$T_s = T_e = T_f = T(z,t)$$

i.e., concentrations in the free and entrapped liquor region are held equal, and likewise phase temperatures are held equal due to an imposed condition of isothermal equilibrium.

The following headings will discuss how reaction kinetics, mass transfer (mass balances of phases components) and heat transfer (energy balances of the phases) influence the time-dependence variation of woodchips basic concentrations, liquors concentrations, and vessel temperature. Before starting this discussion, let us define some terms needed in the next headings.

7.2.2.2.1 Definitions

Equations 7.27 and 7.28 express respectively average retention times of chips and free liquor in an infinitesimal control volume

$$\tau_c = \frac{A\Delta z(1-\eta)}{F_c} = \frac{\Delta z(1-\eta)}{u_c} = \frac{\Delta z}{v_c} \quad \textbf{7.27}$$

$$\tau_f = \frac{A\Delta z\eta}{F_f} = \frac{\Delta z\eta}{u_f} = \frac{\Delta z}{v_f} \quad \textbf{7.28}$$

These terms will be used to formulate the components mass balances. Also, integrals of these values along the vessel length are used to delay the exiting signals of chips and free liquor phases, thus compensating the loss of true momentum dynamics that a fluid parcel would have experienced inside a vessel. As seen during preliminary results, these accessory elements result useful to improve model accuracy during dynamic simulation.

Energy balances, for sake of simplicity, are formulated using the volume-specific heat capacities of the multiple phases. Estimates of these capacities are given below

$$\bar{C}_{P,s} = C_{P,s}\sum_{i=1}^{5}\rho_i \quad \textbf{7.29}$$

$$\bar{C}_{P,c} = \bar{C}_{P,s} + \varepsilon\bar{C}_{P,e} \quad \textbf{7.30}$$

$$\bar{C}_{P,e} = C_{P,ls}\sum_{j=1}^{5} C_{e,j} + C_{P,s}\sum_{j=6}^{11} C_{e,j} + C_{P,w}\rho_w \quad \textbf{7.31}$$

$$\bar{C}_{P,f} = C_{P,ls}\sum_{j=1}^{5} C_{f,j} + C_{P,s}\sum_{j=6}^{11} C_{f,j} + C_{P,w}\rho_w \quad \textbf{7.32}$$

The numbering of the j index follows the order in which the components were listed above. Because of the simplifications on the wood degradation model, heat capacities of entrapped and free liquor phases are the same, i.e.,

$$\bar{C}_{P,e} = \bar{C}_{P,f} = \bar{C}_{P,l}$$

7.2.2.2.2 Reactions kinetics

The kinetic model represents an essential mathematical foundation for the complete process model. As indicated in Section 4.1, the Purdue model outperforms alternative models when balancing model complexity and accuracy, which justifies its use as a key element of this work. Furthermore, the Purdue model is implemented in a way, such that the WBL heating value can be estimated based on the liquor composition of dissolved wood components. Equations 7.33 to 7.39 describe the implemented Purdue model.

$$-R_i = e_f\left(k_{ai}{C_{NaOH}}^{1/2} + k_{bi}{C_{NaOH}}^{1/2}{C_{NaSH}}^{1/2}\right)(\rho_i - \rho_i^{\infty}) \quad \textbf{7.33}$$

$$k_{\Theta i} = k_{\Theta 0 i}\exp\left(\frac{-E_{\Theta i}}{R_g T}\right) \quad \Theta \in \{a, b\} \quad \textbf{7.34}$$

$$\rho_i^{\infty} = \alpha_i \rho_{i,fed} \quad \textbf{7.35}$$

$$R_{NaOH} = \gamma\left(\beta_{EAL}\left(R_{L_F} + R_{L_S}\right) + \beta_{EAC}(R_C + R_G + R_X)\right) \quad \textbf{7.36}$$

$$R_{NaSH} = \gamma\beta_{ESL}\left(R_{L_F} + R_{L_S}\right) \quad \textbf{7.37}$$

$$-R_{\Theta_r} = R_{\Theta} \quad \Theta \in \{NaOH, NaSH\} \quad \textbf{7.38}$$

$$-R_{D\Theta} = \gamma R_{\Theta} \quad \Theta \in \{L_F, L_S, C, GM, X\} \quad \textbf{7.39}$$

The reacted masses of sodium hydroxide and of sodium hydrosulfide are accounted to comply with mass balance constraints, though they actually undergo a chemical reaction that transforms these components in new ones. In

reality, these reacted mass quantities should be distributed among pulp and degraded wood components; however, modelling this distribution can be extremely difficult, and the error due this assumption, estimated as the ratio $\frac{x_{NaOH_r}+x_{NaSH_r}}{c}$, results to be less than 0.01% of the outflow bone dry pulp mass at the digester bottom.

Rigorously, the volume ratio γ should be defined equal to ε, meaning that the degraded wood substance is being transferred to the entrapped liquor phase. From there, dissolved organics could diffuse to the free liquor phase, and from the free liquor phase active inorganic reagents would diffuse back into the entrapped liquor phase to continue the delignification and carbohydrates degradation process. However, all these phenomena are simplified by defining the volume ratio as

$$\gamma = \frac{1-\eta}{\eta} \qquad \textbf{7.40}$$

which implies instantaneous diffusion of dissolved organics into the free liquor phase. Likewise, the concentration of inorganics reagents in the entrapped phase has been assumed equal to the concentration in the free region, representing also a kind of instantaneous diffusion process.

The error associated to the above simplifications cannot be estimated without an improved degradation model. Since diffusion is not considered in the current model, the calibration of effectiveness factor in the reaction rates will be compensating this phenomenon in a certain manner. However, it should be mentioned that the Arrhenius parameters in the rate constant expressions were originally correlated by Christensen (1982) against bulk concentration of reagents, not entrapped concentration. The reader can consult Nieminen et al. (2014a) for a detailed discussion about alternatives manners to regress kinetic models and the implications on the values of pre-exponential factor and energy barrier.

It is worth noting that if $\alpha_i \neq 0$ in Eq. 7.35, then implicit invariants components are created that represent “unreactive” portion of pulp polymers. In principle, no mass is unreactive, thus this term actually means a pulp fraction reacting at an infinitely slow rate. Modern kinetic models, such as Andersson, Nieminen, or fractal kinetic models, avoid introducing invariants components to describe the reactivity of pulp

polymers; however, we will represent a small fraction of lignin as unreactive in order to improve the calibration of the Purdue model. To some extent, this unreactive lignin portion is justifiable to better account for the residual lignin fraction, which would have a different reactivity than fast and slow lignin components of the original Purdue model. Nevertheless, the concepts of residual and unreactive lignin fraction are not equivalent, i.e., the former refers to the total lignin that remains at the end of the cook, while the latter represents an extremely slow reacting fraction remaining intact all along the digesting stage. The reader is encouraged to consult Andersson et al. (2003) for a comprehensive discussion on this issue.

7.2.2.2.3 Chips phase components continuity

The mass balance equation of woodchips components in an infinitesimal control volume can be established as follows

$$A(1-\eta)\Delta z\big(\rho_i(z,t+\Delta t)-\rho_i(z,t)\big) = F_c\Delta t\rho_i(z,t) - F_c\Delta t\rho_i(z+\Delta z,t) + R_i A(1-\eta)\Delta z\Delta t \quad \textbf{7.41}$$

multiplying by $\frac{1}{\Delta t\Delta z}$, taking limits as $\Delta t \to 0 \wedge \Delta z \to 0$, introducing Eq. 7.3, and clearing the temporal derivative we get

$$\frac{\partial \rho_i}{\partial t} = -\frac{u_c}{1-\eta}\frac{\partial \rho_i}{\partial z} + R_i = -v_c\frac{\partial \rho_i}{\partial z} + R_i \quad \textbf{7.42}$$

This simple PDE can be implemented into a Simulink S-function through the method of lines, i.e. discretizing the spatial derivates and maintaining continuity for the temporal derivate.

For practical reasons, however, we will implement an alternative form of this equation in terms of the average chips retention time in the control volume. Introducing Eq. 7.27 in 7.42, we arrive to the Eq. 7.43 that results from backward discretization and is actually implemented in the S-function representing vessel zones.

$$\frac{d\rho_{i,k}}{dt} = -\frac{1}{\tau_{c,k}}\big(\rho_{i,k}-\rho_{i,k-1}\big) + R_{i,k} \quad \textbf{7.43}$$

$$\tau_{c,k} = \frac{A_k\Delta z(1-\eta_k)}{F_c(t)} \quad \textbf{7.44}$$

7.2.2.2.4 Liquor phase components continuity

Analogously to the chips phase case, we postulate a mass balances equation for the free liquor phase components as follows

$$A\eta\Delta z\left(C_j(z,t+\Delta t)-C_j(z,t)\right) = F_l\Delta t C_j(z,t)-F_l\Delta t C_j(z+\Delta z,t)+R_j A\eta\Delta z\Delta t \quad \textbf{7.46}$$

multiplying by $\frac{1}{\Delta t\Delta z}$, taking limits as $\Delta t\to 0 \wedge \Delta z\to 0$, introducing Eq. 7.4, and clearing the temporal derivate we get

$$\frac{\partial C_j}{\partial t} = -\frac{u_l}{(\eta+\iota)}\frac{\partial C_j}{\partial z}+R_j = -v_l\frac{\partial C_j}{\partial z}+R_j \quad \textbf{7.45}$$

then we arrive to the final, backward-discretized form to implement in the vessel zone S-function by using Eq. 7.28

$$\frac{dC_{j,k}}{dt} = -\frac{1}{\tau_{l,k}}\left(C_{j,k}-C_{j,k-1}\right)+R_{j,k} \quad \textbf{7.47}$$

$$\tau_{l,k} = \frac{A_k\Delta z(1-\eta_k)}{F_l(t)} \quad \textbf{7.48}$$

Certainly, balance Eqs. 7.41 and 7.46 could be sophisticated, incorporating, for example, axial diffusion or disperssion effects, radial difussion between phases, or the derivatives of volume fractions. Moreover, we have established continuity equations for the components in the free liquor phase, omitting the balances of the entrapped liquor components under the assumption of instataneous diffusion. Althouhg the latter is obviously unreal, mass balances are consistent and the wood degradation model proves to be a good aproximation as the simulation results will show us in the next Chapter.

7.2.2.2.5 Thermal equilibrium energy balance

Assuming local thermal equilibrium of the multiple phases in the radial direction, we can establish the energy balance of an infinitesimal control volume as follows

$$\begin{aligned}\left(A(1-\eta)\Delta z\bar{C}_{P,c}+A\eta\Delta z\bar{C}_{P,f}\right)\left(T(z,t+\Delta t)-T(z,t)\right) &= F_c\Delta t\bar{C}_{P,c}T(z,t)+F_f\Delta t\bar{C}_{P,f}T(z,t)-F_c\Delta t\bar{C}_{P,c}T(z+\Delta z,t)\\ &-F_f\Delta t\bar{C}_{P,l}T(z+\Delta z,t)-A(1-\eta)\Delta z\Delta t\sum_i R_i H_{Ri}\end{aligned} \quad \textbf{7.49}$$

regrouping

$$A\Delta z\left((1-\eta)\bar{C}_{P,c}+\eta\bar{C}_{P,f}\right)\left(T(z,t+\Delta t)-T(z,t)\right) = \Delta t\left(F_c\bar{C}_{P,s}+F_l\bar{C}_{P,l}\right)\left(T(z,t)-T(z+\Delta z,t)\right) - A(1-\eta)\Delta z\Delta t\sum_i R_i H_{Ri} \quad \textbf{7.50}$$

multiplying by $\frac{1}{\Delta t\Delta z}$ and taking limits as $\Delta t \to 0 \wedge \Delta z \to 0$, we get

$$A\left((1-\eta)\bar{C}_{P,c}+\eta\bar{C}_{P,f}\right)\frac{\partial T}{\partial t} = -\left(F_c\bar{C}_{P,c}+F_f\bar{C}_{P,f}\right)\frac{\partial T}{\partial z} - A(1-\eta)\sum_i R_i H_{Ri} \quad \textbf{7.51}$$

under the assumption that $H_{Ri} = H_R \; \forall \; i$ and clearing the equation for the temporal derivative we get

$$\frac{\partial T}{\partial t} = -\frac{F_c\bar{C}_{P,c}+F_f\bar{C}_{P,f}}{A\left((1-\eta)\bar{C}_{P,c}+\eta\bar{C}_{P,l}\right)}\frac{\partial T}{\partial z} - \frac{(1-\eta)H_R\sum_i R_i}{(1-\eta)\bar{C}_{P,c}+\eta\bar{C}_{P,f}} \quad \textbf{7.52}$$

Then the final backward-discretized form to implement in the vessel zone S-function corresponds to

$$\frac{dT_k}{dt} = -\frac{\left(F_c\bar{C}_{P,c,k}+F_f\bar{C}_{P,f,k}\right)(T_k-T_{k-1})+A_k\Delta z(1-\eta)H_R\sum_i R_{i,k}}{A_k\Delta z\left((1-\eta_k)\bar{C}_{P,c,k}+\eta_k\bar{C}_{P,f,k}\right)} \quad \textbf{7.53}$$

Certainly, the Eq. 7.49 is valid under the typical, implicit simplifications of energy balances for chemical processes, such as constant mass-specific heat capacities, and negligible kinetic energy, potential energy, shaft work, and enthalpy of mixing*.

The assumption of multiphase thermal equilibrium in radial direction is not commonly hold when modelling digester vessels. Kayihan et al. (1996) used it when constructing a digester benchmark model for system identification and controller design, and later Castro & Doyle (2004a) to construct a complete pulp mill benchmark model for research on plant-wide control design. Although control design is outside the scope of the thesis, this assumption also allows us to considerably reduce model complexity and the numerical burden for the dynamic simulation, but at the obvious cost of losing model accuracy.

* For a clear explanation, the reader is encouraged to consult Skogestad (2009)

7.2.2.3 Quality variables (depolymerization)

To this point, we have obtained expressions to compute pressure, velocity, concentration and temperature variables. As the mathematical models show us, all of them are interdependent, reflecting the intrinsic complexity of phenomena inside the vessels. Indeed, to use these phenomenological models we still need to calculate the kappa number as a requirement of the Härkönen bed porosity correlation.

The kappa number and the pulp yield can be easily derived from states of the wood degradation model. Together with these quality variables (see Section 3.4), we would also like to model the cellulose average degree of polymerization (DP) and pulp intrinsic viscosity, but this will require additional states and equations. Once having models of the pulp intrinsic viscosity and the cellulose DP, several product quality variables could be modelled to describe physico-mechanical properties of the pulp sheet, such as zero-span, tensile and tear indices. Although models of these indices will not be implemented, we discuss their modelling and the need of empirical correlations. Besides the above, the WBL heating value and the blowline pulp carry-over represent important process quality variables, and we will leverage signals generated by the vessel models to estimate them.

The next headings show the mathematical expressions to compute the mentioned quality variables. The set of these equations may be regarded as a quality model of the process and its products built on top of the wood degradation model.

7.2.2.3.1 Kappa number

Experimentally, the kappa number has been found to linearly correlate with the lignin fraction in the pulp, as well as with the fraction of hexenuronic acids formed in the xylan during the kraft cook (see Section 3.2), i.e.,

$$\kappa \propto x_L \quad \wedge \quad \kappa \propto x_{HexA}$$

The lignin fraction in the pulp can be defined in relation to the states of the wood degradation model as follows

$$x_L = \frac{\rho_{L_F} + \rho_{L_S}}{\sum_i \rho_i} \tag{7.54}$$

The fraction of hexenuronic acids cannot be obtained directly from the model states, however, assuming that this fraction is proportional to the content of xylan, i.e.,

$$x_{HexA} \propto \frac{\rho_X}{\sum_i \rho_i} \tag{7.55}$$

we can postulate an expression to compute the kappa number by the following equation

$$\kappa = \theta_{L\kappa} \frac{\rho_{L_F} + \rho_{L_S}}{\sum_i \rho_i} + \theta_{X\kappa} \frac{\rho_X}{\sum_i \rho_i} \tag{7.56}$$

where $\theta_{L\kappa}$ and $\theta_{X\kappa}$ are empirical parameters to be regressed from laboratory data. To the best knowledge of the author, no researcher has attempted to determine a multivariable correlation of the kappa number to the fractions of lignin and xylan in the pulp. However, simple linear correlations between kappa and lignin fraction has been obtained by several authors, from which the value of $\theta_{L\kappa}$ can be taken and calibrated during model testing. It should be noted that those correlations show that the conversion factor $\theta_{L\kappa}$ strongly depends on the wood species and cooking process technology (see Section 4.4.1).

In principle, the kappa number is a function of the amount (and reaction time) of oxidizable (titratable) material by the permanganate method that is concentrated in a pulp sample. Thus, it could be explained as a multivariable correlation considering all pulp components and not limited only to major lumped polymer fractions, such as those represented by the Purdue model. For example, Simão et al. (2005) and Danielsson et al. (2006) have developed kinetic models to describe the change of the hexenuronic acids during the kraft cook; thus, one of this models may be included in our vessel model to improve the accuracy on the kappa modelling by restating Eq. 7.56 as

$$\kappa = \theta_{L\kappa} \frac{\rho_{L_F} + \rho_{L_S}}{\sum_i \rho_i} + \theta_{HexA\kappa}[HexA] \tag{7.57}$$

where $[HexA]$ represents minimolar basic concentration of hexenuronic acid in the pulp xylan, and $\theta_{HexA\kappa}$ can be set equal to 0.0862 (11.6^{-1}) BDkg/mmol, an empirical value found by Li & Gellerstedt (1997) (see Section 3.2). Although these researchers were not trying to identify a multivariable correlation, they did it indirectly by means of distinguishing permanganate consumption of lignin and

hexenuronic acids. Furthermore, they measured hexenuronic acids concentrations in hardwood (birch) kraft pulps of almost 70 mmol/BDkg, which would represent up to 6 units of uncertainty in a kappa number modelled without considering this contribution. The reader may consult Li (1999) for a comprehensive discussion of the experimental methods required to determine the parameter $\theta_{HexA\kappa}$. In terms of mathematical modelling, the approach described evidently implies more states, increasing model complexity, and longer time of implementation, and therefore it remains outside the scope of the thesis.

Although the Eq. 7.57 is of great importance to validate a vessel model against data from an on-line kappa analyzer, no author appears to have delved into this issue. Moreover, some authors, especially those who apply the Gustafson kinetic model, avoid disclosing the conversion equation of lignin to kappa (Agarwal & Gustafson, 1997; Rantanen et al. 2005; Rantanen, 2006; Laakso, 2008). Authors of vessel models built upon the Purdue kinetic model (Kayihan et al. (1996); Wisnewski et al. (1997); Bhartiya et al. (2003); Kayihan et al. (2005)) usually set $\theta_{L\kappa}$ equal to a value of 654 (0.00153^{-1}), apparently regressed from softwood kraft cooking data, without considering other contributions to the kappa number than from the lignin fraction. Michelsen (1995), who applies a simplified Purdue-like kinetics in his vessel model, originally used a value of 769 (0.0013^{-1}) but later changed it to 654 (0.00153^{-1}) (Michelsen & Foss, 1994, 1996). Alternative kinetic models developed by Gilarranz et al. (2002) and Sixta & Rutkowska (2006) used values of 625 (0.0016^{-1}) and 556 (0.0018^{-1}) respectively to model the kappa number in kraft cooking of eucalyptus species. Though the latter included the hexenuronic acids model of Danielsson et al. (2006), they do not seem to have considered hexenuronic acids contribution when modelling the kappa number. In any case, this contribution is known to be of less impact in kraft cooking of softwood pulp (see Section 3.2), which is the condition simulated and discussed in this work.

As a last remark, the uncertainty of the kappa modelling is transferred to the bed compaction model due to the link by the Härkönen correlation. This weakness could be easily overcome by regressing the correlation against lignin fraction (or even considering polysaccharides fractions) instead of kappa number; however, to the author's knowledge this has not been tried yet.

7.2.2.3.2 Cooking yield

Contrary to the subtleties when modelling the kappa number, pulp yield can be straightforward defined as

$$Y = \frac{\sum_i \rho_i}{\rho_{basic}} \tag{7.58}$$

where ρ_{basic} represents the initial basic density of a chips parcel when was fed; and $\sum_i \rho_i$, the current basic density given as the sum of basic concentrations over all pulp components.

As stated above, the Eq. 7.58 would describe the "true" yield of a chips parcel along its trajectory. However, if at the same time we consider $\sum_i \rho_i$ in the blowline and ρ_{basic} in the chips infeed, then we would be calculating an "apparent" cooked pulp yield, which may be compared against a mill estimate in the case that the consistency of the blowline is truly measured.

7.2.2.3.3 Degree of polymerization and intrinsic viscosity

Several product quality variables, such as tensile, tear and burst indices, depend on the DP of the pulp cellulose; therefore, modelling depolymerization phenomena becomes especially important for purposes of process optimization. However, few authors have derived a depolymerization model and/or included a model of this type as part of their vessel models (see Section 4.4.2). Expect Nieminen et al. (2015), other authors have based their models on a simplified approach of pulp cellulose depolymerization published by Kubes et al. (1983). Although they contributed practical solutions, their approaches conceal conceptual inaccuracies that demand a brief discussion and invite us to elaborate a more rigorous solution.

Kubes et al. (1983) derived and postulated the below equation to describe the temporal variation in the DP_w of the pulp cellulose during a batch cook,

$$\frac{1}{DP_{w,C}(t)} - \frac{1}{DP_{w,C}(t_0)} = k_{cs}\hat{C}_{OH}^{m}(t - t_0) \tag{7.59}$$

This expression is today known as the Ekenstam equation in reference to the first author who has theoretically derived it (af Ekenstam, 1936). Ekenstam arrived to this equation in order to explain the loss of viscosity in an acid solution of cellulose acetate over time. Kubes et al. rederived the equation trying to

understand the loss of pulp intrinsic viscosity during kraft cooking. In this sense, the last authors contributed the experimental determination of the depolymerization rate constant k_{cs} and the reaction order m on hydroxide concentration in the Ekenstam model. The foregoing required them to assume that the pulp intrinsic viscosity is solely proportional to the DP_w of the pulp cellulose, a relation that they stated as

$$DP_{w,C} = 0.75[\eta] \tag{7.60}$$

such that the Eq. 7.59 can be restated as

$$\frac{1}{[\eta](t)} - \frac{1}{[\eta](t_0)} = k_{cs}{}'\hat{C}_{OH}^{m}(t - t_0) \tag{7.61}$$

in order to explain straight lines of $\frac{1}{[\eta]}$ against time t observed from batch cooks at constant hydroxide concentration and temperature.

Agarwal & Gustafson (1993, 1997) derived the Eq. 7.61 with respect to time, and from there they justified a specific reaction rate of second-order on $[\eta]$ to describe the change of pulp intrinsic viscosity in a continuous vessel according to

$$R_{[\eta]} = -k_{cs}{}'\hat{C}_{OH}^{m}[\eta]^2 = \frac{d[\eta]}{dt}_{batch} \tag{7.62}$$

Miyanishi & Shimada (2001) followed a similar approach to the previous authors, but they derived instead the Eq. 7.59 with respect to time in order to elaborate a more fundamental approach modelling the change of DP, from which the intrinsic viscosity can be computed, with a specific reaction rate of second-order on $DP_{w,C}$ [*] according to

$$R_{DP_{w,C}} = -k_{cs}\hat{C}_{OH}^{m}DP_{w,C}^{2} = \frac{dDP_{w,C}}{dt}_{batch} \tag{7.63}$$

Then, in both approaches continuity equations were established to describe the temporal and spatial (axial) variation of the intrinsic viscosity and the cellulose DP respectively, which implies treating these variables as conserved quantities although they are not. This may be a good approximated solution, however, it is conceptually wrong because these variables depend on conserved quantities but are not conserved in themselves. The reader should remember that fundamental

[*] They actually formulated the depolymerization model in terms of DP_n

conserved quantities in the context of chemical processes are mass, energy and (linear) momentum. These quantities can be balanced to obtain equations describing the variation of concentration, temperature, and pressure or velocity variables, but the latter should not be balanced directly at least in the context of first-principles modelling. On the other hand, the differential equations of these approaches drag a numerical approximation error implicit in the left-hand side of the Ekenstam equation, an issue that has recently been motive for a thorough discussion by Calvini (2012) on the validity, interpretation and abuse of this equation.

Let us now present a truly rigorous first-principles model of the pulp cellulose depolymerization, from which is also possible to derive Eq. 7.59 and a similar expression to Eq. 7.61. First, we will discuss the relation between the pulp intrinsic viscosity and the cellulose DP in order to clarify the information needed in a depolymerization model that allows simulating the pulp intrinsic viscosity. Later, first-principles balance equations will be established from where it is possible to derive an expression to compute the cellulose DP.

The cellulose DP is usually estimated based on a measurement of the intrinsic viscosity of a pulp sample dissolved in Cuen. However, the measured property depends not only on the cellulose, but rather on all the polymers constituting the pulp. Assuming that the specific viscosity is an additive property in a solution containing different polymers[*], the intrinsic viscosity of the pulp in Cuen can be explained as a weighted average on intrinsic viscosities of pure (isolated) pulp polymers in the same solvent according to

$$[\eta] = \sum_i x_i [\eta]_i \qquad \textbf{7.64}$$

where $[\eta]_i$ represents the intrinsic viscosity of a pure polymer contained in the pulp, such as cellulose, xylan, glucomannan or lignin, and x_i corresponds to the mass fraction of the polymer component in the pulp. Further, the intrinsic viscosity of pure polymers can be related to their viscosity-average degree of polymerization (DP_v) by the Mark-Houwink equation, i.e.,

$$[\eta]_i = K_i {DP_{v,i}}^{\alpha_i} \qquad \textbf{7.65}$$

[*] The reader may consult Kulicke & Clasen (2004) to delve into this issue

From the above, it is clear that the pulp intrinsic viscosity could be computed based on a depolymerization model able to describe the change of DP_v for each polymer component of the pulp, assuming that Mark-Houwink parameters are known for each of them. Several researchers have determined values of Mark-Houwink parameters of pure cellulose dissolved in Cuen (see Section 4.2.2), but no attempt has been found in the published literature to determine these parameters for other pulp polymers. To overcome the lack of information, a practical approach comprises neglecting the contribution from the lignin to the pulp intrinsic viscosity, as well as neglecting depolymerization phenomena of hemicelluloses, i.e., considering a constant DP_v in glucomannan and xylan. Further, we can assume that the Mark-Houwink parameters of hemicelluloses are the same to those of cellulose and that their DP_v can be described by a common value, $DP_{v,H}$. Thus, we could estimate the pulp intrinsic viscosity as follows

$$[\eta] = K_C {DP_{v,C}}^{\alpha_C} x_C + K_C {DP_{v,H}}^{\alpha_C} x_H \qquad \textbf{7.66}$$

As mentioned, several different values of K_C and α_C have been determined, indicating a high uncertainty in this issue. However, da Silva Perez & van Heiningen (2002, 2015) have validated an expression equivalent to Eq. 7.66 using the Mark-Houwink parameters of cellulose in Cuen given in Evans & Wallis (1989) by means of experimentally estimating the intrinsic viscosity contribution from to the hemicellulose fraction. Therefore, we can use the values derived from their equation (Eq. 7.67) as an initial guess to calibrate the pulp intrinsic viscosity model.

$$DP_v = \left(\frac{1.65[\eta] - 116 x_H}{x_C} \right)^{1/0.9} \qquad \textbf{7.67}$$

To this point, the reader may note that the Eq. 7.66 plays an analogous role to the Eq. 7.57 in the modelling of the kappa number. That is, both act as filters of underlying fundamental models providing a comparable output signal for validation of the process model against industrial data, where the underlying models depend on remainder phenomenological variables of the process, including flow rates, temperatures and concentrations.

Having established a relation between cellulose DP and pulp intrinsic viscosity variables, we can now concentrate on the derivation of a first-principles model to

describe the time-dependence variation of the former variable within an infinitesimal control volume of a vessel. The essential of this derivation is to think about the cellulose polymer as composed of a large number of polymer molecules representing a distribution of chain lengths, this led us to postulate a kind of population mass balance for every molecule as follows

$$A\Delta z(1-\eta)\left(\rho_{C,n_m}(z,t+\Delta t)-\rho_{C,n_m}(z,t)\right) = F_c\Delta t\rho_{C,n_m}(z,t)-F_c\Delta t\rho_{C,n_m}(z+\Delta z,t)+R_{C,n_m}A\Delta t\Delta z(1-\eta) \quad \textbf{7.68}$$

where ρ_{C,n_m} represents the basic concentration accounting for a cellulose molecule composed of n_m anhydrous glucose units (AGU), and R_{C,n_m} the volume-specific depolymerization rate of this polymer molecule. This basic concentration could be straightforward estimated as the molecular mass of the monomer times the number of monomers in the molecule. However, we will considered instead the number of glyosidic bonds to define an estimate according to

$$\rho_{C,n_m} \approx \bar{w}_{AGU}(n_m-1) \quad \textbf{7.69}$$

where $\bar{w}_{AGU}$ denotes the monomer molar mass per unit of chip volume. Choosing the number of bonds instead of monomers for estimating the mass of a polymer may appear as an arbitrary decision, nonetheless, it is phenomenologically meaningful because it permits to define mass balances strictly for polymer molecules, and the depolymerization rate becomes intrinsically zero when monomers in a polymer molecule are completely unbound.

Now, we can sum balance equations over all polymer molecules and divide by the molecular mass of the monomer, thus obtaining the following equation

$$A\Delta z(1-\eta)\big(n(z,t+\Delta t)-n(z,t)\big) = F_c\Delta t n(z,t)-F_c\Delta t n(z+\Delta z,t)+R_{sc,n}A\Delta t\Delta z(1-\eta) \quad \textbf{7.70}$$

where n corresponds to the total number of glyosidic bonds in the cellulose fraction per unit chip volume and $R_{cs,n}$ to the sum of specific depolymerization rates over every polymer molecule according to Eq 7.71 and 7.72 respectively.

$$n = \frac{1}{\bar{w}_{AGU}}\sum_{m=1}^{M}\rho_{C,n_m} = \sum_{m=1}^{M}(n_m-1) \quad \textbf{7.71}$$

$$R_{cs,n} = \frac{1}{\overline{w}_{AGU}} \sum_{m=1}^{M} R_{C,n_m} \quad \textbf{7.72}$$

Assuming that the depolymerization rate of a polymer molecule is first-order on its mass and m-order on molar hydroxide concentration, i.e.,

$$R_{C,n_m} = -k_{C,n_m} \hat{C}_{OH}^{m} \rho_{C,n_m} = -k_{C,n_m} \hat{C}_{OH}^{m} \overline{w}_{AGU} (n_m - 1) \quad \textbf{7.73}$$

and that the depolymerization rate constant is the same for every polymer molecule

$$k_{cs} \equiv k_{C,n_m} \quad \textbf{7.74}$$

then we can restate Eq. 7.75 as

$$R_{cs,n} = -k_{cs} \hat{C}_{OH}^{m} n \quad \textbf{7.75}$$

Considering the equivalences given above, we continue transforming the balance expressed in Eq. 7.70 into a differential equation multiplying it by $\frac{1}{\Delta t \Delta z}$ and taking limits as $\Delta t \to 0 \wedge \Delta z \to 0$, thus we get

$$\frac{\partial n}{\partial t} = -\frac{F_c}{A(1-\eta)} \frac{\partial n}{\partial z} + R_{cs,n} \quad \textbf{7.76}$$

From Eq. 7.71 we can also derive an expression to relate the total number of glyosidic bonds to the cellulose number-average degree of polymerization (DP_n) according to

$$n = \sum_{m=1}^{M} (n_m - 1) = N - M = N\left(1 - \frac{1}{DP_n}\right) \quad \textbf{7.77}$$

and applying the rule of the chain we get below the differential of the total number of bonds

$$dn = \frac{N}{DP_n{}^2} dDP_n + \left(1 - \frac{1}{DP_n}\right) dN \quad \textbf{7.78}$$

This expression of the differential dn is introduced in Eq. 7.76 in order to obtain a PDE describing the cellulose depolymerization in terms of DP_n instead of n assuming that dN can be neglected. The latter differential would represent anhydrous glucose units being dissolved in the cooking liquor; however, since the total number of monomers is considerably large, neglecting this term should not

affect the computation of dn to a great extent. After some algebraic manipulation and using Eq. 7.3, we get a first-principles, dynamic equation to describe the variation of the cellulose DP_n along a vessel as follows

$$\frac{\partial DP_n}{\partial t} = -\frac{u_c}{1-\eta}\frac{\partial DP_n}{\partial z} + R_{cs,DP_n} = -v_c\frac{\partial DP_n}{\partial z} + R_{cs,DP} \quad \textbf{7.79}$$

$$R_{cs,DP_n} = -k_{cs}\hat{C}_{OH}^{m}\left(1-\frac{1}{DP_n}\right)DP_n{}^2 \quad \textbf{7.80}$$

Finally, we backward-discretized the PDE by the method of lines, and by using Eq. 7.28 we get below an equation form to implement in the vessel zone S-function

$$\frac{dDP_k}{dt} = -\frac{1}{\tau_{c,k}}(DP_k - DP_{k-1}) + R_{cs,k} \quad \textbf{7.81}$$

$$R_{cs,k} = -k_{cs,k}\left(\frac{C_{NaOH,k}}{w_{NaOH}}\right)^m\left(1-\frac{1}{DP_k}\right)DP_k{}^2 \quad \textbf{7.82}$$

$$\tau_{c,k} = \frac{A_k\Delta z(1-\eta_k)}{F_c(t)} \quad \textbf{7.83}$$

The depolymerization model has been rigorously derived from mass balances of polymer molecules; therefore, we may be tempted to think that the depolymerization rate constant should be identical to one of the degradation rate constants considered in the Purdue kinetic model. However, this interpretation becomes clearly shortsighted if we start thinking in the complex mechanisms involve in the dissolution of pulp polysaccharides, i.e., the reaction mechanisms of peeling, stopping and alkaline hydrolysis, as well as the mass transfer mechanisms that explain reacted polysaccharide mass dissolving into the cooking liquor. The wood degradation represented by the Purdue model is an apparent, average rate of all the above phenomena, including reaction kinetics and mass transfer in the solid-liquid interphase (between wood substance and entrapped liquor); instead, the depolymerization model aims mainly to capture an average rate of peeling and alkaline hydrolysis reactions, as they are the principal causes of the shortening in polymers chains that decrease the degree of polymerization. Indeed, it is surprising to compare the rate constant determined by Kubes et al. (1983) for describing the kinetics in the loss of pulp intrinsic viscosity against the rate constant regressed by Nieminen et al. (2014) specifically for the cellulose alkaline hydrolysis reaction. Both rate constant are

Arrhenius form with activation energies of 179 and 175 kJ/mol, and pre-exponential factors equal to exp(41.2) and exp(36.43) respectively. This similitude in values is remarkable and is not found when comparing the rate constant of Kubes et al. to those of cellulose in the Purdue model.

As a final remark, let us show that the Ekenstam equation can be easily obtained from the depolymerization model here elaborated. Let us consider a batch process where the polymer DP_n variation would be described as follows

$$\frac{dDP}{dt} = -k\left(1 - \frac{1}{DP}\right)DP^2 \qquad \textbf{7.84}$$

but integrating both sides of the equation

$$\int_{DP_0}^{DP} \frac{1}{\left(1-\frac{1}{DP}\right)DP^2}\, dDP = -\int_{t_0}^{t} k dt \qquad \textbf{7.85}$$

we get the following expression

$$\ln\left(1 - \frac{1}{DP}\right) - \ln\left(1 - \frac{1}{DP_0}\right) = -\int_{t_0}^{t} k d\tau_c \qquad \textbf{7.86}$$

Now, applying a numerical approximation of first-order Taylor expansion around x>1 in the left-hand side terms of the equation, i.e.,

$$\ln\left(1 - \frac{1}{x}\right) \approx -\frac{1}{x} \quad x > 1 \qquad \textbf{7.87}$$

we arrive to the common Ekenstam expression

$$\frac{1}{DP(t)} - \frac{1}{DP_0} = \int_{t_0}^{t} k dt \qquad \textbf{7.88}$$

7.2.2.3.4 Zero-span, tensile and tear indices

For market pulp producers, the quality variables of the product may be of greater interest than those of the process concerning their optimization. However, little research has been done regarding modelling of product quality variables (see Section 4.4), such as zero-span, tensile, tear and burst indices of the pulp sheet, in comparison to an extensive effort in modelling digesting vessels, which primarily entails the modelling of process variables.

Based on the findings of Molin & Teder (2002), we can postulate the following empirical models for tensile and tear indices at a particular pulp beating degree*

$$I_{tensile} = \left(\theta_0 + \theta_1 \frac{x_C}{x_H}\right)\left(1 - e^{-\frac{[\eta]}{\theta_2}}\right) \quad \textbf{7.89}$$

$$I_{tear} = \left(\theta_0 + \theta_1 \frac{x_C}{x_H}\right)\left(1 - e^{-\frac{[\eta]}{\theta_2}}\right) \quad \textbf{7.90}$$

The left factor represents the linear correlation between cellulose/hemicellulose ratio as stated by Molin & Teder; the right factor instead, a known behavior of exponential drop in pulp sheet properties after certain shortening of cellulose chains. The empirical parameters of Eqs. 7.89 and 7.90 would be ideally calibrated by means of laboratory experiments, however, it may be also possible to adjust them by exploiting mill signals with an adequate sampling frequency that capture the process dynamics.

The zero-span index can be modelled following the approach of Emsley et al. (1997), who claim that this property can be dynamically described according to

$$\frac{dI_{zspan}}{dt} = \theta_1 \frac{1}{DP^2}\frac{dDP}{dt} + \theta_2 DP \quad \textbf{7.91}$$

where the empirical constant are positive defined and would be obtained from laboratory experiments, or by exploiting mill signals as previously explained.

7.2.2.3.5 Heating value of cooking liquors

The process optimizer will consider the energy flow sent to the recovery line in the WBL stream; therefore, an estimate is needed of the heating value in cooking liquors. Leveraging the information of dissolved wood components generated by the kinetic model, we can simply model the higher heating value of the WBL stream as follows

$$HHV_{WBL}\left[\frac{\text{MJ}}{\text{kg dry}}\right] = HHV_L \tilde{x}_{DL} + HHV_{CH}\tilde{x}_{DCH} + HHV_E \tilde{x}_{DE} \quad \textbf{7.92}$$

The dilution effect of inerts is implicitly accounted since mass fractions are in a dry-basis over the total dry mass of the WBL stream. The estimate could be improved to distinguish between different carbohydrates fractions, including

* PFI revolutions

cellulose, glucomannan and xylan, but no information about HHV of these pure polymers was found.

7.2.2.3.6 Blownline pulp carry-over

Also for purposes of process optimization, a simple estimate of the blowline pulp carry-over is formulated based on the information generated by the digester model.

$$carryover_{pulp}\left[\frac{\text{kgDS}}{\text{BDt}}\right] = \frac{\sum_j x_j}{\frac{c}{1000\,\frac{\text{kg}}{\text{t}}}} \tag{7.93}$$

Although pulp does not carry over itself all the dissolved matter, this estimate becomes to represent a maximum limit or the worst case scenario as if all dissolved matter would be sorbed in the pulp.

7.2.2.4 Top feeding

To solve the differential equations constituting vessel models, we need to define boundary conditions at the origin of the axial dimension ($z = 0$) to represent the information of effective inflow streams at the chips bed top. In the case of concentration variables, the boundary values are directly given by the signals of chips and liquor streams; for temperature variables, instead, we need to estimate a thermal equilibrium value shared by all the streams already before entering the bed, such that the assumption of thermal equilibrium is not violated at its top.

Beside boundary conditions, the variable coefficients in PDEs must be updated along the time of integration (simulated time), either with information from internal signals, as in the case of the digester subsystem, or from external signals acting as inputs of the process simulator, as in the case of the impregnator subsystem. Because we are not dynamically solving momentum balances, velocity variables (equivalent to retention times) appears as variable coefficients that depend on the flow rates of entering streams to the vessels. In the digester subsystem, flow rates are trivially computed; in the impregnator case instead, externals signals, such as the chip meter speed or the weightometer reading, must be converted into flow rates of chips and liquor.

The next headings will now clarify the above ideas and give their mathematical formulations.

7.2.2.4.1 Impregnator chips infeed

The chip meter is designed to deliver a specific volume of chips per revolution, let us denote it by

$$\theta_{cm} \ [=] \frac{\mathrm{m^3st}}{\mathrm{rev}} \tag{7.94}$$

considering the chips compaction within the chip chute, the infeed flow of chips can be estimated as

$$F_c = s_{cm}\theta_{cm}(1-\eta_{chute}) = s_{cm}\theta_{cm}\frac{\rho_{bulk}}{\rho_{basic}} \tag{7.95}$$

Alternatively, we may estimate the same flow based on the reading of a weightometer as

$$F_c = \tilde{F}_{wm}(1-m^{wet})\frac{1}{\rho_{basic}} \tag{7.96}$$

This latter instrument is usually placed in the conveyor belt, feeding the impregnator, just before the chip chute, thus the delay between the above estimates should be neglegible. Further, the difference between these estimates quantifies an uncertainty interval associated to measurement errors in the determination of basic density, bulk density and chips moisture, as well as errors in the measurement themselves of the chip meter speed and the weight in the conveyor belt.

The chips infeed implies a water inflow associated to moisture cointained whithin chips, i.e., their moisture content. The volumetric flow of water is a portion of the volumetric chips flow according to

$$F_w = \varepsilon_w F_c \tag{7.97}$$

where ε_w represents the volume fraction of water. Naturally, we would expect this fraction to comply with

$$\varepsilon = \varepsilon_w + \varepsilon_{air} \tag{7.98}$$

i.e., the chips internal void volume (chips porosity) is filled either with water or air. The moisture content is usually defined on the basis of the total wet mass of the sample. However, in the context of wood processing, it may also be defined on

the basis of the bone dry wood mass. Equations 7.99 and 7.100 express both definitions respectively.

$$m^{wet} = \frac{F_w \rho_w}{F_c \rho_{basic} + F_w \rho_w} = \frac{\varepsilon_w \rho_w}{\rho_{basic} + \varepsilon_w \rho_w} \quad \textbf{7.99}$$

$$m^{dry} = \frac{F_w \rho_w}{F_c \rho_{basic}} = \frac{\varepsilon_w \rho_w}{\rho_{basic}} \quad \textbf{7.100}$$

Thus, the value of ε_w needed to calculate the flow of water can be estimated by one of the above equations depending on the available measurements at the mill according to

$$\varepsilon_w = \frac{m^{wet} \rho_{basic}}{(1 - m^{wet}) \rho_w} = \frac{m^{dry} \rho_{basic}}{\rho_w} \quad \textbf{7.101}$$

$$m^{dry} = \frac{m^{wet}}{(1 - m^{wet})} \qquad \text{V} \qquad m^{wet} = \frac{m^{dry}}{(1 + m^{dry})} \quad \textbf{7.102}$$

The water flow is mixed with the top liquor, the recycle stream to the upper part of the impregnator, and the resulting stream corresponds to the total liquor flowing through the chips column in the impregnator, assuming that chips are completely and instantaneously penetrated with liquor just entering the impregnator. The error in the latter assumption can be estimated, though it requires some previous discussion on the concepts of moisture and penetration degree.

Equation 7.12 express an estimate of the internal chips porosity ε based on the density of the wood substance and the basic density of the chips. In reference to this value, the penetration degree can be expressed as

$$P_\varepsilon = \frac{\varepsilon_w}{\varepsilon} \quad \textbf{7.103}$$

and the maximum moisture content can be estimated for each moisture definition according to

$$m_{max}^{wet} = \frac{\varepsilon \rho_w}{\rho_{basic} + \varepsilon \rho_w} \quad \textbf{7.104}$$

$$m_{max}^{dry} = \frac{\varepsilon \rho_w}{\rho_{basic}} \quad \textbf{7.105}$$

Now, let us consider a case example with the following data: basic density equal to 382 kg/m^3, water density at 1000 kg/m^3, wood substance density of 1500 kg/m^3, and moisture content of 57.3% on wet-basis (134% on dry-basis). Hence,

we estimate a chips internal porosity of 0.745 by Eq. 7.12, a water volume fraction equal to 0.513 by Eq. 7.101, and an initial penetration degree of 68.8% by Eq. 7.103. Logically, the higher the moisture content the smaller the assumption error of instantaneous penetration. Further, the estimated maximum moisture content is equal to 66.1% on wet-basis (195% on a dry-basis), and this value could be compared against laboratory measurement to assess the validity of the equations.

Chips moisture represents a significant disturbance for the digesting process as it impacts on the control of L/W ratios and the wash zone DF. To aid mill personnel weighing the disturbance load associated, we can defined a new monitored variable that scales the chips moisture to its maximum possible value, which we may referred as the relative moisture content given by Eqs. 7.106 and 7.107 for each definition of moisture.

$$m_{rel}^{wet} = \frac{m^{wet}}{m_{max}^{wet}} \tag{7.106}$$

$$m_{rel}^{dry} = \frac{m^{dry}}{m_{max}^{dry}} \tag{7.107}$$

Introducing the estimates of the initial moisture and maximum moisture given above, we arrive to the following relations

$$m_{rel}^{dry} = \frac{\varepsilon_w}{\varepsilon} = P_\varepsilon \tag{7.108}$$

$$m_{rel}^{wet} = \frac{\varepsilon_w}{\varepsilon}\frac{\left(1+\frac{\varepsilon\rho_w}{\rho_{basic}}\right)}{\left(1+\frac{\varepsilon_w\rho_w}{\rho_{basic}}\right)} = P_\varepsilon\frac{\left(1+m_{max}^{dry}\right)}{\left(1+m^{dry}\right)} \tag{7.109}$$

which show us that the penetration degree could be directly estimated from laboratory measurements of the chips (current) moisture and maximum moisture content.

7.2.2.4.2 Vessels top temperatures

The assumption of thermal equilibrium requires calculating a common temperature value for all the streams entering a vessel that will form part of a bed, and this value represents a boundary condition at the top of the chips bed. The values of the chips bed top temperatures can be computed by means of steady-state enthalpy balances.

The enthalpy balance in the impregnator case is

$$\tilde{F}_{imp\ top} h_{imp\ top} = \tilde{F}_{imp\ fed} h_{imp\ fed} + \tilde{F}_{top\ liq} h_{top\ liq} \quad \textbf{7.110}$$

and the equation terms are

$$\tilde{F}_{top\ liq} h_{top\ liq} = F_{top\ liq} \bar{C}_{P,top\ liq} \left(T_{top\ liq} - T_{ref}\right) \quad \textbf{7.111}$$

$$\tilde{F}_{imp\ fed} h_{imp\ fed} = \left(F_c \rho_{basic} C_{P,s} + \tilde{F}_w C_{P,w}\right)\left(T_{imp\ fed} - T_{ref}\right) \quad \textbf{7.112}$$

$$\tilde{F}_{imp\ top} h_{imp\ top} = \left(F_c \rho_{basic} C_{P,s} + \tilde{F}_w C_{P,w} + F_{top\ liq} \bar{C}_{P,top\ liq}\right)\left(T_{imp\ top} - T_{ref}\right) \quad \textbf{7.113}$$

introducing the terms expressions in the balance equation we get

$$T_{imp\ top} = \frac{\left(F_c \rho_{basic} C_{P,s} + F_w \rho_w C_{P,w}\right) T_{imp\ fed} + F_{top\ liq} \bar{C}_{P,top\ liq} T_{top\ liq}}{F_c \rho_{basic} C_{P,s} + F_w \rho_w C_{P,w} + F_{top\ liq} \bar{C}_{P,top\ liq}} \quad \textbf{7.114}$$

In the case of digester, even if the thermal equilibrium assumption is discarded we will still need to model the heat transfer involved in the mixing of the cooking liquor with the MP steam. The enthalpy balance for the digester case is

$$\tilde{F}_{dig\ top} h_{dig\ top} = \tilde{F}_{dig\ fed} h_{dig\ fed} + \tilde{F}_{steam} h_{steam} \quad \textbf{7.115}$$

and the terms of the equation are expanded as

$$h_{steam} = C_{P,w}\left(T_{sat}(P_{steam}) - T_{ref}\right) + \lambda_{steam}(P_{steam}, T_{steam}) \quad \textbf{7.116}$$

$$\lambda_{steam} = h_{sup\ steam}(P_{steam}, T_{steam}) - h_{sat\ liq}(T_{sat}(P_{steam})) \quad \textbf{7.117}$$

$$\tilde{F}_{dig\ fed} h_{dig\ fed} = \left(F_c \bar{C}_{P,c} + F_f \bar{C}_{P,f}\right)\left(T_{dig\ fed} - T_{ref}\right) \quad \textbf{7.118}$$

$$\tilde{F}_{dig\ top} h_{dig\ top} = \left(F_c \bar{C}_{P,c} + F_f \bar{C}_{P,f} + \tilde{F}_{steam} C_{P,w}\right)\left(T_{dig\ top} - T_{ref}\right) \quad \textbf{7.119}$$

which introduced in the previous balance give

$$T_{dig\ top} = \frac{\left(F_c \bar{C}_{P,c} + F_f \bar{C}_{P,f}\right) T_{dig\ fed} + \tilde{F}_{steam}\left(C_{P,w} T_{sat} + \lambda_{steam}\right)}{F_c \bar{C}_{P,c} + F_f \bar{C}_{P,f} + \tilde{F}_{steam} C_{P,w}} \quad \textbf{7.120}$$

Should be noted that λ_{steam} is the latent heat of the steam plus the sensible heat due to its superheated condition, thus it is referred as the effective latent heat. This term can be calculated by imaging any reversible path from the reference

temperature to the steam temperature, since the result is independent of the chosen path.

Equations 7.114 and 7.120 are implemented in one S-function per vessel. The S-function for the impregnator contains also the formulas needed to compute the chips infeed flow rate based on the chip meter speed, as well as the water inflow rate associated to the chips moisture. The S-functions for the digester is linked to a code library that implements steam tables, thus the effective latent heat can be computed for changing conditions of temperature and pressure in the MP steam signal.

7.2.2.5 Digester wash zone

The plug flow motion is presumably an inaccurate model to apply in the wash zone of the digester, especially to describe the flow of liquors. The wash liquor enters radially and also at the bottom of the digester, where it flows counter-currently to the chips motion. The liquor from the cook zone 2 flowing co-currently with the chips stream will be partially extracted and partially mixed with the wash liquor. Considering the above, at least the co-current plug flow model, assumed in the remainder zones, should be change to a counter-current representation. However, since we are not modelling diffusion between entrapped and free liquor, even a counter-current plug flow description would not properly “wash” the pulp. Thus, an ideal washer model is used as an alternative approach to describe this zone.

Consequently, the wash zone is modelled as a single, steady-state, washing operation. Based on the equations of an ideal, single-stage, washing operation[*], the standard terms in a mass flow basis are defined as follows

$$V_1 = \frac{F_{low\ ext}\rho_{low\ ext}}{\tilde{F}_{pulp}} \quad \textbf{7.121}$$

$$L_0 = \frac{\tilde{F}_{dig\ bot}(1-c_{dig\ bot})}{\tilde{F}_{pulp}} \quad \textbf{7.122}$$

$$V_2 = \frac{F_{wash}\rho_{wash}}{\tilde{F}_{pulp}} \quad \textbf{7.123}$$

$$L_1 = \frac{\tilde{F}_{blow}(1-c_{blow})}{\tilde{F}_{pulp}} \quad \textbf{7.124}$$

[*] Also referred as a leaching operation in the lexicon of unit operations in chemical engineering

$$L_1 = L_0 + V_2 - V_1 \tag{7.125}$$

$$c_{blow} = \frac{1}{L_1 + 1} \tag{7.126}$$

$$X_{1,j} = X_{0,j} - DR\left(X_{0,j} - Y_{2,j}\right) \tag{7.127}$$

$$Y_{1,j} = \frac{\left(L_0 Y_{0,j} + V_2 Y_{2,j} - L_1 X_{1,j}\right)}{V_1} \tag{7.128}$$

$$x_{blow,j} = X_{1,j}(1 - c_{blow}) \tag{7.129}$$

$$x_{low\ ext,j} = Y_{1,j} \tag{7.130}$$

The above describes the overall mass transfer occurring in the wash zone. The displacement ratio acts as an efficiency parameter, which would be affected by the dilution factor, diffusion rates, and retention times of the pulp and liquor streams but which is held as a constant here for sake of simplicity.

For obvious reasons, heat transfer is usually not described when calculating washing operations; however, we do need to consider the variation of temperature variables. A simple approach is to apply enthalpy balances to determine the temperature of the filtrate and the pulp out, representing the lower extraction and blowline streams respectively. The equations used are given below

$$T_{blow} = \frac{1}{\tilde{F}_{blow}\left((1-c_{blow})C_{P,w} + c_{blow}C_{P,s}\right)}\Big(\tilde{F}_{dig\ bot}\left((1 - c_{dig\ bot})C_{P,w} + c_{dig\ bot}C_{P,s}\right)T_{dig\ bot} - DR\left(\tilde{F}_{dig\ bot}(1 - c_{dig\ bot})C_{P,w}T_{dig\ bot} - F_{wash}\bar{C}_{P,wash}T_{wash}\right)\Big) \tag{7.131}$$

$$T_{low\ ext} = \frac{1}{\tilde{F}_{low\ ext}C_{P,w}}\Big(\tilde{F}_{dig\ bot}\left((1 - c_{dig\ bot})C_{P,w} + c_{dig\ bot}C_{P,s}\right)T_{dig\ bot} + F_{wash}\bar{C}_{P,wash}T_{wash} - \tilde{F}_{blow}\left((1 - c_{blow})C_{P,w} + c_{blow}C_{P,s}\right)T_{blow}\Big) \tag{7.132}$$

In the above equations, enthalpy is assumed to be exchanged only due to displacement of the liquor (free and entrapped phases). The liquor and chips streams flowing down from the cook zone 2 has been lumped and converted to a mass flow variable that is denoted by $\tilde{F}_{dig\ bot}$. Since we have to convert all flow

variables from volumetric basis into mass basis and perform balances in the latter, we lose the information about the density of the exiting streams.

The estimate of the specific heat capacity could be improved in the case of liquor phases; however, the preferable alternative for further development is including a description of diffusion and applying a counter-current plug flow model to represent the wash zone. In this latter scenario, the ideal washer model would be used solely to describe the pressure diffuser.

7.2.2.6 Levels

Modelling a vessel and its variations of liquor and chips levels represents a challenging task. Michelsen (1995) seems to have been the only author to originally disclose an idea to achieve it. By using a continuous stirred-tank reactor (CSTR) model as a "top section", he was able to simulate variations of levels up to a certain upper threshold* in the vessel. The latter is due to the fact that the plug flow model, which axially describes the remainder vessel length, requires an origin that represents both phases coexisting at the same level. To overcome this limitation, we will apply an alternative modelling approach exploiting the coupling of overall mass balances with continuity statements, such that the extension of the plug flow model is dynamically changed. The origin of the plug flow model will thus represent a matching level, which may be equal to the liquor level if the chips level is higher or to the chips level on the contrary.

Let us denote the overall entering and exiting streams of vessel by the following subscripts

$$i \in \{input\ streams\ of\ the\ vessel\}$$

$$o \in \{output\ streams\ of\ the\ vessel\}$$

such that the variation in total masses of chips and free liquor phases are described according to Eqs. 7.133 and 7.134

$$\frac{dM_c}{dt} = \sum_i (F_c \rho_c)_i - \sum_o (F_c \rho_c)_o - \tilde{F}_t \qquad \textbf{7.133}$$

$$\frac{dM_f}{dt} = \sum_i \left(F_f \rho_f\right)_i - \sum_o \left(F_f \rho_f\right)_o + \tilde{F}_t \qquad \textbf{7.134}$$

* The bottom in the definition of his vessel "top section"

where the term $\tilde{F}_t$ lumps the overall mass transfered from the chips phase to the free liquor phase. On the other hand, these total masses should comply with

$$M_c = \text{abs} \int_{z_{end}}^{z(h_c)} A(1-\eta)\rho_c dz \tag{7.135}$$

$$M_f = \text{abs} \int_{z_{end}}^{z(h_l)} A\eta\rho_f dz \tag{7.136}$$

where h_c and h_l denote the levels of chips and liquor from the vessel bottom (z_{end}), and $z(h_c)$ and $z(h_l)$ are their associated values as measured from the vessel top. Therefore, after having initialized the dynamic simulation at a certain (known) pair of levels and total masses for each phase, we can change the origin of the plug flow model according to

$$z_{match} = \max\big(z(h_c), z(h_l)\big) = z\big(\min(h_c, h_l)\big) \tag{7.137}$$

That is, the chips and liquor levels are computed by implicitly solving Eqs. 7.135 and 7.136 to follow the values calculated by the differential equations. Since z_{match} as well as h_c and h_f are updated at every time step, this approach simulates the physical phenomenon of interdependent variation of chips and liquor levels without a threshold restriction. Furthermore, the difference between chips and liquor levels allows us to define a meaningful boundary condition for the top compacting pressure as follows

$$P_{c,ext} = \begin{cases} \rho_c g\big(h_c - h_f\big) & if \quad h_c > h_f \\ 0 & otherwise \end{cases} \tag{7.138}$$

Although the conceptual model is simple, its implementation is rather complex, and the simulation model may become numerically unstable due to the introduced algebraic loops. On one hand, a virtual section with a special compaction profile is needed to compute levels when total masses are rising; on the other hand, when total masses decrease, the integral would be more accurately calculated from the (old) top to the (new) bottom as we expect that a bottom section is being removed from the column. More on these issues will be discussed in the following chapter.

7.2.3 Heat-exchangers

Even though heat-exchangers are known to be well modelled by the plug flow representation, we will use instead the perfect mixing tank as the underlying model for modelling the units in the local heat-recovery network. Logically, we aim in this way to reduce the numerical burden of the whole process model.

Having in mind a common notation for heat-exchangers[*], we establish energy balances for each side of a generic unit from which the outlet temperatures of hot and cold sides become described by

$$\frac{dT_{ho}}{dt} = \frac{F_h \bar{C}_{P,h}(T_{hi} - T_{ho})}{V_h} - \frac{UA\Delta T_m}{\bar{C}_{P,h} V_h} \quad \textbf{7.139}$$

$$\frac{dT_{co}}{dt} = \frac{F_c \bar{C}_{P,c}(T_{ci} - T_{co})}{V_c} + \frac{UA\Delta T_m}{\bar{C}_{P,c} V_c} \quad \textbf{7.140}$$

where ΔT_m is a function of the inlet and outlet temperatures (four variables) that can be empirically determined. However, we will used the standard definition of the log mean temperature difference to a give form to this term, i.e.,

$$\Delta T_m = \Delta T_{lm}(T_{hi}, T_{ho}, T_{ci}, T_{co})$$

and we apply Eqs. 7.142 and 7.141 depending whether the heat-exchanger is operated in counter-current or co-current flow regimen respectively.

$$\Delta T_{lm,count} = \frac{(T_{ho} - T_{ci}) - (T_{hi} - T_{co})}{\ln\big((T_{ho} - T_{ci}) - (T_{hi} - T_{co})\big)} \quad \textbf{7.142}$$

$$\Delta T_{lm,co} = \frac{(T_{hi} - T_{ci}) - (T_{ho} - T_{co})}{\ln\big((T_{hi} - T_{ci}) - (T_{ho} - T_{co})\big)} \quad \textbf{7.141}$$

Likewise, the volume-specific heat capacities are estimated as in the vessel model according to Eq. 7.32.

7.2.4 Mill controlled variables

As mentioned in Section 3.4, the conventional controlled variables of a digesting stage comprise liquor-to-wood (L/W) ratios, alkali charge (A/W), and H-factor. Additionally, digester vessels with a built-in washing functionality create the need for controlling a dilution factor associated. Though the H-factor depends on

[*] The reader should consult Geankoplis (1993)

retention time and temperature profiles, it is usually controlled only by influencing on the digester top temperature through the manipulation of the steam flow (see Chapter 6), since trying to affect retention times would basically mean disturbing the production rate.

The control theory for systems described by PDEs (distributed parameter systems) is a subject of current research*; therefore, the conventional control structure of a continuous digesting stage is still based on theory more suitable for systems described by ODEs (lumped parameter systems). In practical terms, it means that the control structure found on a mill does not consider the axial profiles of the vessels, but rather some lumped approximations of the profiles stablished in the vessels zones. Certainly, this is not only due to an immature control theory for PDEs systems, but also because of the high instrumentation cost that would involve sensing a whole profile instead of few points along it. For example, the control structure may be defined to cascade control the alkali concentration in the extraction streams by changing the fresh alkali charge through manipulation of the white liquor flow rate and splitting, however, the control system has no information about how the alkali concentration drops along the vessel zone ahead of the extraction point. Unfortunately, pulp sheet properties depend more on these kinds of history profiles of reagents concentrations and temperatures than on punctual values of them as measured in the extraction streams.

Analogous to the cooking yield definition (see Section 7.2.2.3.2), L/W and A/W ratios may be calculated within the simulator as apparent or “true” values, nonetheless, the control system of the mill can only calculate the apparent value as it cannot measure the true yield of a chips parcel. Moreover, the control system has no means to measure effective flow rates of liquor and chips phases inside the vessels; therefore, its formulas are estimates based on physically measurable signals, such as flow rates of liquor and steam streams, chip meter speed, and wood moisture in the chips infeed. In order to calculate set-points useful for a mill DCS, we obviously need to use in the simulator the same formulas used by it. Concerning the alkali control structure, although alkali concentration in the extraction streams may be the primary controlled variable in the cascade structure, we would also like to compare the signals of fresh alkali

* The reader can consult Imanuvilov (2005)

and total alkali charge to facilitate the interpretation of optimization results. The formulas needed to compute all the mentioned controlled variables are given below.

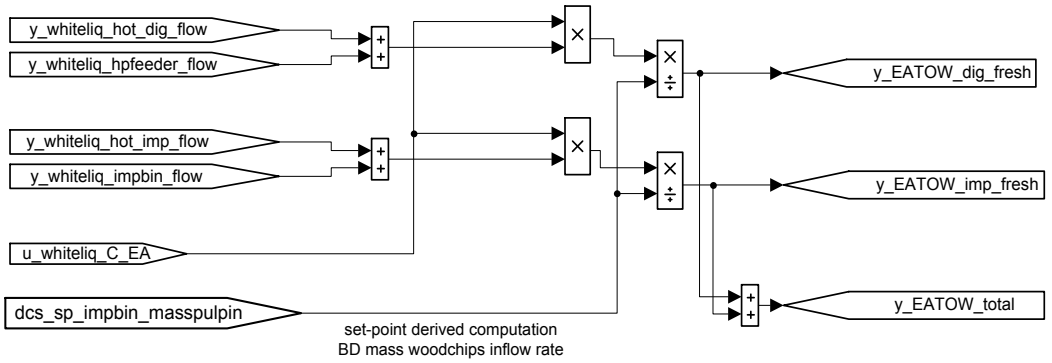

Eq. 7.143. Graphical equations for computing EA/W ratios as found in the mill DCS

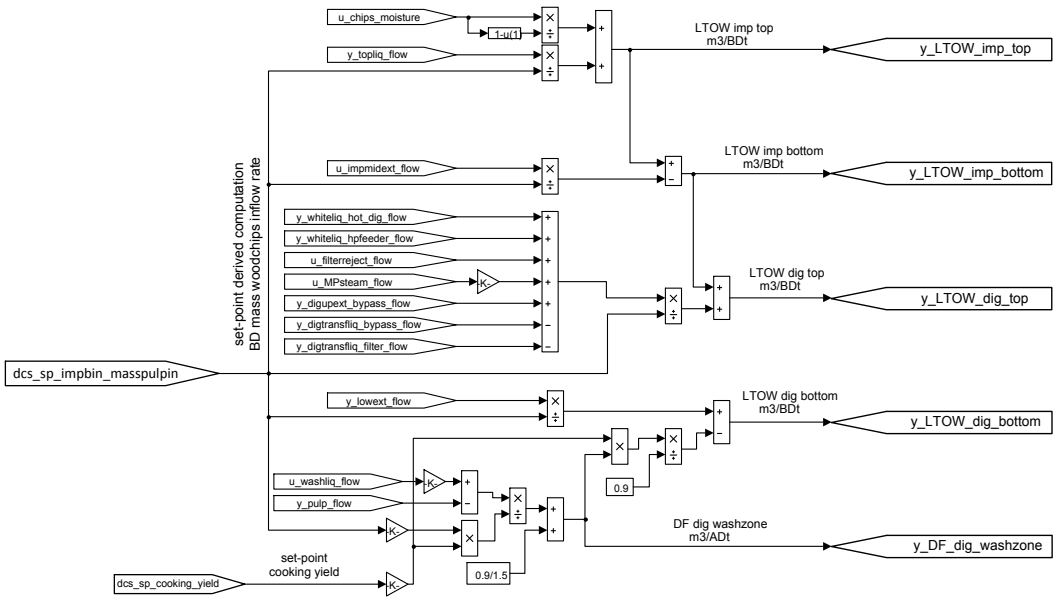

Eq. 7.144. Graphical equations for computing L/W ratios and wash zone DF as found in the mill DCS

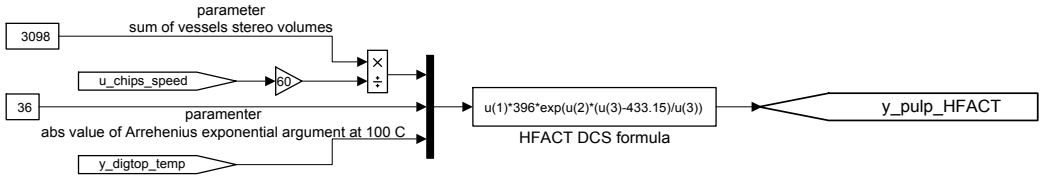

Eq. 7.145. Graphical equation for computing H-factor as found in the mill DCS

Should be noted that the DCS H-factor is far from the original expression stated by Vroom (1957). Obviously, one of the reasons is that the control system cannot measure all the information needed for the original formula, but there are other

limitations in the DCS formula that could be overcome by leveraging available instrumentation. For example, the DCS neglects the chips levels and compaction of the vessels affecting the retention time of the chips stream, and it lumps the temperature profile along the impregnator and digester into a single value corresponding to the digester top temperature. These both simplifications could be improved exploiting other signals, such as from temperatures sensors along the vessels and chips levels sensors. However, as long as the control structure remains the same, we just need to use this formula as given.

8 Simulation Results

The simulation model can be used for several purposes in the domains of process dynamics, control, monitoring and optimization research. The first domain can be straightforward investigated, thus we could elaborate an extensive discussion on CompactCooking™ G2 dynamics by analyzing step responses and process interactions. However, our aim in this Chapter is the validation of the simulator for optimization purposes; thus, we will restrict us to discuss model parameters and its adjustment, data acquisition and conditioning for testing and validation runs, and the comparison of mill and simulated output signals. After this, a procedure to identify a steady-state from mill data is presented and the associated steady-state profiles of the vessels are shown. The identified steady-state will later serve us as a base case scenario for process optimization.

From mill data, 200 h of operating history are used to test and validate the simulation model. Testing is performed with the first 50 h at a time step of 1 min, thus 3000 points of information are actually used for calibration. The remainder data also simulated is considered as a validation run, in the sense that no further adjustment of model parameters was done to improve correlation between mill and simulated outputs. During the whole period the process stage exhibits a stable operation, i.e., without long interruptions of the chips infeed (conveyor belt detentions), events of chips bed plugging (vessel “hangs”), or significant variation in vessels levels, all conditions which the simulator could not handle by design. These limitations are due to the mathematical formulation of the conceptual vessel model, partly owing to the omission of dynamic momentum balances, the discretization of PDEs in terms of retention times instead of flow velocities, and the inactivation of the S-function computing vessels levels. The latter features of

the simulator can be modified in order to allow it handling long infeed interruptions, as long as the vessel levels modelling approach is successfully implemented avoiding the numerical instability experienced in this work. On the contrary, modelling chips bed plugging represents a major effort as it provokes a discontinuity of the chips column, which is actually the difficult characteristic to be modelled and simulated. In any case, in the context of steady-state optimization, the chips infeed is not supposed to be interrupted, and vessels levels can be held constant representing unchanged set-points. Thus, even if the simulator is limited regarding the whole description of the system dynamics occurring during process faults, it do provides the essential dynamic features for validation against stable operating data and further use for model-based optimization.

8.1 Parameters and data acquisition

Mathematically, model parameters and input data play a common role in the numerical integration; thereby, some values treated as parameters may be regarded as input variables and vice versa. In our model architecture, woodchips basic and bulk densities are considered inputs while wood composition is held constant as a set of parameters. Although this could be changed to allow simulating grade transition phenomena (wood species changes), it is obviously not necessary for steady-state optimization.

Table 8.1 attempts to list most of the model parameters grouping them into their associated phenomelogical models. Since an exhaustive list would be fairly extensive, implicit values are referenced to their original source. Thus, explicit values are associated to adjustable parameters useful for improving the correlation between mill and simulated signals. That is, parameters of phenomenological submodels, including kinetic, compaction and depolymerization models, should be already validated in their respective domain by laboratory experiments, the source of physical reality for the mathematical equations; and validating the process model actually means adjusting the models ensemble to match the system-level behavior of an industrial realization as measured by the available instrumentation.

In theory, all parameters could be “guessed” by minimizing the correlation error between mill and simulated outputs; however, it is an impossible task to determine all of them in this way due to limitations in the available computing

power and the stability of numerical methods. These are some of the reasons to use empirical values from literature (laboratory experiments) and to adjust only a small set of parameters.

Table 8.1. Model parameters.

Parameter name		Value
General parameters		
Density of wood substance	kg/m^3	1500
Density of water	kg/m^3	1000
Heat capacity of wood substance	kJ/kgK	1.47
Heat capacity of liquor solids	kJ/kgK	1.47
Heat capacity of water	kJ/kgK	4.18
Wood composition (SW)		
Total lignin	%	27.30
Fast/slow lignin ratio		30/70
Cellulose	%	42.70
Glucomannan	%	16.10
Xylan	%	10.10
Other polysaccharides*	%	3.20
Extractives	%	0.60
Compaction model (Härkönen-like)		
Wall friction coefficient		0.2
Minimum allowed bed porosity	m^{3}f/m^{3}st	0.1
Other values same as Härkönen (1987)†		
Kinetic model (Purdue-like)		
Lignin-kappa conversion factor		657
Unreactive lignin (fast/slow)	%	1.50/1.50
Heat of reaction	kJ/kg	-400
Other values same as softwood case in Wisnewski et al. (1997)‡		
Depolymerization model		
Cellulose DP	AGU	3000

* Evenly distributed among remainder polysaccharides fractions
† Coefficients of bed compaction and liquid pressure drop correlations
‡ Coefficients for five reaction rate equations

Hemicellulose [η]	ml/g	70.30
Cellulose depolymerization rate same as kraft case in Sixta (2006)*		
Cellulose Mark-Houwink parameters same as Evans & Wallis (1989)†		
Heat-exchanger model		
Area-global heat transfer coefficient (UA)	J/(min·K)	100,000
Hold up volume per side	m^3	2
Vessels parameters		
Axial discretizing step in vessel zones	m	0.2
Digester top compacting pressure	kPa	5
Impregnator top compacting pressure	kPa	0
Displacement ratio (DR) in wash zone		0.9

The reader should note that the same value of specific heat capacity is used to describe the wood substance and the liquor solids. Although this is not strictly rigorous regarding the heterogeneous composition of liquor solids, it is a good approximation since: (i) a significant fraction of liquor solids correspond to dissolved wood substance, assumed to have the same heat capacity than unreacted wood substance; and (ii) sodium hydroxide is another significant fraction of liquor solids whose heat capacity, 1.4 – 1.7 kJ/kgK (Chase, 1998), lies in the range of the wood substance property, 1.2 – 1.5 kJ/kgK (Simpson & TenWolde, 2007). In particular, the given values for these properties follows the work of Wisnewski et al. (1997).

The Purdue kinetic model explicitly defines several parameters to improve the model fit to industrial data that are referred as effectiveness factors. The latter modify the reaction rate of pulp components by multiplying the originally regressed rate equations. Although these elements are purely heuristic, they provide a key point of adjustment for the whole process model. Table 8.2 shows the values of effectiveness factors reached during model testing. The adjustment of these factors results to be closely connected to changes in the heat of reaction, which may be expected as the temperature is a key driving-force of wood reactions. The heat of reaction was adjusted in the range of -520 to -260

* Coefficients for one depolymerization rate equation
† Coefficients of Mark-Houwink equation for cellulose dissolved in Cuen

kJ/kg, an empirical interval determined for softwood kraft cooking by Courchene et al. (2005).

Table 8.2. Effectiveness factors calibration

Vessel zone	Rate equation				
	L_F	L_S	C	GM	X
Imp top	12.0	12.0	1.10	1.10	1.10
Imp bottom	12.0	12.0	1.10	1.10	1.10
Cook zone 1	1.30	1.30	0.70	0.70	0.70
Cook zone 2	0.8	0.8	0.30	0.30	0.30

In a homogenous reacting system, these effectiveness factors should not depend on position nor time. However, wood degradation corresponds to a complex heterogeneous reacting system, which is even describable by fractal kinetics (see Section 4.1), and therefore the change of these factors with the position (chips trajectory) may be reflecting structural modification of the woodchips that affect reaction rates. In any case, it must be noted that factors adjustment has been done subject to achieving a monotonous decreasing kappa profile, and that the actual component reaction rate is not necessarily following a decreasing trend along the chips trajectory.

The geometry of the vessels represents also a key set of model parameters. These are introduced in the simulator by means of a cross-sectional area vector meshed according to the axial discretizing step. For sake of simplicity, those values are graphically depicted in Figure 8.1. The wash zone is not depicted in the figure since it was modelled as a lumped parameter system with no retention time. The inaccuracy of this approach would not be significant presuming that the digester behavior can be mainly captured in the upper zones where wood reactions take place. Besides the geometry of stereo space (“empty-tower”), the simulator requires a (initial) value of matching level to partially represent the actual filled space of chips and liquor phases in a vessel. Above the matching level, the filled space could be simulated by the approached proposed in this thesis (see Section 7.2.2.6) or as done by Michelsen (1995); however, this part was omitted from the simulation runs due to numerical limitations, i.e., vessels levels were assumed to be constant. In the impregnator case, the difference between chips and free liquor levels is neglected and thus the top compacting

pressure equals zero; in the digester instead, chips level is assumed 1 m higher than the liquor level resulting in approximately 5 kPa of top compacting pressure, an estimate based on simulated data and presuming a conical formation of the chips pile above the matching level.

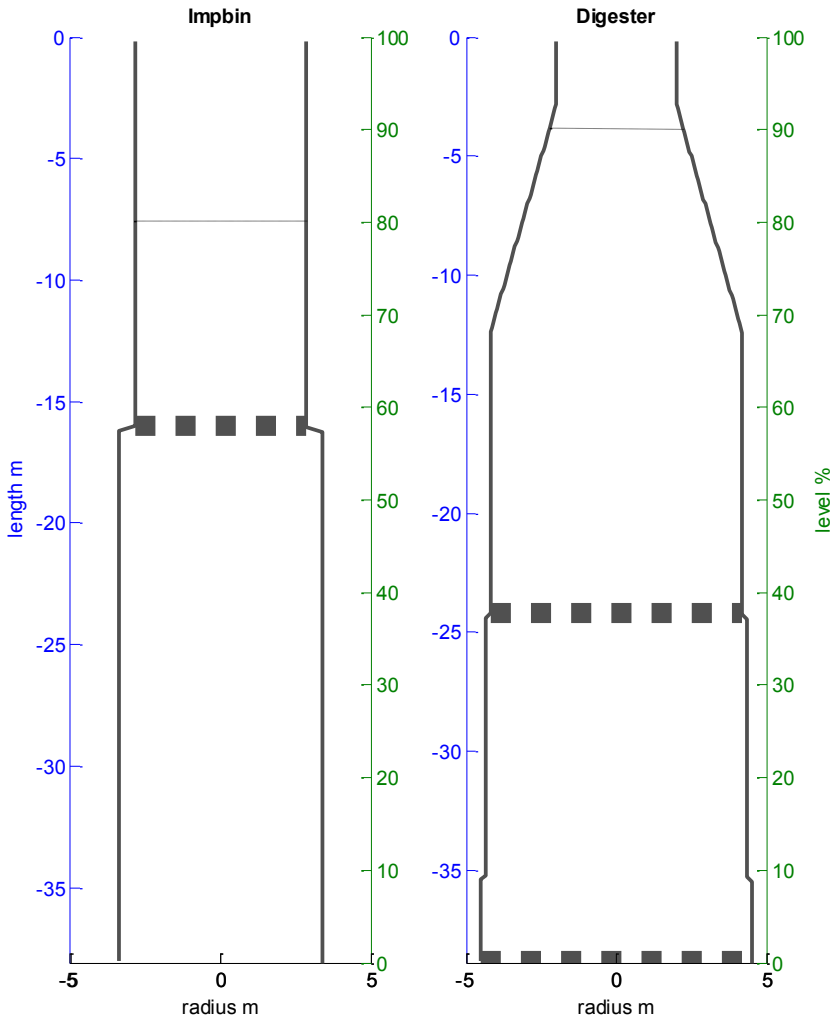

Figure 8.1. Geometry of the vessels and estimated matching levels.

The position of extraction screens is indicated by broad bands, while levels correspond to dotted lines.

In principle, matching levels should be estimated based on mill data. However, due to unreliable mill signals of vessels levels the values shown in Figure 8.1 correspond to “good guesses” that can be adjusted to improve model fit. Analogously, parameters describing heat-exchangers represent “good guesses” as the mill lacked of sufficient temperature sensors to monitor overall heat-transfer coefficients, and equipment design information was not available to define hold-up volumes.

The adjustment of parameters is performed running the simulation model several times, aiming to achieve the best possible correlation between simulated outputs and mill data. To reduce noise in mill signals (used as inputs and comparable outputs), a zero-phase delay moving-average filter is applied using Matlab filtfilt() function; the time window of the filter varies from 20 min for flow rate and temperature variables up to 200 min for smoothing laboratory off-line signals.

The available data in the process historian was incomplete in relation to the minimum number of signals for a rigorous simulation (see Section 7.1). The mill lacked of several sensors to measure process disturbances despite some of them can be easily instrumented, including (cold) white liquor, wash liquor and reject liquor temperatures; consequently, signals estimates have to be used for the unavailable information. Unmeasured temperature disturbances were to some extent observable, thus based on simple physical models we could obtain an estimate for them.

Figure 8.2 and Figure 8.3 show respectively input and output data utilized during model testing and validation. Three input signals were not filtered but taken as seen by the DCS: basic density, bulk density and moisture of chips infeed. This is because they are used in the computation of mill controlled variables to be compared, L/W ratios and wash zone DF, thus we need the same original information to perform equivalent computations. Likewise, we should follow this approach for the white liquor composition signals: NaOH and NaHS concentrations; however, DCS signals were not available and thus we opted to smooth laboratory data such that the corresponding inputs are more “realistic”. Certainly, we could improve the simulator design by keeping two layers of inputs, such that a set of signals tries to capture “realistic” changes truly used in the DAEs model, while another set is only used to emulate DCS computations. However, for sake of simplicity this sort of features is not considered in this work.

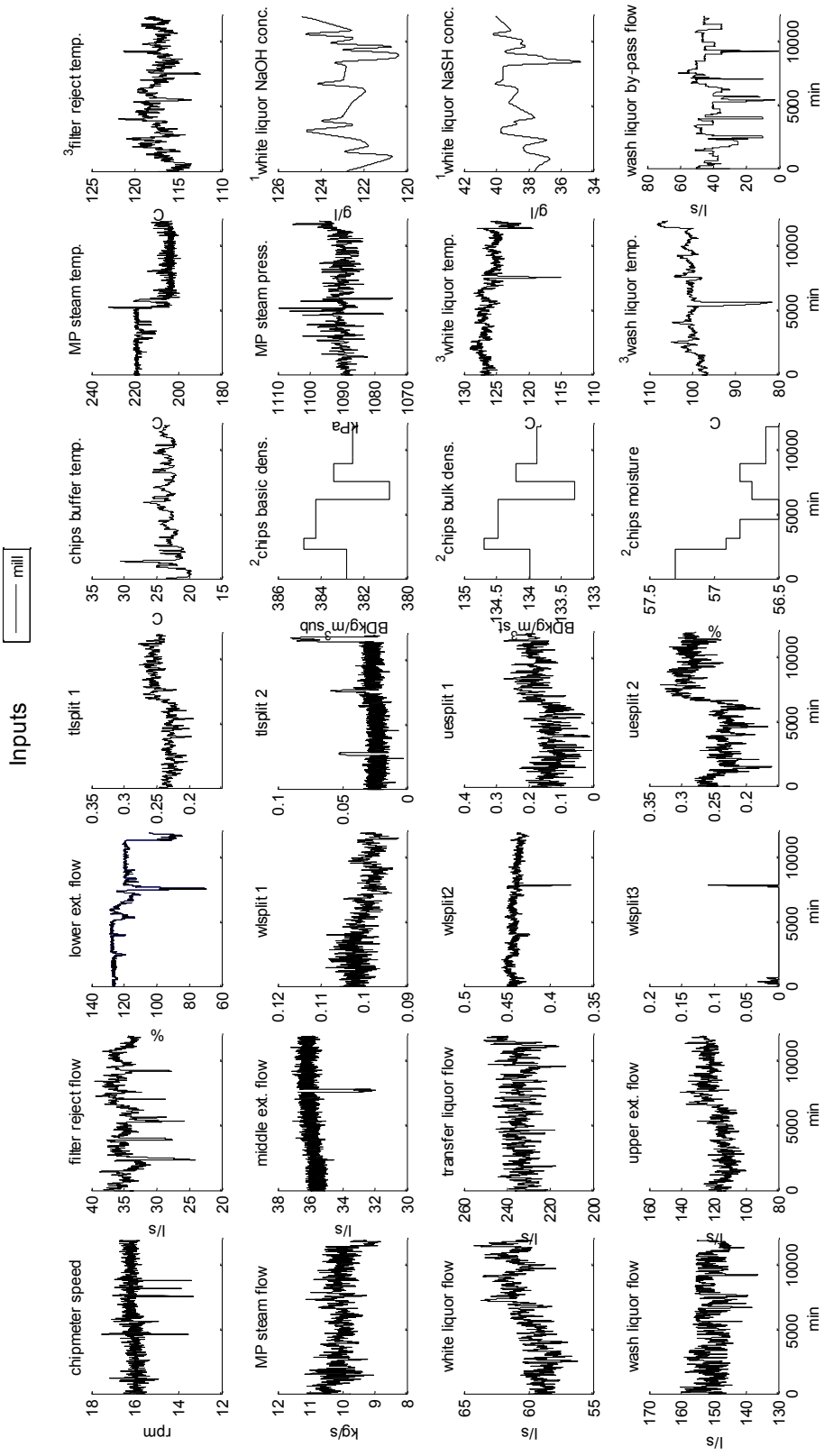

Figure 8.2. Input data for the simulation task.

[1]Off-line lab measurement, [2]DCS input based on lab measurement, [3]own estimate (no instrument at the mill). First 3000 min were used for calibration and the remainder interval is considered as a validation run.

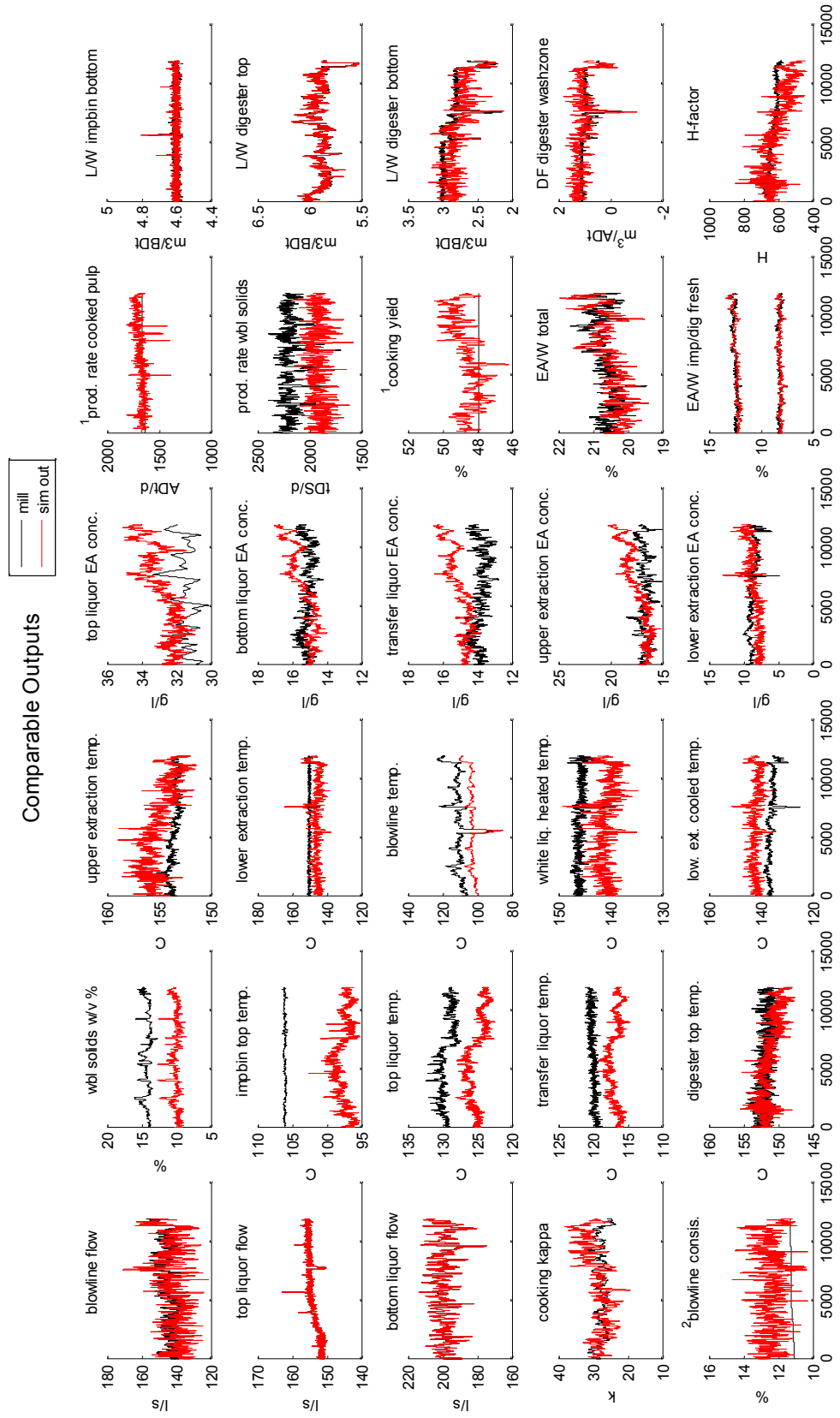

Figure 8.3. Comparable output data of the simulation task.

[1]DCS set-point, [2]DCS estimate (no instrument at the mill).

Regarding mill outputs, two signals are actually set-point values and another one is a DCS estimate based on set-point values: production rate and yield of cooked pulp, and blowline consistency. In this case, the reason behind is the lack of a consistency sensor in the blowline, a key signal that would allow to monitor (or even to control) the cooked pulp yield and production. Obviously, the uncertainty in those outputs poses a barrier to the validation of the overall mass balances; however, the availability of kappa, alkali, temperature and WBL solids sensors allows ("partially") validating energy and component mass balances

8.2 Testing and validation

As it has been explained, vessels are conceptually modelled by a system of PDEs with boundary conditions imposed at z_{match}, point defined as the match of chips and liquor levels. Although PDEs are reduced to ODEs by the method of lines, the complete process model results in a system of DAEs with several algebraic loops introduced by the representation of liquor recycles. To obtain a practical solution for a current average PC, two of these loops had to be "opened" and thus the fiber filter and the pressure diffuser were excluded from the process model. Obviously, this may have consequence concerning the quality of simulation outputs. Nonetheless, the ability to still simulate three liquor recycles represents a unique feature of this work, which is expected to capture the essential dynamic behavior of the whole stage.

The reader may have noted that Figure 8.3 already shows the simulations results compared against mill data. As a first impression, we can realize that results are in a good agreement to mill data. Despite high uncertainty in some inputs, the simulator captures very well dynamic trends though with bias in several cases, such as temperatures and WBL solids signals. Temperature bias may be explained by the poor adjustment of heat-exchanger parameters, as well as the use of simple signal estimates instead of true sensors data, due to the lack of sensors previously mentioned. On the other hand, WBL solids bias can mostly be attributed to the absent of inerts data, i.e., the fact that the simulator is run assuming no inerts in input streams, an obviously unreal description. From this general view of the results, we can also recognize a degradation trend in alkali signals that correlates with a deviation in the digester top temperature trend. In fact, due to the bias in temperature signals the latter variable had to be corrected already during calibration by introducing an adjustment factor in its associated

enthalpy balance. But let us now analyze the simulation results with further detail case by case.

Figure 8.4 aims to show the principal validable signals in terms of mass balances and their relation to the digester top temperature. The simulated top liquor EA concentration may also be included in this group, but since the mill data correspond to off-line lab measurements we may regard it as a less reliable variable for comparison. Although kappa signals show a poor correlation in the figure, the correlation in the remainder signals is outstanding.

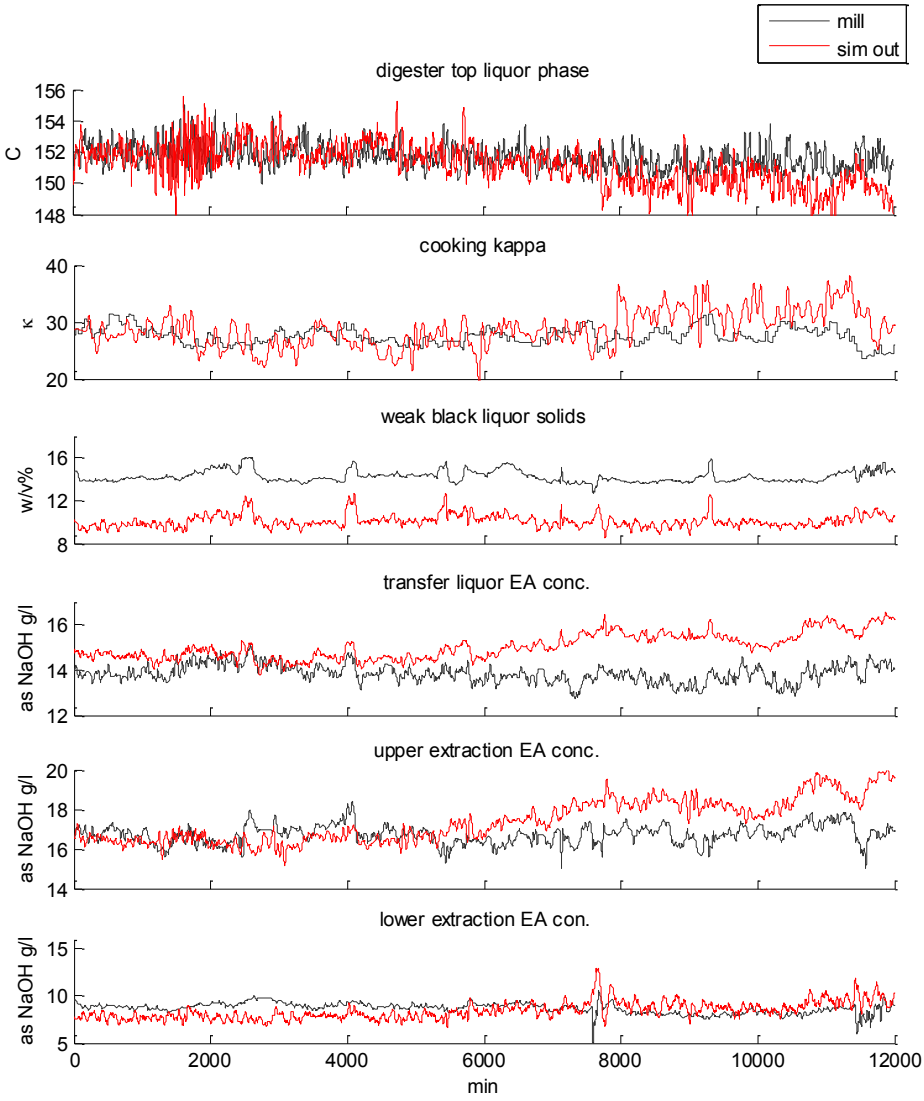

Figure 8.4. Fidelity of the process model: component mass balances.

After the time t = 6000 min, the simulation starts exhibiting a degradation trend in alkali and kappa signals that correlates with a deviation in digester top

temperature. This can be traced back to a change in the liquor splits around the same time (see Figure 8.2), thus it may be explained as the results of degradation in temperature signals, which in turn can be attributed to poor quality information in our temperature estimates and/or a poor calibration of heat-exchangers parameters. However, from a process analysis viewpoint the foregoing suggests that the digester behavior is extremely sensitive to interactions in temperature variables. The reader is referred to the Appendix A for further insights in process analysis of the CompactCooking™ G2 digesting stage

Figure 8.5 shows the available temperatures signals within the heat-recovery network of the stage. Except case of the lower extraction liquor, simulated signals are strongly correlated with the top liquor temperature; this is obviously a good result for the latter variable but not for the remainder signals. Most probably, the isothermal equilibrium description in the vessel model is limiting the capacity to simulate a greater independence between temperature variables, thus resulting all of them intensely correlated between each other even more than in the real process. This limitation may be also involved in the model degradation discussed above. Moreover, the sharp variability seen in the upper extraction liquor temperature negatively correlates with the kappa signal, hence explaining its higher variability compared to mill data. Again, the isothermal hypothesis can be an inadequate description allowing the propagation of higher variability than real one in the temperature profile of the vessels; however, a need for improving parameters adjustment can also be responsible of this behavior, including the heat of reaction and effectiveness factors of Purdue model, as well as bed compaction coefficients of Härkönen correlations. In reality, many elements of the simulator can be attributed to cause higher simulated variability, such as a poor filtering of input data or even numerical issues on the integration algorithm, especially when applied to distributed parameter models implemented through the method of lines. In any case, a systematic improvement of the simulation results should pass through discarding the isothermal hypothesis, as well as acquiring data from true temperature sensors, i.e., demanding better instrumentation from the mill.

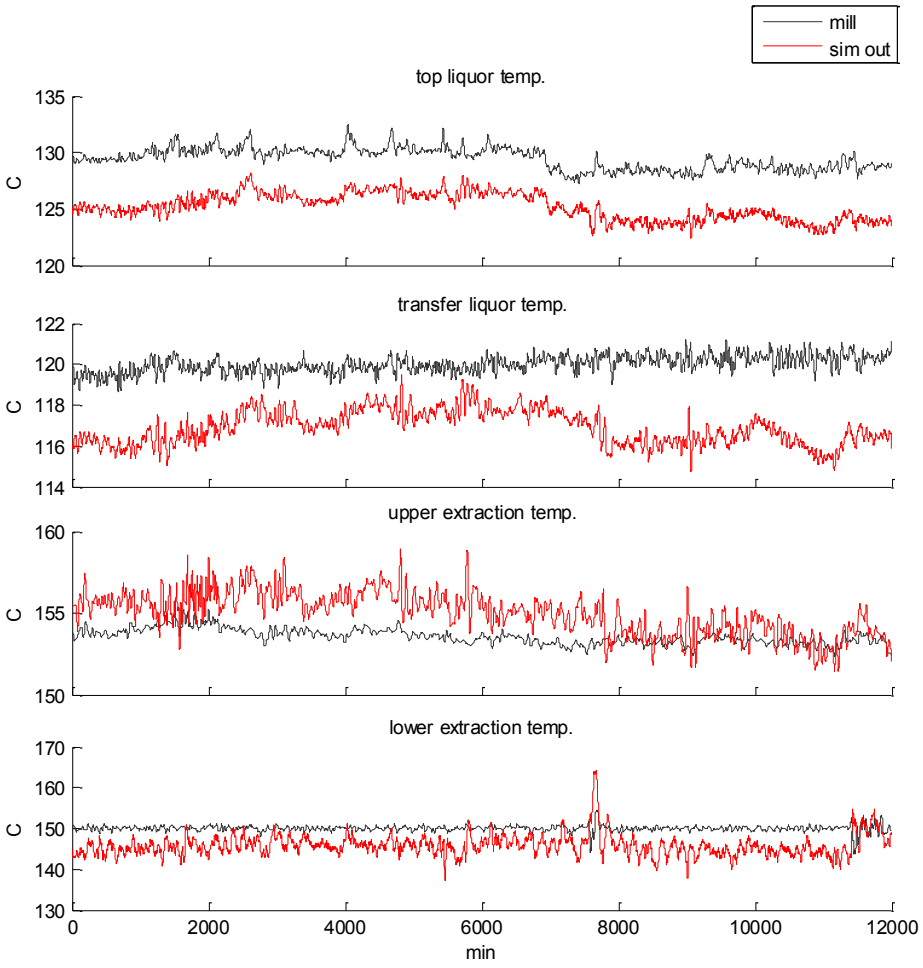

Figure 8.5. Fidelity of the process model: energy balances.

Considering the discussion on the above figures, we can state that the process model is valid based on qualitative criteria. Furthermore, a path for improvements has been established to lessen model degradation, thus we can continue testing the simulator against process data outside the calibration data set. To the best knowledge of the author, no other simulation work on pulp digester has performed a validation process using a similar diversity of signals as in this thesis. In fact, except Rantanen (2006) it seems that no author has even shown the comparison of dynamic signals in such a long period of time. Although we have not performed quantitative analyses, the good agreement in such signals diversity is a powerful reason supporting the use of the simulator for optimization purposes. Before finishing this section, let us review some issues of importance for understanding the optimization part in the next Chapters.

The process optimizer will compute a list of set-points to be given to the control system of the mill. This is coherent as long as the controlled variables, associated to these loops, are simulated in agreement to the “real” process as seen by the DCS. From Figure 8.3 we realize that all controlled variables are in perfect agreement to DCS computations, except two signals that show a small bias and one that shows higher variability than real: the L/W in the cook zone 2 (digester bottom) and the DF of digester wash zone, and the H-factor of the stage. The latter disagreement is related to issues on temperature signals already discussed, whereas the former issues are connected to higher variability in the blowline flow rate as evidenced in Figure 8.6.

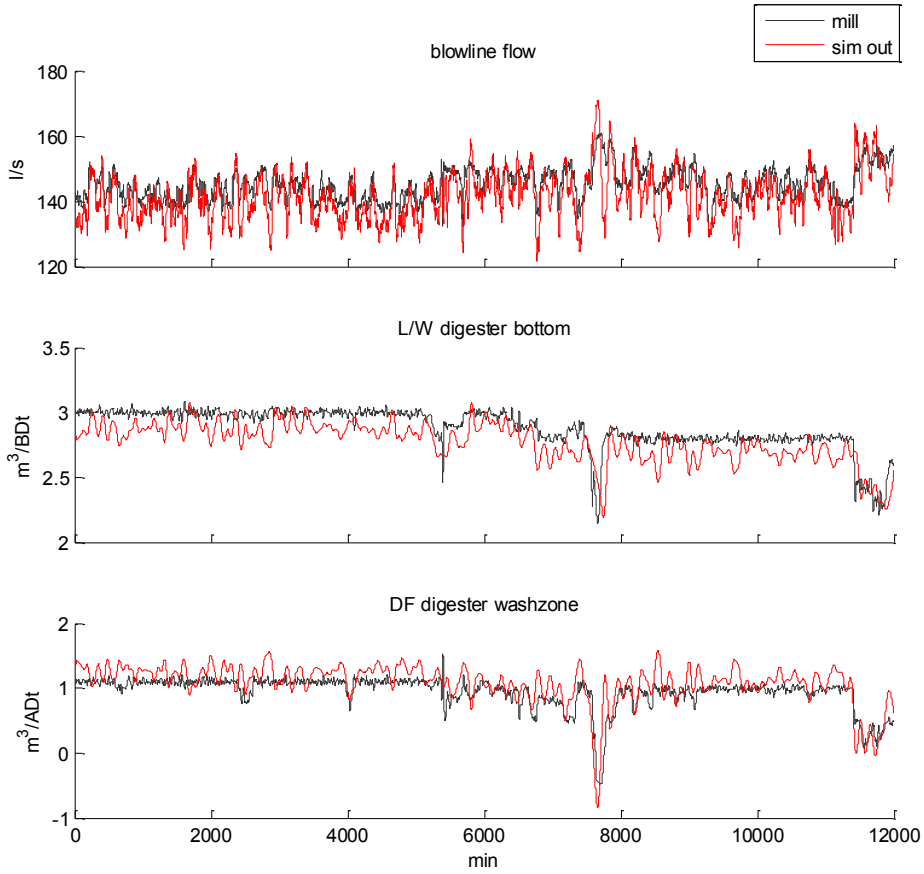

Figure 8.6. Influence of blowline flow rate on the computation of digester bottom L/W and wash zone DF.

This higher variability in the blowline flow rate signal can have several explanations as discussed above, including noise in input data and/or unreliable data, especially related to the chips moisture signal. However, there may be also a modelling issue regarding the use of an ideal washer formulated on a mass-

basis instead of volume-basis description as the rest of the digester vessel. The substance of this issue deals with the computation of the blowline flow density. As its discussion may deviate from our current scope, we just mention this and add that replacing the ideal washer with a counter-current vessel section model is the advisable step for further improvement.

The selection of the final cooking kappa is primarily connected to the optimization of the whole fiberline process design, therefore its optimization will not be considered in our problem. However, the intrinsic viscosity of the pulp can be considered as an optimization objective, as it is feasible to maintain the same final kappa while favoring the preservation of the cellulose DP (see Chapter 3). This phenomenological fact is reproduced in the simulation as shown in Figure 8.7. Unfortunately, mill data on intrinsic viscosity were available for comparison; hence, we cannot assess the validity of the signal dynamics as seen in part a nor of the quantified optimization window (~100 ml/g) as seen in the part b of the figure. In any case, this signal is most probably also suffering of higher variability due to its connection to the temperature profile of the digester.

Finally, let us try to discuss the validity of the compaction model. Though it is a key component of the vessel description, the compaction model cannot be assessed directly as a comparison of the selected outputs defined in Section 7.1. In fact, the compaction degree of a chips column cannot (still) be measured online, and this is an impassable barrier to validate any compaction model through comparison of dynamic signals. However, an associated variable like the liquor pressure drop may be used instead for model testing and validation, as long as several pressure sensors are placed along the vessel. More commonly, vessel instrumentation incorporates pressure differential indicators for every extraction mesh, and these signals might be to some extent related to the liquor pressure drop along the chips column; despite that the latter instrument measures a pressure difference in the radial axis between vessel out and inside, whereas the former would be measuring a difference in the axial axis always inside the vessel. In any case, the pressure drop in extraction meshes were compared to the pressure difference measured by mill indicators but no significant correlation was found. In principle, to be truly coherent in this comparison we should extent the model by including a second spatial dimension,

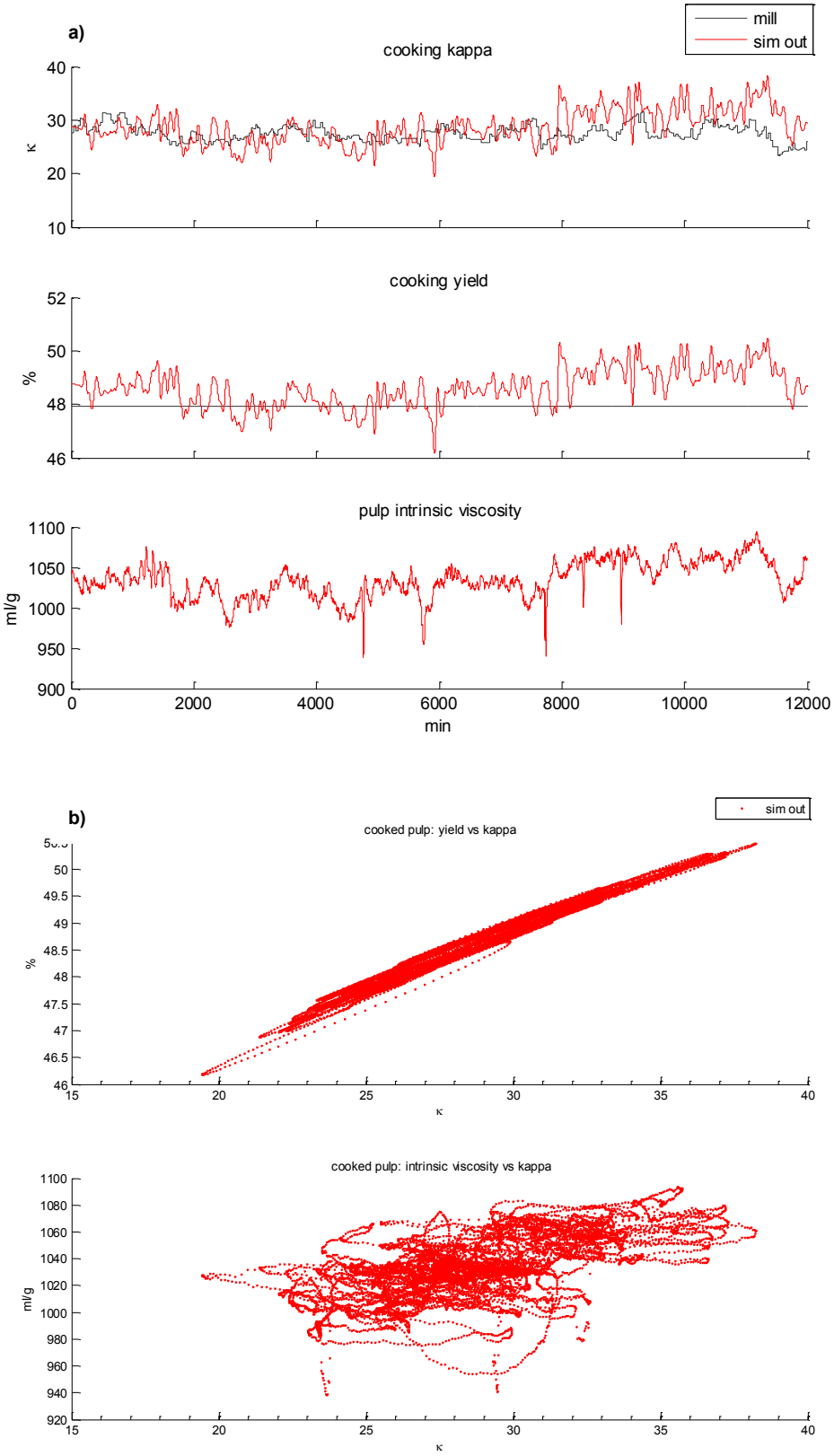

Figure 8.7. Internal correlation in kappa, yield and intrinsic viscosity of the cooked pulp: a) dynamic signals, b) one-to-one plot

describing radial changes in flow velocity and pressure variables, and by solving the dynamic equations of momentum balances; both requirements are obviously very time-consuming and pose several difficulties in process modelling and simulation.

In spite of the above, we can still indirectly assess the impact of the compaction model in other signals by deactivating the time-varying computation of the compaction profile, i.e., comparing simulation results with fixed and varying compaction profiles. In this way, we can at least visualize the effects of changes in bed porosity on the remainder signals by a sort of simulated experiments. Figure 8.8 shows an example of this idea by comparing kappa signals obtained with a fixed and time-varying compaction profiles.

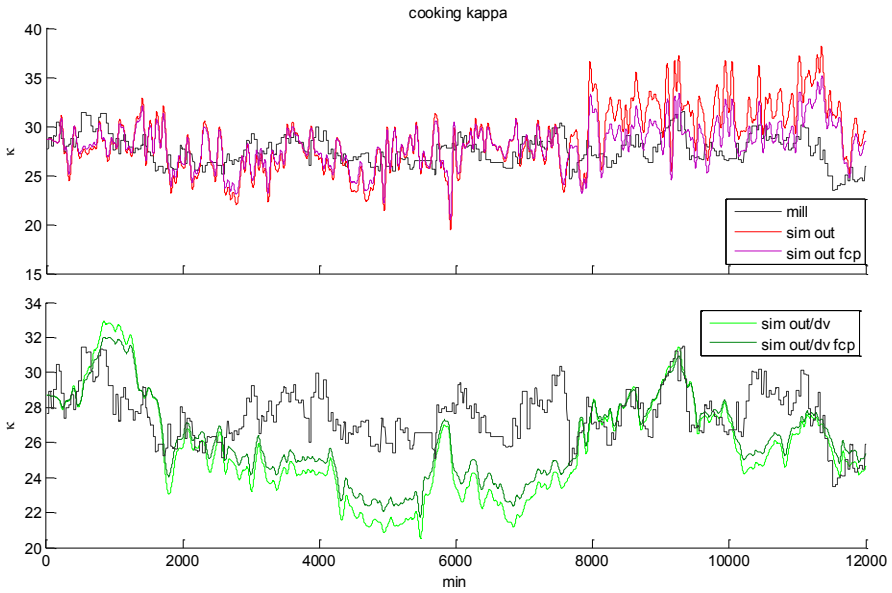

Figure 8.8. Indirect evaluation of compaction model through cooking kappa dynamics. *Signals labeled as fcp mean that a fixed compaction profile (from a determined steady-state) was maintained during the simulation run. Signals labeled as sim out/dv correspond to simulated contributions from the process disturbance (see Appendix A)*

From the simulated experiment, we would deduce that compaction changes do not affect kappa dynamics in a significant way. That is, the kappa variability is far better explained by temperature variations than due to compaction dynamics. However, it must be noted that changes in the coefficients of Härkönen correlations do have an extreme impact on the model behavior, i.e., compaction

variations would be significant if the characteristics of the chips furnish change over time (chips size distribution and/or wood species).

8.3 Steady-state identification

To finalize this Chapter, let us see how to identify the most probable steady-state of the process and to show associated steady-state profiles of the vessels. The procedure described below will be referred as steady-state identification or detection.

First, we need to identify a period of stable operation without set-point changes in the production rate. Then, by taking the average or statistical mode of the input signals, as seen in Figure 8.9, we have a set of constant values to run the simulator such that the outputs reach the steady-state. In this way, we have obtained a process condition to hold as the most probably steady-state that the process could have achieved without noise in manipulated variables or disturbances. Figure 8.10 shows the output values reached after this procedure. This condition will be onwards denoted as identified or base steady-state.

Having an identified steady-state, we can easily obtained vessels profiles of any variable of interest. Figure 8.11 shows several of them to exemplify. In this figure, several profiles are computed based on the theoretical definition of the variable rather than using mill DCS formulas. A reader skilled in the art should understand that those formulas cannot be used to calculate profiles, and that the values in these theoretical calculations are not comparable to the numbers given by the DCS.

The procedure for steady-state identification plays a key role in the design of the process optimizer, as it allows calculating a starting point for the optimization algorithm. Indeed, since we will use a linear programming approach, a well-defined base steady-state is crucial for the whole task.

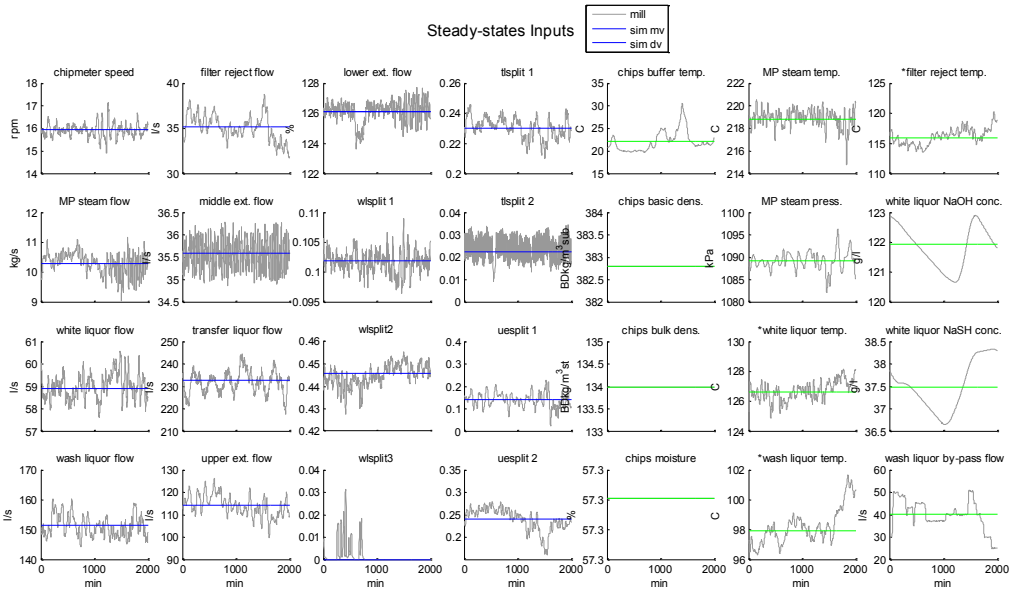

Figure 8.9. Inputs of the identified steady-state

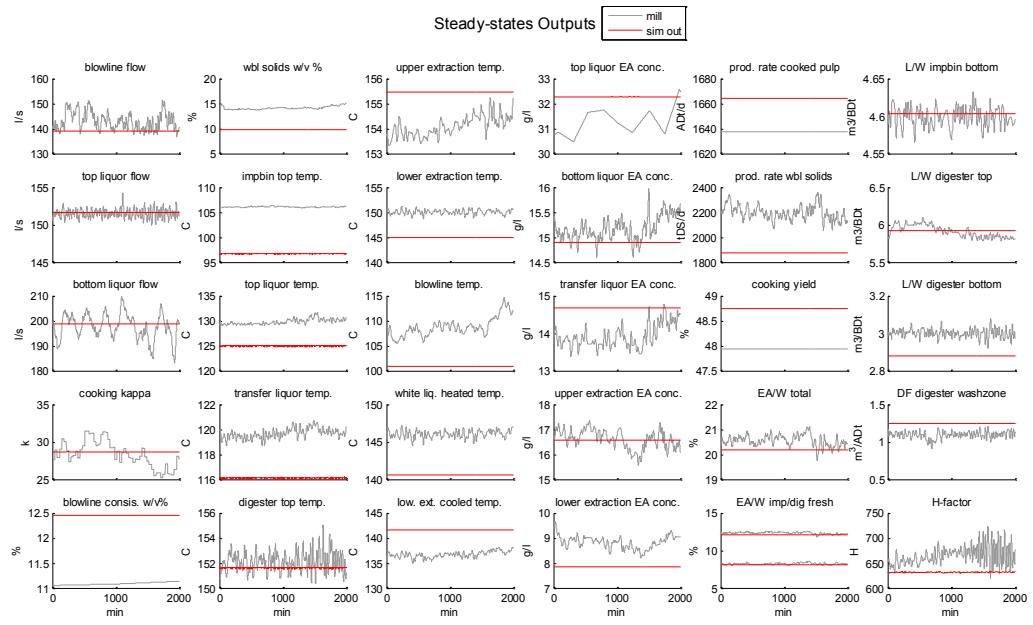

Figure 8.10. Outputs of the identified steady-state

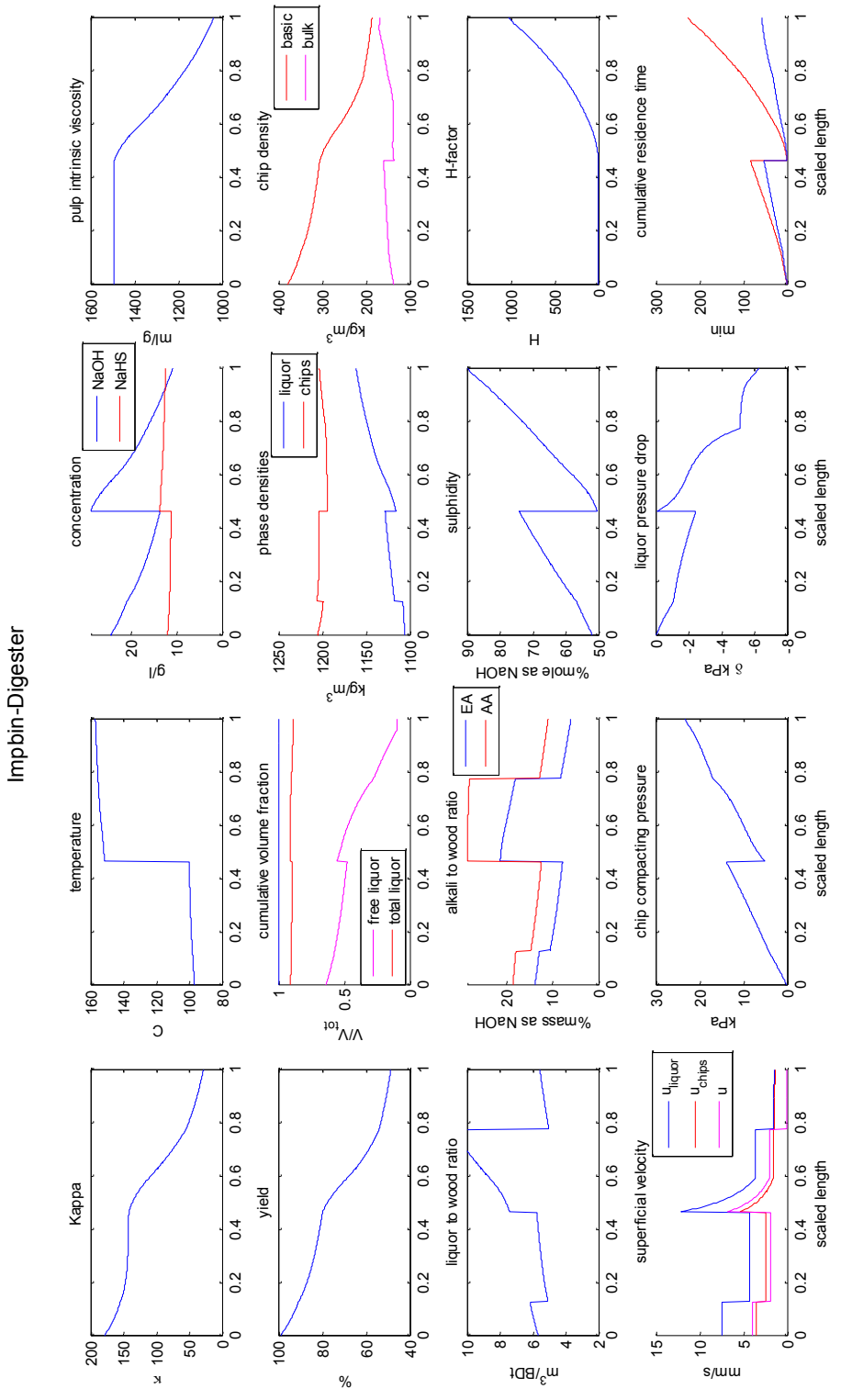

Figure 8.11. Simulated steady-state profiles along vessels from impbin top to digester bottom.

Digester profile starts at 0.467 and its end corresponds to the middle of the lower extraction screen.

9 Optimizer Design

The process studied is highly non-linear and interacting due to liquor recycling combined with heat integration. Therefore, its optimization by means of physical models is likely an impossible task, since lab-scale digesters, including the M/K or CRS reactors commonly found in pulping research centers, do not provide enough means for simulating these key interactions. This barrier is logically overcome by means of applying optimization algorithms on mathematical models of the process, a method in which the results will be reliable as long as the process models have been properly validated.

There exists a large collection of optimization algorithms and several ways of formulating the optimization problem[*]. However, we will use a relatively simple approach of steady-state optimization based on single-objective formulation, model linearization and a linear programming algorithm, such as the simplex, interior-point, or active-set algorithms, aiming to test the feasibility of optimizing the process economics in significant numbers. The workflow diagram for the optimization task is shown in Figure 7.1.

The optimizer should be able to find a new steady-state that achieve same production rate and cooking kappa as the base steady-state, while diminishing the specific consumption of MP steam or the overall EA charge, and/or increasing the cooking yield or the WBL heating value. These conditions define objective functions that are to be optimized by the linear programming algorithm subject to operational constraints on the process (model). From the new steady-state, new set-point values can be recognized in the output variables, and these can be applied at industrial-scale passing them directly to the mill DCS. This last step is actually more complex than as described but will be explained later.

In the context of process economics optimization, the objective function is sometimes referred as the economic model, while the process model and its operational constraints constitute the so-called operating model. Let us now explain the design of both models and how linear programming is used.

[*] The reader can consult Edgar & Himmelblau (1988)

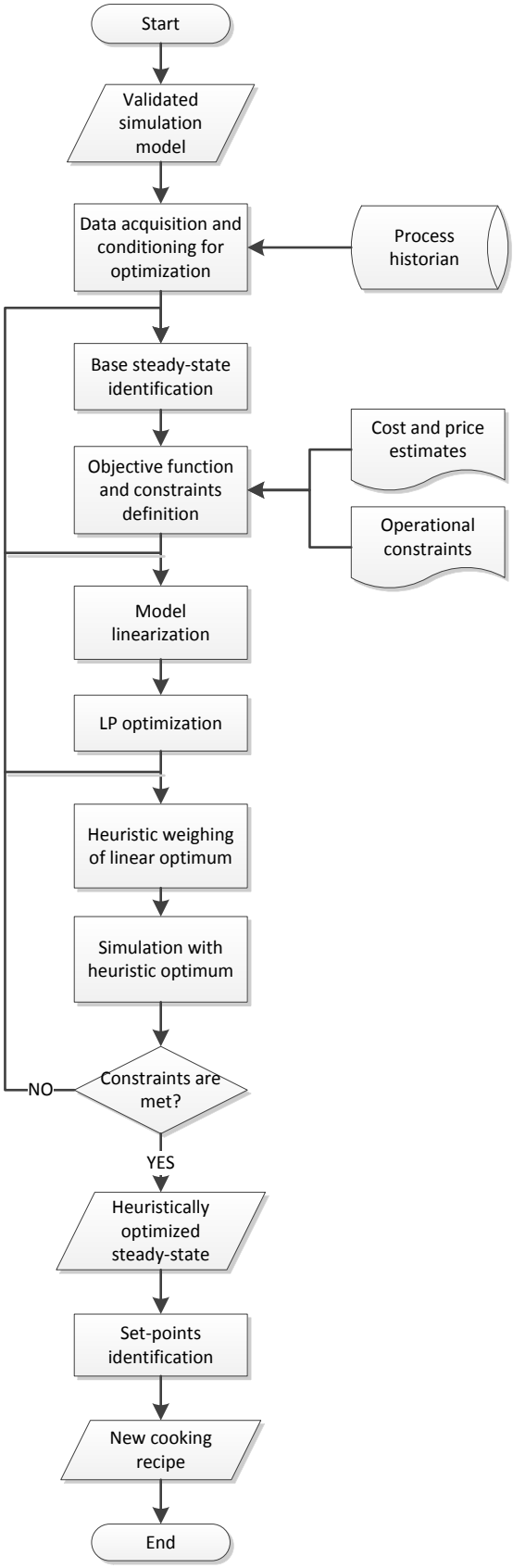

Figure 9.1. Workflow diagram for the design of the optimizer.

9.1 Economic and operating models

In general, the optimization problem of business processes can be formulated either as the maximization of profit or the minimization of operating costs, since both problems are equivalent in most cases. However, this is usually not the case for chemical processes, in which the profit mainly depends on the process yields or the conversion degrees of several reactions that are affected by changes in manipulated variables, i.e., costs minimization does not necessarily imply a profit increment. Having noticed this, we can formulate two independent optimization problems of steady-state process economics in the following general (non-linear) forms

$$\max_{\vec{u}_{ss}} \quad f_{\text{Profit rate}}(\vec{y}_{ss}(\vec{u}_{ss}), \vec{u}_{ss}) \quad \text{V} \quad \min_{\vec{u}_{ss}} \quad f_{\text{Cost rate}}(\vec{u}_{ss}) \tag{9.1}$$

$$\text{such that} \begin{cases} \vec{u}_{lb} \leq \vec{u}_{ss} \leq \vec{u}_{ub} \\ \vec{y}_{lb} \leq \vec{y}_{ss} \leq \vec{y}_{ub} \end{cases}$$

These formulations consider the rates of the profit and operating costs at the steady-state. Nonetheless, process plants usually assess the process economics in terms of specific profit or cost per unit product or educt (raw material), which in the case of a pulp mill translates into objective functions stated as specific values per unit air dried ton of pulp (ADt) or per unit cubic meter of wood as solid under bark (m^3sub, chip phase volume). Naturally, these definitions of specific values can be easily obtained according to

$$f_{\cdot \text{ per ADt}} = \frac{f_{\cdot \text{ rate}}}{F_{pulp}} \tag{9.2}$$

$$f_{\cdot \text{ per m}^3\text{sub}} = \frac{f_{\cdot \text{ rate}}}{F_{wood}} \tag{9.3}$$

Although the above originates other four independent formulations of optimization problems on process economics, it is expected that they are strongly correlated to the original formulations in terms of rates. Let us see now how the latter can be defined to consider the main economic aspects of the digesting stage in the context of a mill able to sell electrical energy to the grid (excess of process steam).

9.1.1 Objective functions

The operating costs of the process studied are fundamentally related to the consumption of wood, white liquor and MP steam. The consumption of these first two elements is accounted in a mass-basis, while the latter is accounted in an energy-basis (enthalpy) since its consumption involves an opportunity cost of energy conversion and sale to the grid. Equation 9.4 expresses the cost rate function of the process stage.

$$f_{\text{Cost rate}}(F_{wood}, F_{WL}, Q_{steam}) = p_{wood}F_{wood} + p_{WL}F_{WL} + \eta_{TG}p_{EE}Q_{steam} \quad \textbf{9.4}$$

On the other hand, the profit is primarily associated to the production of pulp, but we should not forget that the WBL solids constitute a fuel for the recovery line and therefore it must be accounted as additional revenue in an energy-basis (HHV). Equation 9.5 expresses the profit rate function of the process stage.

$$f_{\text{Profit rate}}(F_{pulp}, Q_{WBL}, F_{wood}, F_{WL}, Q_{steam}) = p_{pulp}F_{pulp} + \eta_{RL}p_{EE}Q_{WBL} - f_{\text{Cost rate}}(F_{wood}, F_{WL}, Q_{steam}) \quad \textbf{9.5}$$

The reader will have noted that energy flows are multiplied by conversion efficiency factors. This is an important requirement that can be used to calibrate the weight given to these opportunity revenues and costs. Although not the whole chemical energy provided by the WBL solids is transformed into electrical energy for sale, we do not need to considered an additional factor to describe this condition as it can be included in the value of η_{RL}. Table 9.1 shows the values given to prices and conversion efficiencies.

Table 9.1. Economic model parameters.

Parameter	p_{pulp}	p_{EE}	p_{wood}	p_{WL}	η_{RL}	η_{TG}
Unit	USD/ADt	USD/MWh	USD/m^{3}sub	USD/tNa_2O		
Value	500	100	38	60	0.2	1

Though the units in the variables of the objectives functions are not exactly the same from the input and outputs variables of the process model (see Algebraic Notation), they can be easily converted from one to another; therefore, these operations are implemented graphically in the Simulink model file, wrapping them in a subsystem block that represents the economic model as shown in Figure 9.2.

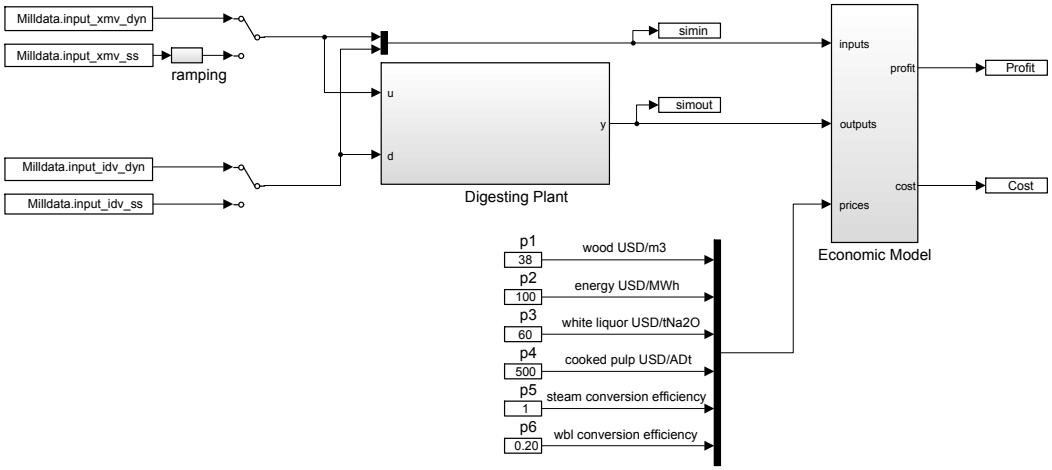

Figure 9.2. Economic model connected to the process model in Simulink interface.

9.1.2 Steady-state model and constraints

Given the implementation of the economic model, objective functions are always evaluated in parallel to the simulation of the dynamic process model. However, we are concern only with values at the steady-state, i.e., complying with

$$\vec{y}_{ss} = \vec{y}\left(\vec{u}_{ss}(t \to \infty)\right) \qquad \textbf{9.6}$$

where $\vec{u}_{ss}$ is maintained constant. The infinite time of this condition is approximated by 2000 min (~1.4 d) of dynamic simulation without delay elements in order to accelerate computations (see Section 7.2.2.1.4). Despite the latter, we still needed a long value to deal with the intrinsically slow process dynamics. By solving the simulation model in this way, we are using the simulator as a steady-state process model, which we can be denoted as the static operating model for the optimization task.

The process optimizer is basically searching for $\vec{u}_{ss}$ input vectors that improve a selected objective function and comply with a set of constraints on manipulated variables and outputs. A reader skilled in the art will understand that (i) the "true" optimal $\vec{u}_{ss}$ cannot be found, (ii) an infinite number of input vectors may actually improve the objective functions, and (iii) an improved input vector under certain disturbance conditions may become detrimental for the process economics when disturbances change. The foregoing motivates the development of real-time and dynamic process optimization techniques, but these topics are outside the scope of the thesis. In any case, we need to understand that manipulated variables and

outputs are physically connected in the nature of the process itself, but also logically connected through the control structure. In this sense, two set-points values of the process will define constraints for our formulation of the optimization problem: bleached pulp production rate and cooking kappa.

Figure 9.3 shows how the control system changes the chip meter speed tracking set-point changes given by the operator. The signal noise is most probably contributed from process noise due to the difficulty of maintaining a stable frequency of rotation. The horizontal line in the upper subplot corresponds to the value calculated by the DCS to comply with the production rate set-point in the first step of the ladder. This value will be used as a constraint on manipulated variables, thus we aim to optimize the process for a production rate of 1535 ADt/d. This problem formulation is likely unconventional, but it is the right one as long as the control system changes the chip meter speed without truly controlling the cooked pulp production rate (cooking and bleaching yields are already "known" and assumed constant).

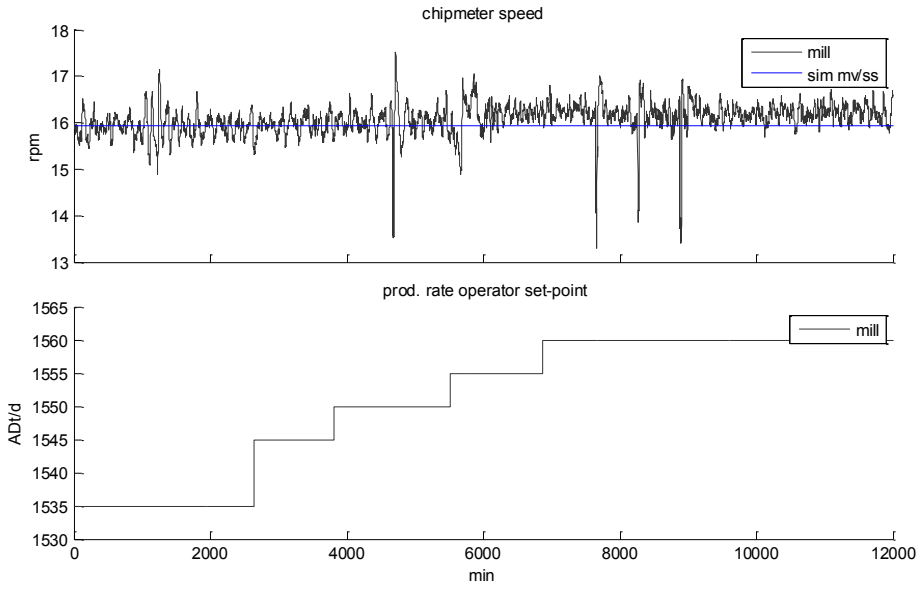

Figure 9.3. Selection of the pulp production rate condition to be optimized.

Table 9.2 summarizes all the constrain values used in the optimization task. These numbers reflect the process knowledge of the author together with the guidance from mill operators. The maximum compacting pressure is a difficult criterion to define numerically, as it depends on an unmeasurable variable involved in vessel plugging. Here, its higher bound was simply set as a rounded

value near the maximum pressure simulated during model testing and validation. The lower bound on EA concentration in liquor streams is meant to avoid lignin condensation and precipitation, a detrimental phenomenon for pulp production known to occur at very low alkali concentration (see Chapter 3).

Table 9.2. Summary of constraint values for the optimization task.

			Lower bound	Higher bound
Manipulated variables				
1	Chip meter speed	rpm	15.925	15.925
2	Flow rate of MP steam	kg/s	0	30
3-8	Flow rate of liquor streams	l/s	0	300
9-16	Splits fraction		0	1
Outputs				
1	Cooking kappa*		28.66	28.66
6	Blowline consistency	%w/v	11	13
23-28	EA conc. of liquor streams	g/l	5	M
42-43	Vessels max. compacting pressure	kPa	0	30
	Remainder outputs		0	M

9.2 Linear programming approach

The general form of the optimization task stated in Eq. 9.1 is a non-linear problem that can be extremely difficult to be solved given the size of the process model and most likely it would at least demand the use of advanced computing. Instead, a linearized form of the task is a routine problem for an average PC, which could be solved even at fixed time intervals, thus creating the basis for a real-time optimization technology. In order to use a linear programming algorithm, the optimization problem must be translated into the standard form for LP-solvers given below

$$\min_{\vec{x}} \quad \vec{f}^T \vec{x} \tag{9.7}$$

* Nominal set-point is 28 but here it is considered the average value during the steady-state identification period

$$\text{such that} \begin{cases} A\vec{x} = \vec{b} \\ \vec{x}_{lb} \leq \vec{x} \leq \vec{x}_{ub} \end{cases}$$

This can be achieved by linearizing the objective function as well as the steady-state process model. As we need to define a point around which the functions are linearized, the natural solution is to use an identified steady-state from mill data that represents the condition to be optimized (see Section 8.3). Let us show then how the linearization is done.

Below indices j and i enumerate the input and outputs variables of the operating model in the following ranges,

$$j \in \{1, \dots, m\}$$

$$i \in \{1, \dots, n\}$$

i.e., we work with an operating model having m inputs and n outputs. Should be noted that these numbers are not necessarily the same of the original process model; in fact, we only need to consider manipulated variables as inputs and a set of outputs relevant for optimization purposes. The linearized form of the objective function is explained by Eqs. 9.8 to 9.11 as follows,

$$f(\vec{u}) \approx f(\vec{u}_0) + \vec{c}^T(\vec{u} - \vec{u}_0) \quad \textbf{9.8}$$

$$\min_{\vec{u}} \quad f(\vec{u}) \implies \min_{\vec{u}} \quad \vec{c}^T\vec{u} \iff \min_{\vec{x}} \quad \vec{f}^T\vec{x} \quad \textbf{9.9}$$

$$\vec{f} = \begin{bmatrix} \vec{c} \\ - \\ 0 \end{bmatrix} \qquad \vec{f} \in \mathbb{R}^{m+n\times 1} \quad \textbf{9.10}$$

$$\vec{x} = \begin{bmatrix} \vec{u} \\ - \\ \vec{y} \end{bmatrix} \qquad \vec{x} \in \mathbb{R}^{m+n\times 1} \quad \textbf{9.11}$$

Equations 9.12 to 9.16 explain the linearized form of the static operating model that is introduced as a constraint domain in the optimization task.

$$\vec{y}(\vec{u}) \approx \vec{y}(\vec{u}_0) + K(\vec{u} - \vec{u}_0) \quad \textbf{9.12}$$

$$-K\vec{u} + I\vec{y}(\vec{u}) = \vec{y}(\vec{u}_0) - K\vec{u}_0 \quad \textbf{9.13}$$

$$[-K \quad | \quad I]\begin{bmatrix}\vec{u}\\-\\\vec{y}\end{bmatrix} = \vec{y}(\vec{u}_0) - K\vec{u}_0 \tag{9.14}$$

$$A = [-K \quad | \quad I] \qquad A \in \mathbb{R}^{n\times m+n} \tag{9.15}$$

$$\vec{b} = \vec{y}(\vec{u}_0) - K\vec{u}_0 \qquad \vec{b} \in \mathbb{R}^{m+n\times 1} \tag{9.16}$$

The elements of the $\vec{c}$ vector and K matrix are determined by a series of simulated experiments with the process model. Essentially, these elements approximate the gradient (or Jacobian) of the linearized function at the identified state-steady. The goodness of the approximation is critical for the whole task, since the gradient guides the optimization algorithm to its final result. A basic idea to determine these elements consist of changing each variable of the initial $\vec{u}_0$ only two times while maintaining all the remainder variables the same. Assuming that each variable can be incremented and decremented, we will have per each manipulated variable 2 input values (u_j^u and u_j^d), 2 values of the objective function (f_j^u and f_j^d) and 2·n output values (y_{ij}^u and y_{ij}^d), with this amount of data the c_j and K_{ij} elements are defined as follows,

$$c_j = \frac{\Delta f_j}{\Delta u_j} \tag{9.17}$$

$$K_{ij} = \frac{\Delta y_{ij}}{\Delta u_j} \tag{9.18}$$

$$\Delta f_j = f_j^u - f_j^d \tag{9.19}$$

$$\Delta y_{ij} = y_{ij}^u - y_{ij}^d \tag{9.20}$$

$$\Delta u_j = u_j^u - u_j^d \tag{9.21}$$

In this work, however, we use a slightly improved procedure that consists of including the data from the initial $\vec{u}_0$ in the calculation of the gradient. In principle, this should increase the accuracy of the aproximation as more data points are used to compute the elements c_j and K_{ij}. The idea behind this modification should be easily understood by a geometrical reasoning. We are now considering three points for approximating the gradient around the base identified steady-state, thus as a natural linear estimate we can used the least square regression leading to the following forms

$$c_j = \left[\mathbf{X_u}^{\mathrm{T}}\mathbf{X_u}\right]^{-1}\mathbf{X_u}^{\mathrm{T}}\mathbf{\Upsilon_f} \tag{9.22}$$

$$K_{ij} = \left[\mathbf{X_u}^{\mathrm{T}}\mathbf{X_u}\right]^{-1}\mathbf{X_u}^{\mathrm{T}}\mathbf{\Upsilon_y} \tag{9.23}$$

where the matrices with observations are defined according to

$$\mathbf{\Upsilon_f} = \begin{bmatrix} f_j^u - f_0 \\ 0 \\ f_j^d - f_0 \end{bmatrix} \tag{9.24}$$

$$\mathbf{\Upsilon_y} = \begin{bmatrix} y_{ij}^u - y_{0,i} \\ 0 \\ y_{ij}^d - y_{0,i} \end{bmatrix} \tag{9.25}$$

$$\mathbf{X_u} = \begin{bmatrix} u_j^u - u_{0,j} \\ 0 \\ u_j^d - u_{0,j} \end{bmatrix} \tag{9.26}$$

In practical terms, the above method requires a good selection of the increment and decrement in the manipulated variable. The increment (decrement) should not be too large or too small in order to capture a significant trend in the output. Obviously, this qualitative condition can only be assessed by trial-and-error. In the case that the manipulated variable cannot be increased (decrease), we can still gather more points by increasing the original increment. In fact, we can collect as much points as we desire near the linearization point, but this does not imply improving the estimate accuracy if we start moving too far from the original point.

All the above operations are implemented as a Matlab script that runs the simulator $2m + 1$ times, which can take several minutes especially depending on the approximation of the infinite time needed to obtain steady-state responses. Once enough data have been collected, $\vec{c}$ vector and K matrix are computed and the optimization problem is solved calling a linear programming algorithm (through Matlab linprog() function). The latter step takes a very short time; however, the linear optimum thus found $\vec{u}_l^*$ is not the final result. The last part of the method involves a heuristic modification of the computed values, such that the operating constraints are actually met in the non-linear process model. A simple heuristic is a weighted sum of the initial $\vec{u}_0$ vector and the linear optimum $\vec{u}_l^*$ according to

$$\vec{u}_h^* = \vec{\alpha} .* \vec{u}_0 + \vec{\beta} .* \vec{u}_l^* \quad \text{9.27}$$

where weighting factors in the vectors $\vec{\alpha}$ and $\vec{\beta}$ are adjusted until complying with the operating constrains. Obviously, if we choose values such that $\alpha_j + \beta_j = 1$, we are sure that at some point of the iteration constraints will be met, however, we may "lose" to some extent the optimization effort. The adjustment of these factors is better done based on process knowledge. That is, analyzing the direction of change proposed by the linear optimum and then deciding which manipulated variables should be let more near to the $\vec{u}_l^*$ vector and which ones to the $\vec{u}_0$ vector. Clearly, the adjustment of the weighting factors should also consider changes in the value of the objective function, thus we are evaluating which variables are "worth" to be optimized.

The optimization method has been designed in the basis of an input-output model of the process itself, i.e., without the need for including the control structure. Though we optimize by changing the manipulated variables directly, the relevant results lie in the output variables, in which we finally recognize optimized set-points for the control system at the mill. The set-point values can be passed to the supervisory control of the digesting stage, which will be compelled to manipulate the process in similar way as given by the manipulated variables found through the optimizer. More on this topic is discussed in the next chapter.

The above procedure could be classified as a heuristic, single-objective, single-step, linear-programming process optimization method. Nonetheless, it could be easily expanded into a multi-objective and multi-step (iterative) method by minor changes while maintaining the linear programming approach. Since the linear form of the operating model may imply a considerable linearization error, alternatives approximations, which can reduced the numerical burden of using the original non-linear model, are appealing approaches to improve the optimization results. In this sense, the recent work of Zakharov & Jämsä-Jounela (2011) is especially attractive by suggesting means to use more accurate quadratic approximations that can be the basis for designing an improved process optimizer. In any case, the current design is already useful and effective as evidenced by the results of its application.

10 Optimization Results

Let us now show and discuss the results of the optimization method as applied to maximize the profit rate or minimize the cost rate of the simulated CompactCooking™ G2 stage, considering a particular scenario with nominal production rate of 1535 ADt/d and cooking kappa 28. As explained at the beginning of this Chapter, these two problems are formulated and solved independently of each other by selecting a different objective function (Eq. 9.4 or Eq. 9.5) in the course of the method application.

For sake of simplicity, the below result corresponds to the final heuristically modified vectors $\vec{u}_h^*$ and their associated steady-state outputs $\vec{y}_h^*$. Likewise, the scope of the discussion reduces to assess the applicability of the method, rather than thoroughly evaluating these particular results.

10.1 Heuristic optima

Table 10.1 summarizes the values on manipulated variables in the base identified steady-state, the profit maximization problem, and the cost minimization case. The input values on disturbance were maintained same as the base case (see Section 8.3). In this sense, the below values are near-optimal as long as disturbances do not move far from this identified steady-state. Obviously, important changes in disturbances, such as those provoked by seasonal temperatures or raw material variations, would demand an effort of real-time optimization.

Table 10.1. Steady-state optimization results: manipulated variables.

		Ubase	Uprofit	Ucost
Chip meter speed	rpm	15.925	15.925	15.925
MP steam flow rate	kg/s	10.27	8.07	9.40
White liquor flow rate	l/s	58.89	70.16	51.74
Wash liquor flow rate	l/s	151.41	149.39	140.87
Middle extraction flow rate	l/s	35.58	146.08	32.88
Transfer liquor flow rate	l/s	232.52	274.69	151.14
Upper extraction flow rate	l/s	114.11	42.79	179.17

Lower extraction flow rate	l/s	126.10	132.90	99.18
*Filter reject flow rate	l/s	35.15	198.00	22.84
Filter reject split fraction	v/v%	15.76	51.01	10.72
White liquor split fraction 1	v/v%	10.19	48.45	06.62
White liquor split fraction 2	v/v%	44.55	16.71	28.96
White liquor split fraction 3	v/v%	0.00	18.86	06.57
Transfer liquor split fraction 1	v/v%	23.00	65.41	14.95
Transfer liquor split fraction 2	v/v%	2.23	36.84	1.45
Upper liquor split fraction 1	v/v%	13.97	5.24	9.08
Upper liquor split fraction 2	v/v%	24.06	71.52	50.64

As seen in the above table, the optimizer has detected opportunities to increase profit or reduce operating costs by decreasing the consumption of MP steam. In the cost minimization case, the algorithm suggests the possibility to decrease white liquor and MP steam consumption at the same time. However, in the profit case, it indicates a need for increasing the fresh alkali charge in the digester, perhaps as a compensation for the higher decrease in MP steam. The latter can be understood observing also the output values given in Table 10.2. In any case, the discrepancy in the trend between profit and cost optimization could be better explained by the “opening” of the recycling path of the filter reject liquor, especially because the profit case requires a significant increment in the filter reject ratio, from 15.76% to 51.01%, which provokes a higher dilution of the alkali concentration since the “opened” recycle brings no dissolved component. That is, the discrepancy in digester fresh alkali charges may be an artificial result provoked by the dilution effect of an “opened” recycle. Whatever the case, this is a very interesting result that highlights the relevance of interactions caused by liquor recycling, and it demands us to consider the use of advanced computing such that no recycle be omitted. In principle, average computing power could have been used to perform the optimization tasks with the simulator including all recycles, but computation times may have ranged from days to weeks (at least under the sequential-modular solving strategy used by Simulink).

Table 10.2 shows the optimization results for the whole set of output variables included in the operating model. Constraints on outputs are well met in both tasks: profit maximization and cost minimization. While the results from the latter

* Not an actual input of the simulator, shown to support the discussion

may slightly decrease yield, from 48.74% to 48.71%; in the former case, we find a cooking recipe able to increase it significantly in 0.75%, equivalent to a 1.54% rise of the effective production rate. This yield increase is also reflected in the reduction of the WBL solids fraction, which constitutes a concomitant and expected result.

The fact that the process can have a higher yield even at the same kappa number is explained by the general rate of wood substance degradation. That is, a particular kappa number value represents a combination of lignin and carbohydrates basic concentrations (kg/m^3sub), which can be preserved at different values of them while changing the resultant basic density of the chips. The reader should remember that the sum of these basic concentrations is the actual basic density of a woodchips parcel, which is decreasing along its trajectory through the digesting vessels and represents the yield loss of the cook.

In the profit maximization case, and according to our heating value estimate (see Section 7.2.2.3.5), WBL HHV would decrease and the total chemical energy flow sent to recovery line would be almost 0.5% less. On the contrary, WBL HHV increases in the cost minimization case; however, the total chemical energy flow still declines because the washing efficiency in the digester falls, i.e., cooked pulp carries over a higher amount of dissolved matter than in the base case.

Table 10.2. Steady-state optimization results: outputs.

		Ybase	Yprofit	Ycost
Cooked pulp prod. rate	ADt/d	1663.88	1689.62	1662.80
WBL prod. rate	tDS/d	1874.78	1947.90	1823.43
Cooking kappa	κ	28.66	28.62	28.62
Cooking yield	w/w%	48.74	49.49	48.71
Cooking wood specific cons.	m^3sub/ADt	4.82	4.75	4.83
Blowline consistency	w/v%	12.46	11.70	12.49
WBL solids fraction	w/v%	9.78	7.62	10.20
Cooked pulp intrinsic viscosity	ml/g	1039.52	1043.01	1054.78
Cooked pulp carry-over	kgDS/BDt	49.12	41.96	50.97
Impbin top temp.	C	97.06	95.49	99.54
Digester top temp.	C	151.63	153.06	152.88
Top liquor temp.	C	125.46	121.33	131.83

Transfer liquor temp.	C	116.50	117.27	122.36
Upper extraction temp.	C	155.45	157.74	156.40
Lower extraction temp.	C	144.89	151.66	146.67
Blowline temp.	C	100.86	100.96	100.91
White liquor hot temp.	C	140.60	145.53	141.30
Lower extraction cold temp.	C	141.63	147.03	142.48
Top liquor EA conc.	g/l	32.26	24.24	29.64
Bottom liquor EA conc.	g/l	14.86	13.12	13.09
Transfer liquor EA conc.	g/l	14.63	12.95	12.49
Upper extraction EA conc.	g/l	16.57	13.70	14.98
Lower extraction EA conc.	g/l	7.85	7.10	6.36
Top liquor flow rate	l/s	151.61	166.09	137.37
Bottom liquor flow rate	l/s	198.67	147.75	201.03
Blowline flow rate	l/s	139.15	150.49	138.70
EA/W total	w/w%	20.05	21.97	18.83
EA/W impbin fresh	w/w%	8.02	5.77	6.70
EA/W digester fresh	w/w%	12.03	16.20	12.13
L/W impbin top	m^3/BDt	5.58	5.98	5.18
L/W impbin bottom	m^3/BDt	4.58	3.44	4.22
L/W digester cook zone 1	m^3/BDt	5.89	5.33	6.56
L/W digester cook zone 2	m^3/BDt	2.86	3.30	2.62
DF digester wash zone	m^3/ADt	1.24	0.60	0.99
H-factor	H	631.41	714.71	703.77
Impbin Pc max	kPa	13.88	14.92	12.99
Digester Pc max	kPa	23.37	31.50	23.99
WBL energy flow as HHV	MJ/min	21431.71	21327.60	21390.47
MP steam energy flow as λ_{eff}	MJ/min	1224.36	1093.45	1172.67
WBL HHV	MJ/kg dry	16.46	15.77	16.89

In order to fulfill the constraint on the final kappa, the algorithm tries to change the cooking temperature by taking into account the interactions caused by changes in compaction (retention times) and reagents concentrations. The capacity to ponder interactions when deciding changes on manipulated variables is a unique feature of this model-based optimization method, which would not be achievable by any experimental procedure. The fact that this constraint is met successfully represents a remarkable result of the method, considering that

otherwise any isolated change in a manipulated variable would likely drive the process away from the set-point kappa. Since the optimizer is manipulating flow rates, vessels will experience changes in their compaction profiles that might eventually provoke a vessel plugging. To avoid this, constraints on compacting pressures have been set; however, as discussed in Section 8.2, compacting pressures cannot be directly measured and therefore it is difficult to determine maximum allowable values. Alternatively, we could set constraints on the compaction degree of the vessels directly by experimentally determining critical values during actual plugging incidents at the mill.

In summary, in the case of profit maximization the optimizer has found higher economical value by increasing yield rather than chemical energy sent to the recovery line. The increased yield could be explained as a decrease of yield loss in the impregnator by means of reducing its fresh alkali charge and temperature, and a faster and more selective delignification in the digester by exploiting the difference in activation energy of wood reactions. In the case of cost minimization, the algorithm has found lower operating costs mainly by diminishing alkali charge while maintaining the cooking yield almost unaffected. Naturally, the difference between results is caused by the definition of the objective function, which highlights the relevance of distinguishing between profit and cost of a chemical process in the context of its optimization.

10.2 Economic assessment

Although we already know that the optimization problems formulated are solvable, we still need to assess the economic significance of the optimized set-point in order to judge the applicability of the method. That is, the whole procedure could be useless if optimized set-points do not report a significant improvement of the process economics. In this sense, the determination of external prices and the estimation of internal costs parameters, including the white liquor cost and conversion efficiencies, are important steps to attain meaningful results.

Likewise, optimization results should be statistically significant against the dynamic variability of the process, i.e., the improvement of the objective function must be distinguishable from normal fluctuations in the base steady-state due to process noise and disturbances. The latter, however, is not easily verifiable

especially because it involves the performance of the control system, which may even increase the variability of the closed-loop process response if controllers are poorly tuned or the whole control scheme is ill-defined. In this sense, we should remember that process optimization relies on the inferior layers of the automation pyramid, i.e., any optimization effort will be useless if the control and instrumentation layers work improperly. In fact, we have already mentioned that the lack of temperature sensors negatively affects the model calibration, but it also means that the control system is hampered to reject disturbances provoked by fluctuations of these unmeasured temperature variables, and thus these unrejected disturbances will obviously increase the variability of the process.

It has been explained above that the linear programming algorithm decides moves in manipulated variables in order to optimize a linearized economic model of the process (objective function). These moves are then heuristically modified to fulfill operating constraints, thus delivering the final optimization results from where near-optimal set-points are recognized. However, we still need to compute the actual improvement of the original (non-linear) economic model to confirm that the optimization has economical value. Figure 10.1 shows the results of profit rate maximization and cost rate minimization tasks comparing them to the base case scenario at steady-state and dynamic conditions, i.e., to the base identified steady-state and to the dynamic evaluation of the economic model during the period of identification. The figure additionally shows the previous optimization results as evaluated by other four economic models derived from the original ones (see Section 9.1). That is, though the figure depicts six subplots of different objectives functions, only two of them were actually used in the optimization tasks.

In terms of profit rate increment, the results from the profit maximization task are clearly superior to those of the cost minimization task. Interestingly, when comparing the optimization results in terms of profit per ADt, both tasks seem to yield the same improvement. This apparent contradiction is explained by the fact that the profit per ADt evaluation ignores the effective rise of the production rate. Profit increases in at least 3 USD/ADt in both cases, thus considering the nominal production rate of 1535 ADt/d and a conservative mill availability of 90%, it can range between 1 – 2 million USD the annual benefits experienced by the plant from these optimization efforts.

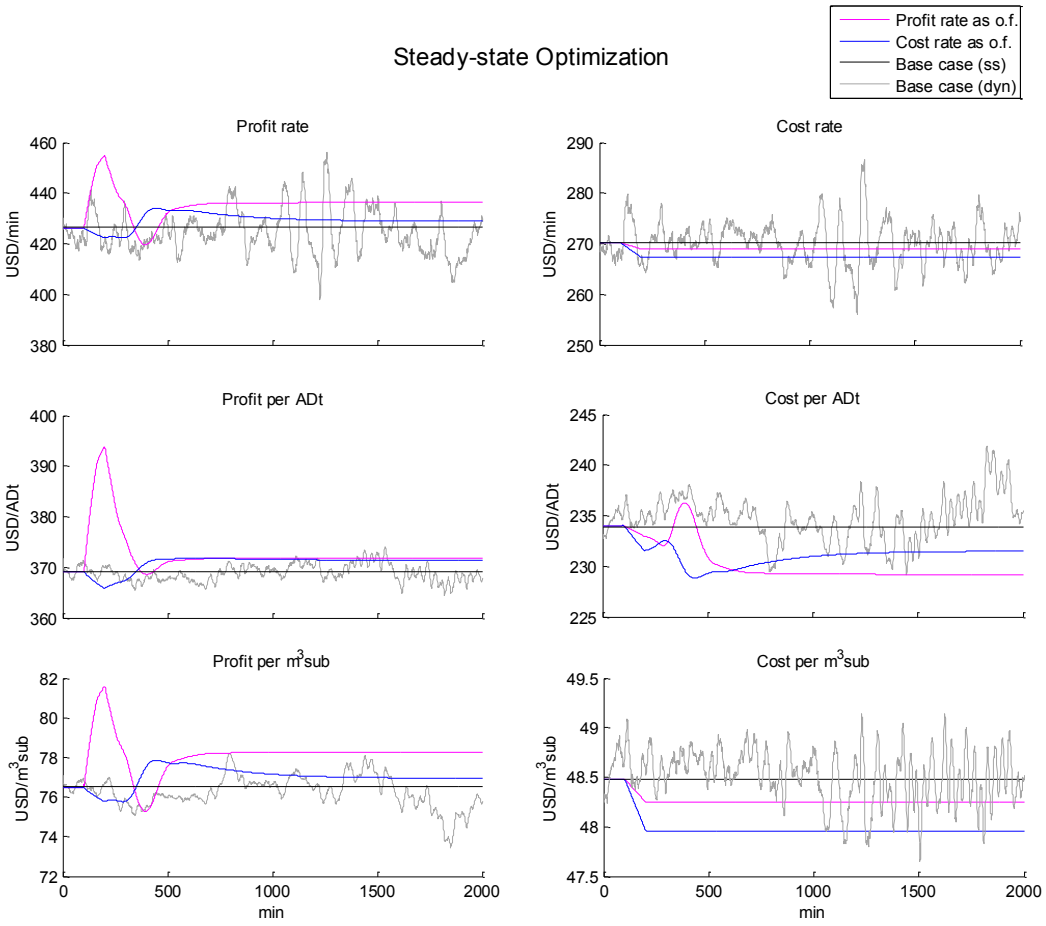

Figure 10.1. Comparison of optimization results as expressed by different economic models.

During first 100 min the process is run at the base, identified steady-state, after that it is ramped up to the optimized states found for the tasks of profit rate maximization (magenta signal) and cost rate minimization (blue signal). The dynamic variability of process economics at the identification period is plotted in the background (gray signal).

Since the profit expressed by the economic models is only an indicative number and not as "concrete" as the computed operating costs, we can recalculate our previous estimation in terms of cost savings. In this sense, both tasks are able to reduce costs in at least 2 USD/ADt, which still yields the same range of economic value in annual savings under equal considerations of production rate and mill availability. Should be noted also that by means of evaluating the optimization results in terms of profit or cost per m^3sub (of processed wood), we can realize that the new set-points are statistically significant against process variability, at least as seen during the period of identification.

Finally, let us summarize in Table 10.3 our optimization results expressed as two new cooking recipes for the mill DCS. Whether these recipes are effective or not

remains a question that can be solely answered by industrial testing. In any case, it must be recalled that these values represent just examples of application of the model-based optimization method designed in this work, which is to be ideally leveraged as the basis for a real-time optimization technology.

Table 10.3. New cooking recipes obtained from the profit maximization and cost minimization tasks.

		Base	Profit	Cost
Constraint set-points *(nominal)*				
Bleached pulp prod. rate	ADt/d		1535	
Cooking kappa	κ		28	
Computed set-points				
EA/W total	%	20.05	21.97	18.83
EA/W impbin fresh	%	8.02	5.77	6.70
EA/W digester fresh	%	12.03	16.20	12.13
L/W impbin top*	m^3/BDt	5.58	5.98	5.18
L/W impbin bottom	m^3/BDt	4.58	3.44	4.22
L/W digester cook zone 1	m^3/BDt	5.89	5.33	6.56
L/W digester cook zone 2	m^3/BDt	2.86	3.30	2.62
DF digester wash zone	m^3/ADt	1.24	0.60	0.99
H-factor	H	631.41	714.71	703.77
Filter reject split fraction	%	15.76	51.01	10.72
Simulated variables				
Cooking kappa	κ	28.66	28.62	28.62
Digester top temp.	C	151.63	153.06	152.88
MP steam flow rate	kg/s	10.27	8.07	9.40
Cooked pulp prod. rate	ADt/d	1663.88	1689.62	1662.80
Cooking yield	%	48.74	49.49	48.71
Cooking wood sp. cons.	m^3sub/ADt	4.82	4.75	4.83

* Eventually used as a degree of freedom by the control system, thus not available as a set-point in the supervisory control layer

11 Conclusions

This thesis provides a method to compute optimal set-points for a CompactCooking™ G2 kraft digesting stage based on mathematical modelling, numerical simulation, and linear optimization. Thus, a model-based optimization method has been successfully designed and evaluated. The method proved to be a valuable tool for process economics optimization as applied to a particular implementation of this process technology, in which it found a potential for increasing yield or reducing operating costs that can lead to annual benefits between 1 – 2 million USD depending on production rate and mill availability.

The background information for modelling unit operations considered is available as published material; hence, the added value by the thesis is to have successfully designed and implemented a dynamic simulator and a steady-state optimizer of the process studied based on it. Furthermore, this work has several merits given its novel contributions: (i) a simulation model architecture to represent a CompactCooking™ G2 process stage; (ii) a linear programming approach to search for optimal set-points of this process; and additionally, (iii) a first-principles depolymerization model, appropriate to describe pulp intrinsic viscosity and cellulose depolymerization; and (iv) a model-based process analysis technique, elaborated in Appendix A, that allows explaining the variability of the cooking kappa in the real process. Indeed, regarding the current publishing conventions, these four contributions may be further expanded and publish as separated research articles.

Besides the limitations of any linear programming approach for process optimization, i.e., model linearization error, the method can also suffered from non-linear model inaccuracy, input data uncertainty, and lack of comparable output data for model calibration. On one hand, several features of modelled phenomena were neglected because of the time limitation for the thesis work, which represents a known source of model inaccuracy. Likewise, two liquor recycles had to be “opened” from the originally designed model architecture, thus reducing the number of algebraic loops in order to decrease computation times. In this sense, we have lost interaction effects due to recycling of the fiber filter reject liquor and the pressure diffuser filtrate. Nevertheless, all these simplifications contributed to short computation times that enabled the use of the simulation model for optimization purposes on an average PC. On the other

hand, the lack of temperature data from inflow and outflow streams of heat-exchangers, due to the absence of sensors in the mill, made very difficult the calibration of heat-exchanger models parameters and a significant bias was generated in temperature signals when using simple data estimates.

Despite the above, the process simulator showed a very good agreement with industrial data during testing and validation in a time span of 200 hours at stable operation. Liquors residual alkali, weak black liquor solids, and blowline kappa signals correlate fairly well to industrial data, which confirms the fidelity of the Purdue wood reactions kinetic model used as a foundation for the process simulator. In any case, simulated kappa showed higher sensitivity to temperature fluctuations than the plant signal, likely indicating the need for more phenomenological detail especially in modelling of heat transfer phenomena.

Regarding the design of the process optimizer, several economic models have been defined for the CompactCooking™ G2 stage. The ability to choice among them, when applying the optimization procedure, allowed understanding the relevance of properly identifying the structure of costs and benefits in the process and the implications for process economics optimization.

Although this thesis was developed with data from a particular mill, the designed method can be applied in any other implementation of the CompactCooking™ G2 process by recalibrating the process model. Estimated economic benefits of applying this model-based optimization method should encourage industrial testing and further development in order to create a real-time optimizer software technology for the pulp and paper industry.

References

af Ekenstam, A. (1936). Über das Verhalten der Cellulose in Mineralsäure-Lösungen, II. Mitteil.: Kinetisches Studium des Abbaus der Cellulose in Säure-Lösungen. *Berichte Der Deutschen Chemischen Gesellschaft (A and B Series)*, *69*(3), 553–559. http://doi.org/10.1002/cber.19360690315

Agarwal, N. (1993). *Modeling of continuous pulping* (Doctoral Dissertation). University of Washington. Retrieved from http://www.worldcat.org/oclc/29459398

Agarwal, N., & Gustafson, R. (1997). A contribution to the modeling of kraft pulping. *The Canadian Journal of Chemical Engineering*, *75*(1), 8–15. http://doi.org/10.1002/cjce.5450750104

Ahvenlampi, T., Rantanen, R., & Tervaskanto, M. (2006). Fault tolerant control application for continuous kraft pulping process. In Z. Zhang (Ed.), *Fault Detection, Supervision and Safety of Technical Processes* (Vol. 6, pp. 849–854). Tsinghua University, P.R. China: IFAC. http://doi.org/10.3182/20060829-4-CN-2909.00141

Akhtaruzzaman, A. F. M., & Virkola, N. E. (1979). Influence of chip dimensions in kraft pulping. IV. Effect on screened pulp yield and effective alkali consumption; predictive mathematical models. *Paperi Ja Puu*, *61*(12), 805–814.

Akhtaruzzaman, A. F. M., & Virkola, N. E. (1980). Influence of chip dimensions in kraft pulping. V. Effect on total yield and screening rejects; predictive mathematical models. *Paperi Ja Puu*, *62*(1), 15–26.

Alaqqad, M., Bennington, C. P. J., & Martinez, D. M. (2012). The permeability of wood-chip beds: The effect of compressibility. *The Canadian Journal of Chemical Engineering*, *90*(5), 1278–1288. http://doi.org/10.1002/cjce.20638

Andersson, N. (2003). *Modelling of Kraft Cooking Kinetics Using Near Infrared Spectroscopy*. Karlstad University. Retrieved from http://urn.kb.se/resolve?urn=urn:nbn:se:kau:diva-21541

Andersson, N., Wilson, D. I., & Germgård, U. (2002). Validating continuous kraft digester kinetic models with online NIR measurements. In *Proceedings of the American Control Conference 2002* (pp. 3783–3787 vol.5). Anchorage: IEEE. http://doi.org/10.1109/ACC.2002.1024516

Andersson, N., Wilson, D. I., & Germgård, U. (2003). An improved kinetic model structure for softwood kraft cooking. *Nordic Pulp and Paper Research*

Journal, *18*(02), 200–209. http://doi.org/10.3183/NPPRJ-2003-18-02-p200-209

Aurell, R., & Hartler, N. (1965a). Kraft Pulping of Pine. II. Influence of the charge of alkali on the yield, carbohydrate composition, and properties of the pulp. *Svensk Papperstidning*, *68*(4), 97–102.

Aurell, R., & Hartler, N. (1965b). Kraft pulping of pine. I. The changes in the composition of the wood residue during the cooking process. *Svensk Papperstidning*, *68*(3), 59–68.

Baldea, M., & Daoutidis, P. (2012). *Dynamics and nonlinear control of integrated process systems*. Cambridge: Cambridge University Press.

Bhartiya, S., Dufour, P., & Doyle, F. J. (2001). Thermal-hydraulic digester model using a higher order numerical method. Presented at the American Institute of Chemical Engineers (AIChE) Fall meeting, Reno, Nevada, USA.

Bhartiya, S., Dufour, P., & Doyle, F. J. (2003). Fundamental thermal-hydraulic pulp digester model with grade transition. *AIChE Journal*, *49*(2), 411–425. http://doi.org/10.1002/aic.690490212

Bhat, S., Srinivasa, B. B., & Pathath, P. (2012, March 1). System and a method for optimization of continuous digestion process. Retrieved from http://www.google.co.in/patents/US20120048492

Biermann, C. J. (1996). *Handbook of Pulping and Papermaking* (2nd ed.). San Diego: Academic Press.

Blanco, A., Dahlquist, E., Kappen, J., Manninen, J., Negro, C., & Ritala, R. (2009). Use of modelling and simulation in the pulp and paper industry. *Mathematical and Computer Modelling of Dynamical Systems*, *15*(5), 409–423. http://doi.org/10.1080/13873950903375387

Bogren, J. (2008). *Further insights into kraft cooking kinetics* (Doctoral thesis). Chalmers University of Technology. Retrieved from http://publications.lib.chalmers.se/publication/75043-further-insights-into-kraft-cooking-kinetics

Calvini, P. (2012). The role of the Ekenstam equation on the kinetics of cellulose hydrolytic degradation. *Cellulose*, *19*(2), 313–318. http://doi.org/10.1007/s10570-011-9645-5

Castro, J. J., & Doyle, F. J. (2002). Plantwide Control of the Fiber Line in a Pulp Mill. *Industrial & Engineering Chemistry Research*, *41*(5), 1310–1320. http://doi.org/10.1021/ie010008x

Castro, J. J., & Doyle, F. J. (2004). A pulp mill benchmark problem for control: problem description. *Journal of Process Control*, *14*(1), 17–29. http://doi.org/10.1016/S0959-1524(03)00011-8

Chase, M. W. (1998). *NIST-JANAF Thermochemical Tables* (4th ed.). Woodbury, N.Y.: American Institute of Physics for the National Institute of Standards and Technology.

Christensen, T. (1982). *A Mathematical Model of the Kraft Pulping Process* (Doctoral Dissertation). Purdue University. Retrieved from http://docs.lib.purdue.edu/dissertations/AAI8225697

Courchene, C. E., Mcdonough, T. J., Hart, P. W., Malcolm, E. W., & Carter, B. R. (2005). Determining the heat of reaction of kraft pulping. *Tappi Journal*, *4*(12), 9.

Dahlquist, E. (2008). Process Simulation for Pulp and Paper Industries: Current Practice and Future Trend. *Chemical Product and Process Modeling*, *3*(1). http://doi.org/10.2202/1934-2659.1087

Danielsson, S., Kisara, K., & Lindström, M. E. (2006). Kinetic Study of Hexenuronic and Methylglucuronic Acid Reactions in Pulp and in Dissolved Xylan during Kraft Pulping of Hardwood. *Industrial & Engineering Chemistry Research*, *45*(7), 2174–2178. http://doi.org/10.1021/ie051386v

da Silva Perez, D., & van Heiningen, A. R. P. (2002). Determination of cellulose degree of polymerization in chemical pulps by viscosimetry. In H. Sixta (Ed.), *7th European Workshop on Lignocellulosics and Pulp: Proceedings* (pp. 393–396). Turku: Wiley-VCH.

da Silva Perez, D., & van Heiningen, A. R. P. (2015). Prediction of alkaline pulping yield: equation derivation and validation. *Cellulose*, 1–13. http://doi.org/10.1007/s10570-015-0735-7

Dence, C. W. (1992). The Determination of Lignin. In S. Y. Lin & C. W. Dence (Eds.), *Methods in Lignin Chemistry* (pp. 33–61). Berlin, Heidelberg: Springer Berlin Heidelberg.

Doyle, F. J., & Kayihan, F. (1999). Reaction profile control of the continuous pulp digester. *Chemical Engineering Science*, *54*(13–14), 2679–2688. http://doi.org/10.1016/S0009-2509(98)00363-7

Edgar, T. F., & Himmelblau, D. M. (1988). *Optimization of chemical processes*. New York: McGraw-Hill.

Ek, M., Gellerstedt, G., & Henriksson, G. (Eds.). (2009). *Pulping Chemistry and Technology* (Vol. 2). Berlin: De Gruyter.

Emsley, A. M., Heywood, R. J., Ali, M., & Eley, C. M. (1997). On the kinetics of degradation of cellulose. *Cellulose*, *4*(1), 1–5. http://doi.org/10.1023/A:1018408515574

Ergun, S. (1952). Fluid flow through packed columns. *Chemical Engineering Progress*, *48*, 89–94.

Evans, R., & Wallis, A. F. A. (1989). Cellulose molecular weights determined by viscometry. *Journal of Applied Polymer Science*, *37*(8), 2331–2340. http://doi.org/10.1002/app.1989.070370822

Fan, Y. (2005). *Numerical Investigation of Industrial Continuous Digesters*. University of British Columbia, Vancouver.

FAO. (2014). FAOSTAT Database. Retrieved October 3, 2014, from http://faostat.fao.org/

Fardim, P. (Ed.). (2011). *Chemical Pulping Part 1, Fiber Chemistry and Technology* (2nd ed., Vol. 6a). Helsinki: Paper Engineers' Association/Paperi ja Puu Oy.

Geankoplis, C. J. (1993). *Transport processes and unit operations* (3rd ed). Engelwood Cliffs, N.J: PTR Prentice Hall.

Gilarranz, M. A., Santos, A., García, J., Oliet, M., & Rodríguez, F. (2002). Kraft Pulping of Eucalyptus globulus: Kinetics of Residual Delignification. *Industrial & Engineering Chemistry Research*, *41*(8), 1955–1959. http://doi.org/10.1021/ie0108907

Grénman, H., Wärnå, J., Mikkola, J.-P., Sifontes, V., Fardim, P., Murzin, D. Y., & Salmi, T. (2010). Modeling the Influence of Wood Anisotropy and Internal Diffusion on Delignification Kinetics. *Industrial & Engineering Chemistry Research*, *49*(20), 9703–9711. http://doi.org/10.1021/ie101215a

Gustafson, R. R., Sleicher, C. A., McKean, W. T., & Finlayson, B. A. (1983). Theoretical model of the kraft pulping process. *Industrial & Engineering Chemistry Process Design and Development*, *22*(1), 87–96.

Härkönen, E. J. (1984). *A Mathematical Model for Two-phase Flow* (Doctoral Dissertation). Helsinki University of Technology, Espoo.

Härkönen, E. J. (1987). A mathematical model for two-phase flow in a continuous digester. *Tappi Journal*, *70*(12), 122–126.

Hatton, J. (1973). Development of yield prediction equations in kraft pulping. *Tappi Journal*, *56*(7), 97–100.

Hatton, J. (1976). Kraft pulping equations: Comparison of linear with nonlinear forms. *Tappi Journal*, *59*(12), 132–134.

He, P., Salcudean, M., Gartshore, I., & Bibeau, E. (1999). Modeling of kraft two-phase digester pulping processes. In *Process and Product Quality Conference and Trade Fair* (Vol. 3, pp. 1407–1418). Anaheim, California: TAPPI Press.

Holik, H. (Ed.). (2006). *Handbook of Paper and Board*. Weinheim: Wiley-VCH.

Imanuvilov, O. (Ed.). (2005). *Control theory of partial differential equations*. Boca Raton: Chapman & Hall/CRC.

Immergut, E. H., & Eirich, F. R. (1953). Intrinsic Viscosities and Molecular Weights of Cellulose and Cellulose Derivatives. *Industrial & Engineering Chemistry*, *45*(11), 2500–2511. http://doi.org/10.1021/ie50527a039

Jääskeläinen, A.-S., Saariaho, A.-M., & Vuorinen, T. (2005). Quantification of Lignin and Hexenuronic Acid in Bleached Hardwood Kraft Pulps: A New Calibration Method for UVRR Spectroscopy and Evaluation of the Conventional Methods. *Journal of Wood Chemistry and Technology*, *25*(1-2), 51–65. http://doi.org/10.1081/WCT-200058239

Johnsson, L. (1970). *Mathematical models of the kraft cooking process* (Doctoral Dissertation). Chalmers University of Technology, Gothenburg. Retrieved from http://www.worldcat.org/title/mathematical-models-of-the-kraft-cooking-process/oclc/33266285

Kayihan, F., Bills, A., & Hart, P. W. (2005). Mill application of a new continuous digester model. *AIChE Journal*, *51*(9), 2489–2494. http://doi.org/10.1002/aic.10497

Kayihan, F., Gelormino, M. S., Hanczyc, E. M., Doyle, F. J., & Arkun, Y. (1996). A Kamyr Continuous Digester Model for Identification and Controller Design. In *Proceedings of the 13th IFAC World Congress* (pp. 37–42). San Franciso: Elsevier.

Kerr, A. (1970). The kinetics of kraft pulping: progress in the development of a mathematical model. *Appita Journal*, *24*(3), 180–188.

Kerr, A., & Uprichard, J. (1976). The kinetics of kraft pulping: refinement of a mathematical model. *Appita Journal*, *30*(1), 48–54.

Kes, M., & Christensen, B. E. (2013). A re-investigation of the Mark–Houwink–Sakurada parameters for cellulose in Cuen: A study based on size-exclusion chromatography combined with multi-angle light scattering and viscometry. *Journal of Chromatography A*, *1281*, 32–37. http://doi.org/10.1016/j.chroma.2013.01.038

Kleinert, T. (1966). Mechanisms of alkaline delignification. I. The overall reaction pattern. *Tappi Journal*, *49*(2), 53–57.

Kubes, G. J., Fleming, B. I., Macleod, J. M., Bolker, H. I., & Werthemann, D. P. (1983). Viscosities of Unbleached Alkaline Pulps. II. The G-Factor. *Journal of Wood Chemistry and Technology*, *3*(3), 313–333. http://doi.org/10.1080/02773818308085166

Kulicke, W.-M., & Clasen, C. (2004). *Viscosimetry of Polymers and Polyelectrolytes*. Berlin, Heidelberg: Springer Berlin Heidelberg.

Laakso, S. (2008). *Modeling of chip bed packing in a continuous kraft cooking digester* (Doctoral Dissertation). Helsinki University of Technology, Espoo. Retrieved from http://lib.tkk.fi/Diss/2008/isbn9789512296781/isbn9789512296781.pdf

Lee, Q. F. (2002). *Fluid flow through packed columns of cooked wood chips* (Master Thesis). University of British Columbia, Vancouver. Retrieved from https://circle.ubc.ca/handle/2429/13865

Lee, Q. F., & Bennington, C. P. J. (2005). The Effect of Particle Size Distribution on Pressure Drop through Packed Beds of Cooked Wood Chips. *The Canadian Journal of Chemical Engineering*, *83*(4), 755–763. http://doi.org/10.1002/cjce.5450830416

Leiviskä, K. (Ed.). (2000). *Process Control* (Vol. 14). Helsinki: Fapet Oy.

Lémon, S., & Teder, A. (1973). Kinetics of the delignification in kraft pulping: I. bulk delig- nification of pine. *Svensk Papperstidning*, *76*(11), 407–414.

Li, J. (1999). *Towards an accurate determination of lignin in chemical pulps : The meaning of kappa number as a tool for analysis of oxidable groups*. KTH Royal Institute of Technology, Stockholm. Retrieved from http://urn.kb.se/resolve?urn=urn:nbn:se:kth:diva-2780

Li, J., & Gellerstedt, G. (1997). The contribution to kappa number from hexeneuronic acid groups in pulp xylan. *Carbohydrate Research*, *302*(3-4), 213–218. http://doi.org/10.1016/S0008-6215(97)00125-0

Lindgren, C. T., & Lindström, M. (1997). Kinetics of the bulk and residual delignification in kraft pulping of birch and factors affectingthe amount of residual phase lignin. *Nordic Pulp and Paper Research Journal*, *12*(21), 124–127. http://doi.org/10.3183/NPPRJ-1997-12-02-p124-127

Lindström, M. (1997). *Some factors affecting the amount of residual phase lignin during kraft pulping* (Doctoral Dissertation). KTH Royal Institute of Technology. Retrieved from http://urn.kb.se/resolve?urn=urn:nbn:se:kth:diva-2502

Łojewski, T., Zięba, K., & Łojewska, J. (2010). Size exclusion chromatography and viscometry in paper degradation studies. New Mark-Houwink coefficients for cellulose in cupri-ethylenediamine. *Journal of Chromatography A*, *1217*(42), 6462–6468. http://doi.org/10.1016/j.chroma.2010.07.071

Malkov, S. (2002). *Studies on liquid penetration into softwood chips: experiments, models and applications*. Helsinki University of Technology, Espoo.

Malkov, S., Kuzmin, V., Baltakhinov, V., & Tikka, P. (2003). Modelling the process of water penetration into softwood chips. *Journal of Pulp and Paper Science*, *29*(4), 137.

Marx-Figini, M. (1978). Significance of the intrinsic viscosity ratio of unsubstituted and nitrated cellulose in different solvents. *Die Angewandte Makromolekulare Chemie*, *72*(1), 161–171. http://doi.org/10.1002/apmc.1978.050720114

McKibbins, S. W. (1960). Application of Diffusion Theory to the Washing of Kraft Cooked Chips. *Tappi Journal*, *43*(10), 801–805.

Mercangöz, M., & Doyle, F. J. (2008). Real-time optimization of the pulp mill benchmark problem. *Computers & Chemical Engineering*, *32*(4–5), 789–804. http://doi.org/10.1016/j.compchemeng.2007.03.004

Michelsen, F. A. D. (1995). *A Dynamic Mechanistic Model and Model-based Analysis of a Continuous Kamyr Digester* (Doctoral Dissertation). University of Trondheim, Trondheim. Retrieved from http://folk.ntnu.no/bjarnean/pubs/others/thesis-michelsen.pdf

Michelsen, F. A., & Foss, B. A. (1994). Modeling and simulation of the mass flow and reaction kinetics in a continuous Kamyr steam/liquor phase digester. *Modeling, Identification and Control: A Norwegian Research Bulletin*, *15*(1), 33–53. http://doi.org/10.4173/mic.1994.1.4

Michelsen, F. A., & Foss, B. A. (1996). A comprehensive mechanistic model of a continuous Kamyr digester. *Applied Mathematical Modelling*, *20*(7), 523–533. http://doi.org/10.1016/0307-904X(95)00171-F

Miyanishi, T., & Shimada, H. (2001). Improvement of pulp strength and yield by computer simulation of lo-solids kraft cooking. *Tappi Journal*, *84*(6).

Molin, U., & Teder, A. (2002). Importance of cellulose/hemicellulose-ratio for pulp strength. *Nordic Pulp and Paper Research Journal*, *17*(01), 014–019. http://doi.org/10.3183/NPPRJ-2002-17-01-p014-019

Montané, D., Salvadó, J., Farriol, X., Jollez, P., & Chornet, E. (1994). Phenomenological kinetics of wood delignification: application of a time-

dependent rate constant and a generalized severity parameter to pulping and correlation of pulp properties. *Wood Science and Technology*, *28*(6), 387–402. http://doi.org/10.1007/BF00225458

Neretnieks, I. (1972). Analysis of Some Washing Experiments of Cooked Chips. *Svensk Papperstidning*, *72*(8), 19–825.

Nguyen, K. L., & Dang, V. Q. (2006). The fractal nature of kraft pulping kinetics applied to thin Eucalyptus nitens chips. *Carbohydrate Polymers*, *64*(1), 104–111. http://doi.org/10.1016/j.carbpol.2005.10.036

Nieminen, K. (2015). *Towards a comprehensive model for cooking processes* (Doctoral Dissertation). Aalto University, Helsinki. Retrieved from http://urn.fi/URN:ISBN:978-952-60-6612-7

Nieminen, K., Kuitunen, S., Paananen, M., & Sixta, H. (2014). Novel Insight into Lignin Degradation during Kraft Cooking. *Industrial & Engineering Chemistry Research*, *53*(7), 2614–2624. http://doi.org/10.1021/ie4028928

Nieminen, K., Paananen, M., & Sixta, H. (2014). Kinetic Model for Carbohydrate Degradation and Dissolution during Kraft Pulping. *Industrial & Engineering Chemistry Research*, *53*(28), 11292–11302. http://doi.org/10.1021/ie501359p

Nieminen, K., & Sixta, H. (2012). Comparative evaluation of different kinetic models for batch cooking: A review. *Holzforschung*, *66*(7). http://doi.org/10.1515/hf-2011-0122

Nieminen, K., Testova, L., Paananen, M., & Sixta, H. (2015). Novel insight in carbohydrate degradation during alkaline treatment. *Holzforschung*, *69*(6). http://doi.org/10.1515/hf-2014-0306

Oberlerchner, J., Rosenau, T., & Potthast, A. (2015). Overview of Methods for the Direct Molar Mass Determination of Cellulose. *Molecules*, *20*(6), 10313–10341. http://doi.org/10.3390/molecules200610313

Patankar, S. V. (1980). *Numerical heat transfer and fluid flow*. New York: Hemisphere Publ. Co.

Pougatch, K., Salcudean, M., & Gartshore, I. (2006). A numerical model of the reacting multiphase flow in a pulp digester. *Applied Mathematical Modelling*, *30*(2), 209–230. http://doi.org/10.1016/j.apm.2005.03.016

Poulakka, H.-M., & Kortela, U. (2005). Applicability of the chip compaction model in the controlling of the digester. *Pulp & Paper Canada*, *106*(9), 40–43.

Pu, Q., McKean, W., & Gustafson, R. (1991). Kinetic model of softwood kraft pulping and simulation of RDH process. *Appita Journal*, *44*(6), 399–404.

Rantanen, R. (2006). *Modelling and control of cooking degree in conventional and modified continuous pulping processes*. University of Oulu, Oulu. Retrieved from http://herkules.oulu.fi/isbn9514281500/isbn9514281500.pdf

Rantanen, R., Similä, E., & Ahvenlampi, T. (2004). Modeling of Kappa number in Downflow Lo-Solids cooking using Gustafson's model. *Pulp & Paper Canada*, *105*(5), 31–34.

Richter, J. (1949, July 5). Process and apparatus for continuous digestion of fibrous materials. Retrieved from http://www.google.com/patents/US2474862

RISI. (2014, May). Global pulp production capacity to grow 15% by 2014; demand increase likely to expand by 10%. *RISI PPI*. Retrieved from https://www.risiinfo.com/pulp-paper/ppila/Global-pulp-production-capacity-to-grow-15-by-2014-demand-increase-likely-to-expand-by-10.html

Rolandi, P. A., & Romagnoli, J. A. (2003). Smart enterprise for Pulp and Paper: Digester Modeling and Validation. In A. K. and I. Turunen (Ed.), *Computer Aided Chemical Engineering* (Vol. 14, pp. 1049–1054). Lappeenranta: Elsevier. http://doi.org/10.1016/S1570-7946(03)80256-0

Rolandi, P. A., & Romagnoli, J. A. (2004). Smart enterprise for Pulp and Paper: Optimisation and Transition Planning of a Continuous Industrial Digester. Presented at the 14th European Symposium on Computer Aided Process Engineering (ESCAPE 14), Lisbon: Unpublished. Retrieved from http://www.nt.ntnu.no/users/skoge/prost/proceedings/escape14/papers/pcap079.pdf

Saltin, J. F. (1992). A predictive dynamic model for continuous digesters. In *Tappi 1992 Pulping Conference Proceedings* (pp. 261–268). Boston: TAPPI Press.

Santos, A., Rodríguez, F., Gilarranz, M. A., Moreno, D., & García-Ochoa, F. (1997). Kinetic Modeling of Kraft Delignification of Eucalyptus globulus. *Industrial & Engineering Chemistry Research*, *36*(10), 4114–4125. http://doi.org/10.1021/ie9701940

Sargent, R. (2011). Verification and Validation of Simulation Models. In S. Jain, R. R. Creasey, J. Himmelspach, K. P. White, & M. Fu (Eds.), *Proceedings of the 2011 Winter Simulation Conference*. Phoenix: IEEE. Retrieved from http://www.informs-sim.org/wsc11papers/016.pdf

Sidrak, Y. (1991). Model-based optimization and control of Kamyr digester operation. In K. Najim & E. Dufour (Eds.), *Advanced Control of Chemical*

Processes (pp. 137–142). Tolouse: IFAC. http://doi.org/10.1016/B978-0-08-041267-2.50027-9

Silva, C. M., & Biscaia Jr., E. C. (2003). Multiobjective optimization of a continuous pulp digester. In A. K. and I. Turunen (Ed.), *Computer Aided Chemical Engineering* (Vol. 14, pp. 1055–1060). Lappeenranta: Elsevier. http://doi.org/10.1016/S1570-7946(03)80257-2

Simão, J. P. F., Egas, A. P. V., Baptista, C. M. S. G., & Carvalho, M. G. (2005). Heterogeneous Kinetic Model for the Methylglucuronic and Hexenuronic Acids Reactions during Kraft Pulping of Eucalyptus globulus. *Industrial & Engineering Chemistry Research*, *44*(9), 2997–3002. http://doi.org/10.1021/ie049061m

Simpson, W., & TenWolde, A. (2007). Physical Properties and Moisture Relations of Wood. In U.S. Dept. of Agriculture, *The Encyclopedia of Wood*. Skyhorse Publishing Inc.

Sixta, H. (Ed.). (2006). *Handbook of Pulp*. Weinheim; Chichester: Wiley-VCH ; John Wiley.

Sixta, H., & Rutkowska, E. W. (2006). Comprehensive kinetic study of delignification, carbohydrate degradation, cellulose chain scissions, and hexenuronic acid reactions during Kraft pulping of Eucalyptus globulus. *Lenzinger Berichte*, *86*(2006), 32–45.

Sjöström, E. (1993). *Wood Chemistry: Fundamentals and Applications*. Gulf Professional Publishing.

Skogestad, S. (2009). *Chemical and energy process engineering*. Boca Raton, FL: CRC Press.

Smith, C. C. (1974). *Studies of the mathematical modelling, simulation and control of the operation of a Kamyr continuous digester for the kraft process* (Doctoral Dissertation). Purdue University. Retrieved from http://docs.lib.purdue.edu/dissertations/AAI7620254

Tikka, P. (Ed.). (2008). *Chemical Pulping Part 2, Recovery of Chemicals and Energy* (2nd ed., Vol. 6b). Helsinki: Paper Engineers' Association/Paperi ja Puu Oy.

Valmet. (2014). Valmet - the market leader in cooking. Retrieved June 15, 2014, from http://www.valmet.com/Valmet/products/Vault2MP.nsf/BYWID/WID-100512-2256E-3DC21/$File/CPDU_B_2075_260-02.pdf?OpenElement

Vroom, K. E. (1957). The H factor: A means of expressing cooking times and temperatures as a single variable. *Pulp and Paper Magazine of Canada*, *58*(3), 228–231.

Walkush, K., & Gustafson, R. G. (2002). Application of pulping models to investigate the performance of commercial continuous digesters. *Tappi Journal*, *1*(5), 13–19.

Wilder, H., & Daleski, E. (1965). Delignification rate studies. Part II of a series on kraft pulping kinetics. *Tappi Journal*, *48*(5), 293–297.

Wisnewski, P. A. (1997). *Inferential control using high-order process models with application to a continuous pulp digester* (Doctoral Dissertation). Purdue University. Retrieved from http://docs.lib.purdue.edu/dissertations/AAI9821857

Wisnewski, P. A., Doyle, F. J., & Kayihan, F. (1997). Fundamental continuous-pulp-digester model for simulation and control. *AIChE Journal*, *43*(12), 3175–3192. http://doi.org/10.1002/aic.690431206

Zakharov, A., & Jämsä-Jounela, S.-L. (2011). Iterative optimization of the economic efficiency of an industrial process within the validity area of the static plant model and its application to a Pulp Mill. *Computers & Chemical Engineering*, *35*(2), 245–254. http://doi.org/10.1016/j.compchemeng.2010.10.010

Appendix A

Model-based Process Analysis

Simulated contribution, a simply powerful technique

The technique called here simulated contribution was originally conceived for assessing the quality of input data used in the simulation, thus it may resemble to some extent model sensitivity or uncertainty analyses. However, the results of its application showed that it can be used for more interesting purposes, reason why it is treated here as an additional and relevant contribution of the thesis.

Figure A.1 depicts the basic idea of the method. The initial steady-state values are previously estimated from dynamic data, as performed for example in Section 8.3. The novelty of the method is the ability to attribute cause-effect relations based on the comparison of simulated contributions and the mill signal. Essentially, the method represents a process engineering tool to identify root-cause and cause-effect relations between input and output variables of a process. The method is extremely simple and can be applied to any process if a validated dynamic model is available. Thus, it could be categorized as a model-based analysis technique for process monitoring and diagnosis.

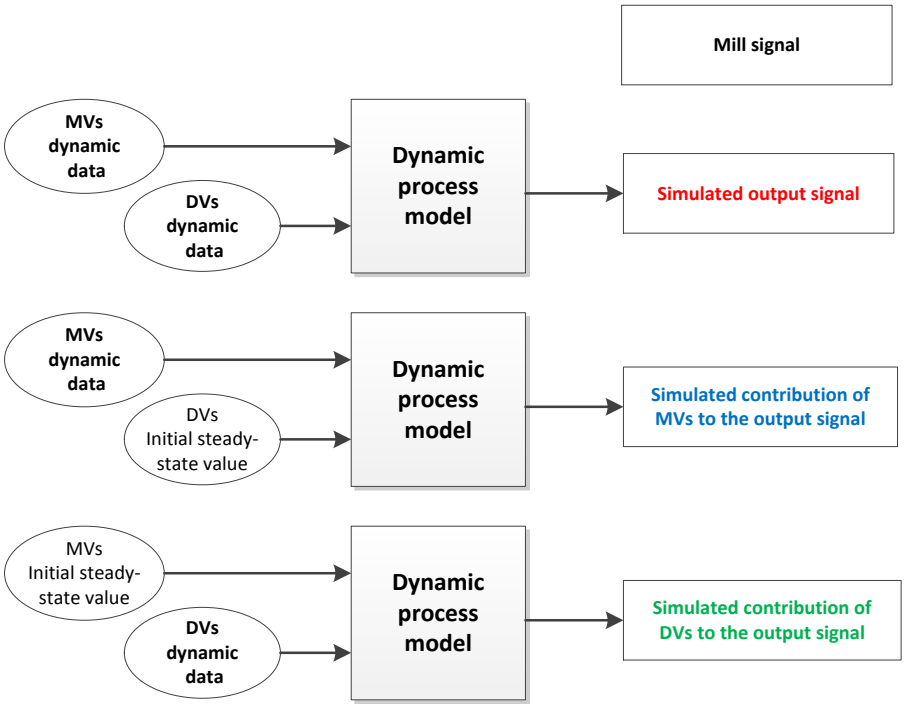

Figure A.1. Concept of the simulated contribution analysis.

An example of application: CompactCooking™ G2 digesting stage

Let us see now an example of applying the method to explain variations of weak black liquor solids and cooking kappa in the process studied.

Figure A.2 compares the mill signal of weak black liquor solids with the simulated output and its associated contribution signals. The simulated contributions clearly explain the main upsets of the mill signal, since we can attribute cause-effect relationships based on the correlation between each upset period in the mill signal and the same period in contributions. Most of the process upsets here can be attributed to the dynamics of disturbances, however, there are two important upsets around t = 8000 and t = 11000 that are instead explained by process manipulation. Regarding the bias between mill and simulated signals, a discussion of this issue can be found in Section 8.2.

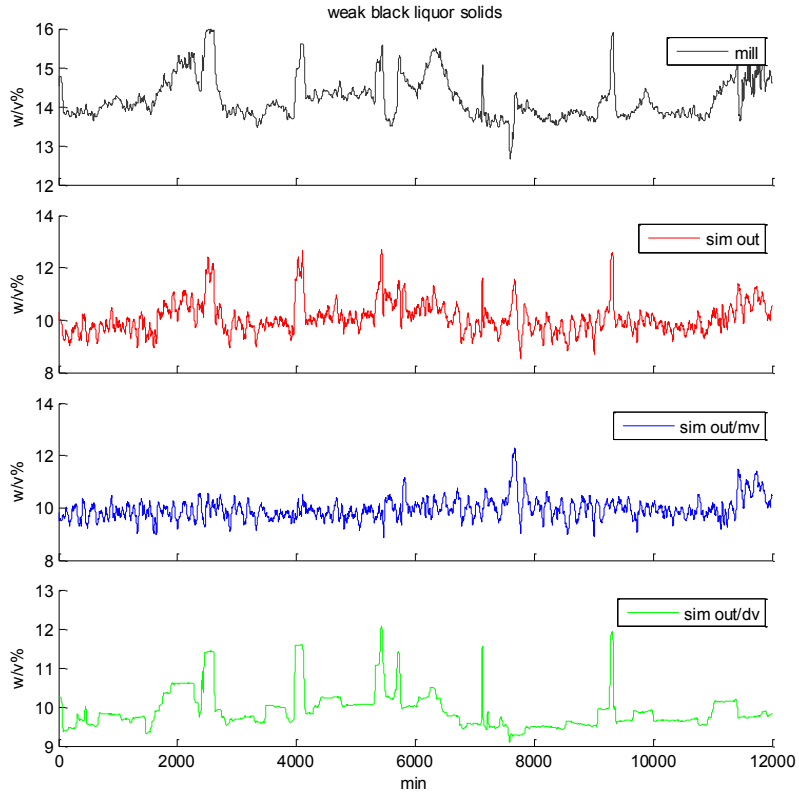

Figure A.2. Simulated contributions in the weak black liquor solids signal. *Red signal corresponds to a normal simulation run with all input data; blue signal, pure-manipulation contribution by maintaining disturbances at their initial steady-state value; green signal, pure-disturbance contribution by maintaining manipulated variables at their initial steady-state value.*

The reader should note that pure-manipulation contribution represents the digesting process stage operating under no disturbance load, meaning no change of entering temperatures, white liquor concentrations, wood moisture, or wood densities; and pure-disturbance contribution, a stage being operated with absolutely constant flow rates of all the streams but under disturbance load. Both situations are naturally imaginary and an industrial process is far from approaching to any of them. In a certain sense, we are using the dynamic model as a filter of the mill output signal, despite we are not filtering the output signal itself, rather input signals as they contribute to the output dynamics.

It is worth noting that the fast dynamics of the mill signal can be attributed to process manipulation, suggesting here that input data has not been filtered enough carrying too much noise to the simulation. The slow dynamics of the signal can be easily attributed to changes in the wash liquor by-pass flow rate, which in the simulator structure is considered a special disturbance variable.

Let us now continue with the analysis of the cooking kappa signal, in which the attribution of cause-effect relations is much more complex. Figure A.3 compares the mill signal of cooking kappa against the normal simulated output and simulated contributions. The normal simulation output shows a noisy signal that is clearly attributed to manipulation at the *model-level*; the pure-disturbance contribution shows instead a very good agreement with the mill signal at the *measurement-level*. This result has several interpretations concerning the simulation model design, as well as the understanding of process dynamics and improvements in the process control scheme. For the model, it suggests that (i) the sensitivities of reaction rates are higher than real, and/or that (ii) the temperature fluctuation experienced by the chip mass are higher than in the actual phenomenon. For the understanding of the process dynamics and control, it means that disturbances are able to generate a slow dynamics that the actual control scheme is not rejecting well enough.

To this point, we have found through the simulated contribution analysis that disturbances are the main causes of cooking kappa fluctuations. However, we would like to know which types of them have the greatest impact on kappa variability. The novel technique could be applied in a selective way, such that the contribution of single signals is simulated, but since we already suspect that temperature fluctuations are related to kappa variations, we will continue an

alternative approach trying to find a root-cause of the variations by analyzing the cooking temperature dynamics.

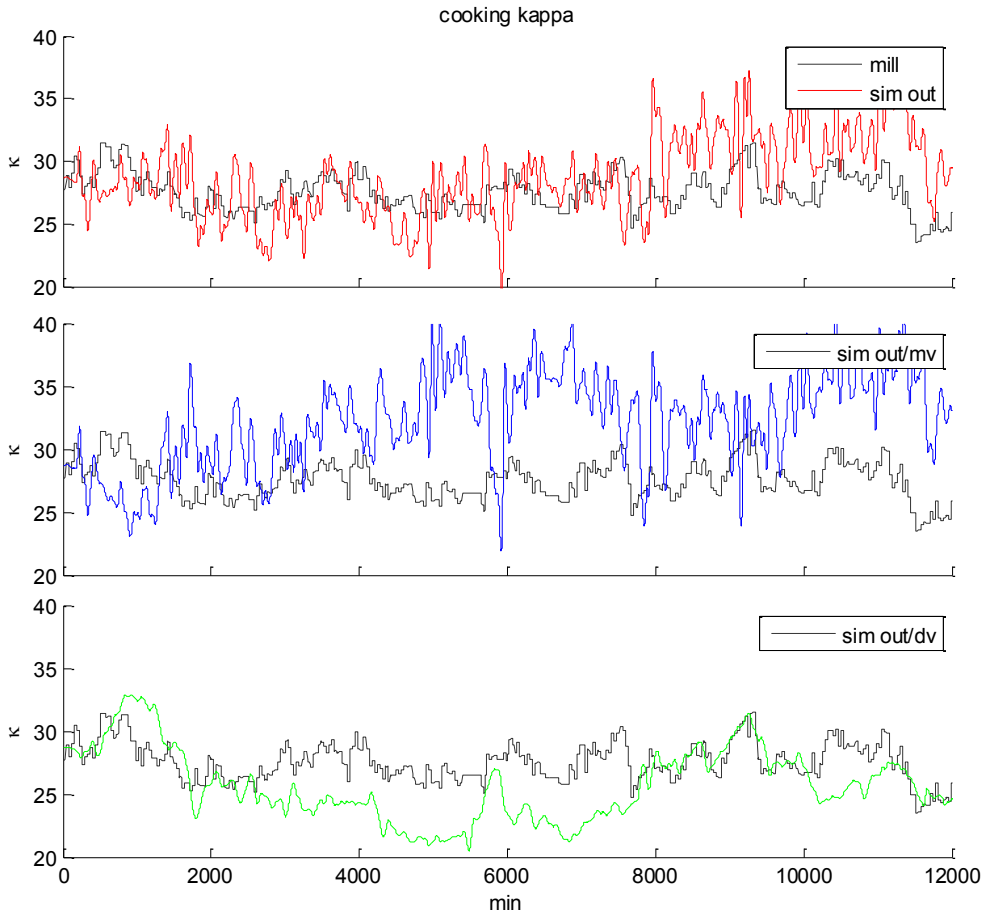

Figure A.3. Simulated contributions in the cooking kappa signal. *Red signal corresponds to a normal simulation run with all input data; blue signal, pure-manipulation contribution; green signal, pure-disturbance contribution.*

Figure A.4 compares several signals related to the cooking temperature, taken as the digester top liquor phase temperature. From this figure, we realize that the cooking temperature experiences a multiple-time-scale dynamics easily separable between fast and slow components. The slow dynamics is contributed by disturbances, including ambient, (cold) white liquor, wash liquor, and MP steam temperatures; the fast dynamics, insteand, is mainly contributed by flow rate manipulation, such as changes in the MP steam and (return) transfer liquor flow rates. Now, when comparing the pure-disturbance contribution signal of the cooking temperature against the mill cooking kappa (see Figure A.5), we find a surprising result that shows that kappa fluctuation inversely correlates to the slow

dynamic component of the cooking temperature. Since mill signal are too noisy, it could be very difficult to recognize this relation, as clearly as the simulated contribution analysis have shown, by alternative means involving statistical methods. In this sense, the technique can be employed as a model-based process diagnosis tool to find root-causes for complex dynamic behaviors. In this case, we have found that the controller of the cooking temperature does not handle well enough the multiple-time-scale dynamic behavior of the CompactCooking™ G2 process, a critical finding to start thinking about future improvements for the stabilizing control layer.

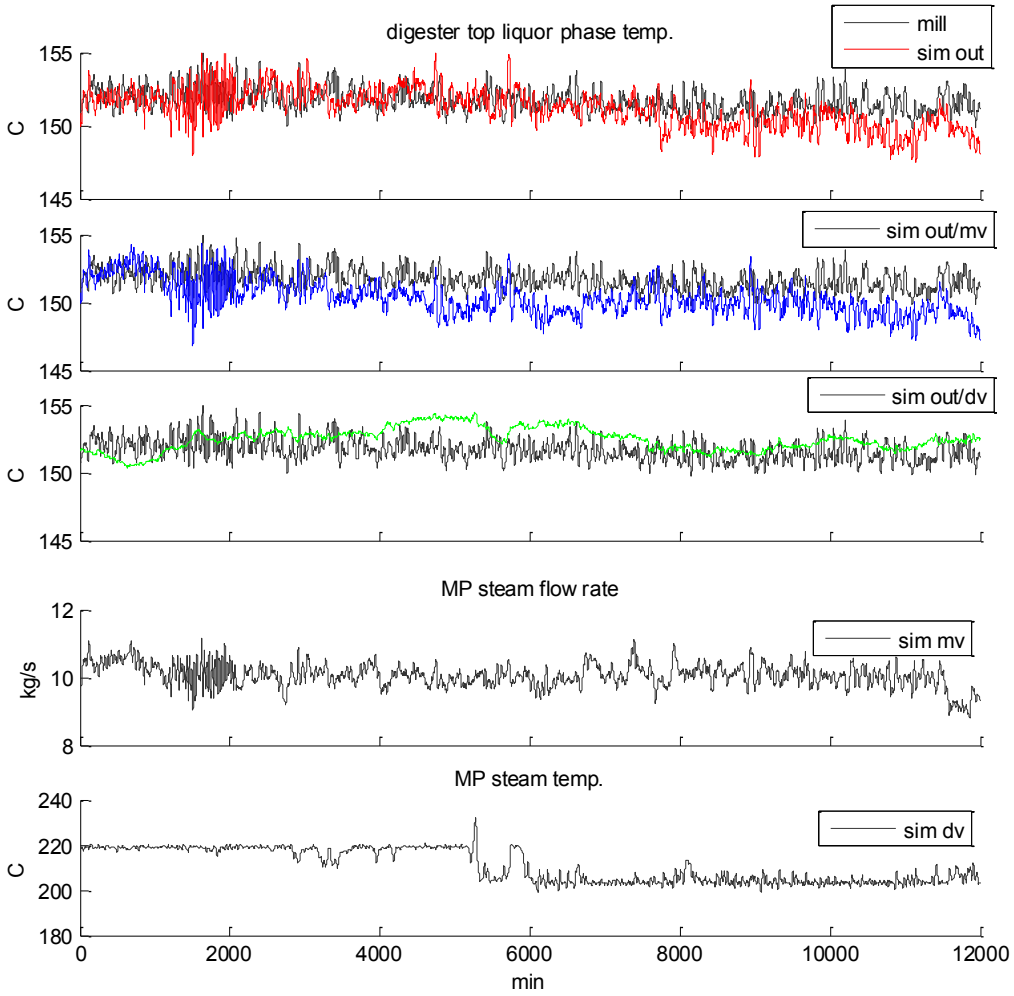

Figure A.4. Simulated contributions in the digester top liquor-phase temperature signal. *Red signal, normal simulation run with all input data; blue signal, pure-manipulation contribution; green signal, pure-disturbance contribution.*

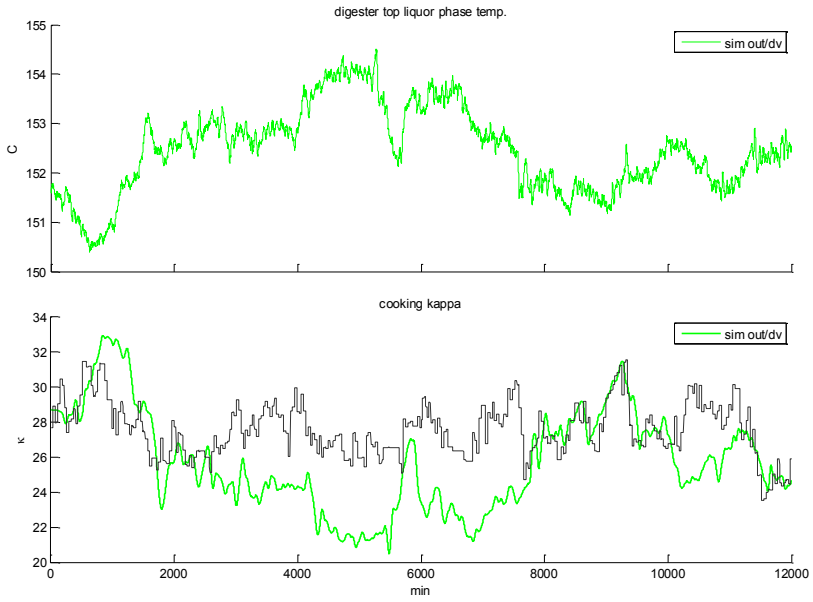

Figure A.5. Root-cause finding of cooking kappa fluctuations.
The slow dynamics of the cooking temperature, considered as the top liquor phase temperature, can mostly explain the variability of kappa; in turn, its slow dynamics is explained as the contribution of process disturbances.

The above results, regarding contribution analyses of cooking kappa and weak black liquor solids signals, are very important in terms of showing a direction for control improvement in the CompactCooking™ G2 digesting stage. Cooking kappa variations greatly affect the remainder stages of the fiber line; and fluctuations of weak black liquor solids content do the same on the whole recovery line. As pure-disturbance contribution signals (sim out/dv) represent most of the root-cause of their fluctuations, the logical conclusion is to strengthen disturbance rejection performance in the control system design. Practical guidelines are the incorporation of: (i) temperature sensors on entering streams of white liquor (cold), wash liquor, and filter reject, as well as on input and output streams of heat-exchangers (which allows monitoring heat-transfer performance); (ii) sensor moisture on the entering woodchips stream; (iii) and on-line white liquor chemical analyzers. All these measurements can be used to implement feed-forward policies on the control system, requiring a low investment on instrumentation with the exception of the white liquor chemical analyzers.

We have performed simulated contribution analyses grouping inputs into two sets of manipulated variables and disturbances; however, there is no limitation to group in any arbitrary way, such that we can analyze how the interactions of

inputs are contributing certain outputs dynamics. As the example of application has shown, the novel technique is a powerful conceptual tool to detect cause-effect and root-cause relations within highly interacting dynamic systems.